B E R I C H T E

aus dem

I N S T I T U T F Ü R M E E R E S K U N D E

an der

Christian-Albrechts-Universität Kiel

Nr. 175

1 9 8 7

S E A R O V E R

DATA REPORT II

NORTH ATLANTIC SUMMER 1983

- N O A '83 -

by

Harry Leach, Norbert Didden, Volker Fiekas,

Jürgen Fischer, Alexander Horch, John Woods

DOI 10.3289/IFM_BER_175

Copies of the Report can be obtained from

Abteilung Regionale Ozeanographie
Institut für Meereskunde an der Universität Kiel
Düsternbrooker Weg 20
D 2300 Kiel 1

ISSN 0341 - 8561

PREFACE

The NOA'83 SEA ROVER experiment was carried out during Cruise 101b of FS "Poseidon" between the Azores, Greenland and the British Isles during the summer of 1983.

The experiment was part of a long-term research programme designed to investigate structures in the seasonal boundary layer. The spectral range covers over three decades in the horizontal ranging from the gyre scale (order 1000 km) to the mesoscale (order 1 km) and it includes finestructure with vertical scales of more than one metre. Covering this broad spectral range was only possible with the development of the "Seasonal and Regional Ocean Variability Explorer" (SEA ROVER). A detailed description of various parts of the system can be found in Fischer et al. (1985), Leach (1984), Horch (1984) and Bauer et al. (1985). Although the first three of these reports represent the present status of the system most of the parts were already operational in 1983. The last describes the status of 1981. A brief description of the system including the data processing will be given within this report.

In 1983 the system was enhanced with an acoustic Doppler current profiler on the ship and on upward-looking radiometer on the fish. The latter was to measure the attenuation of downward irradiance and thus phytoplankton concentration.

There were two main scientific targets:

(1) large-scale variability of the boundary layer between the Azores (38° N) and 55° N,

(2) three-dimensional mesoscale structure of the Polar Front near the Gibbs Fracture Zone.

Although the scientific applications were different, the data sampling, processing and reduction of this large data set was identical for both parts of the experiment, the products are, however, presented separately according to the scientific objectives.

Within this report we describe the experiment and data processing, assess the experimental errors and present a selection of the possible products from various stages of the data processing. Many of the diagnostic techniques were developed to analyse the Batfish data set collected from RRS "Discovery" during GATE (Woods and Minnett, 1979; Woods, Leach and Minnett, 1981; Leach, Minnett and Woods, 1985). This data report does not offer scientific interpretation of the data. It is possible to gain some insight into the variability encountered in the seasonal boundary layer from the selection of products derived from routine computer processing of the data set.

The instrument development, data processing and analysis were carried out at the Institut für Meereskunde an der Universität Kiel. The fieldwork would not have been possible without the invaluable help of the captain and crew of FS "Poseidon".

The Deutsche Forschungsgemeinschaft helped to finance the work through the Sonderforschungsbereich 133 and the Normalverfahrenproject Wo 254/10. The following colleagues contributed to the work reported here by either taking part in the field phase on board FS "Poseidon", by developing the necessary hardware and software of the SEA ROVER system or by processing and discussing the data:

W. Barkmann, B. Burkert, J. Diemer, H.-J. Langhof, C. Meinke, A. Reikowski, V. Rehberg, I. Rodrigues (visiting from University of Lisbon), A. Schiller, D. Stammer and V. Strass.

We also thank Dr. Bauer and his colleagues at the Forschungsanstalt für Wasserschall- und Geophysik der Bundeswehr in Kiel for allowing us to copy their control system for the towed fish (Dettmann, 1981) and Vince Lawford at the Institut of Oceanographic Sciences for his support on the mechanical parts of the fish.

Last, but not least, we would like to thank the members of our cartography section, A. Eisele, I. Oelrichs and E. Petersen, also E. Mempel in the photography laboratory for preparing the figures in this report, and the members of the IfM computer centre for their invaluable help.

Contents

		Page
1.	**INTRODUCTION**	1
1.1	Aims of the experiment	1
1.2	Experimental design	2
1.3	Experimental site and oceanographic conditions	3
1.4	Sonderforschungsbereich 133 "Warm Water Sphere of the Atlantic"	4
1.5	Publications and reports related to the 1983 expedition	5
2.	**INSTRUMENTATION - THE SEA ROVER**	8
2.1	The IfM towed fish system during NOA'83	8
2.2	The radiometer	12
2.3	The "Poseidon" scientific navigation system	13
2.4	The Doppler Current Profiler	15
2.5	Real-time monitoring	16
3.	**THE EXPERIMENT**	17
3.1	The Long Sections	17
3.2	The Polar Front Survey	23
4.	**PROCESSING AND REDUCTION OF HYDROGRAPHIC AND OPTICAL DATA**	26
4.1	Raw data recording: CTD-data and optical data	26
4.2	Navigation data recording and correction	26
4.3	First processing - Editing the raw data	26
4.4	Second processing - Merging fish and navigation data	29
4.5	Third processing - Pressure monotonization and up/down-splitting	29
4.6	Fourth processing - Salinity and pressure correction	29
4.7	Fifth processing - Interpolation to depth levels for attenuation	29
4.8	Sixth processing - Interpolation to depth and sigma-t levels	31
4.9	Seventh processing - Combining 4-hour files to section files	31
4.10	Eighth processing - Interpolation to constant horizontal spacing	31
4.11	Ninth processing - Calculation of thickness	32
4.12	Tenth processing - Reorganisation of data from profiles to surfaces	32
4.13	Objective analysis	32
4.14	Deep CTD dips	32

Page

5. **PROCESSING AND REDUCTION OF CURRENT DATA** 34
5.1 Raw data acquisition 34
5.2 First processing - Calculation of the relative ship's velocities 34
5.3 Second processing - Merging the DCP-data with the corrected navigation data 37
5.4 Fourth processing - Calculation of absolute currents 37
5.5 Fifth processing - Calculation of vertical shear 38
5.6 Sixth and seventh processing - Extraction and objective analysis of surfaces 38

6. **DATA - LONG SECTIONS** 39
6.1 Section plots 39
6.2 One degree averages 43

7. **DATA - FRONT SURVEY** 49
7.1 Maps 49
7.2 Sections 51
7.3 Statistics 52

8. **ANALYSIS OF ERRORS OF HYDROGRAPHIC AND OPTICAL DATA** 74
8.1 Measurement errors and corrections applied during data processing 74
8.2 Numerical estimates of uncertainties in derived quantities . . . 75
8.3 Errors in objectively analysed fields 78
8.4 Synopticity 80
8.5 Errors in the attenuation, K_d 80

9. **ANALYSIS OF ERRORS OF CURRENT DATA** 82
9.1 Measurement errors 82
9.2 Estimate of errors in the objectively analysed fields 83

10. **METEOROLOGY** 84

11. **CONCLUSIONS** 88

12. **REFERENCES** 89

1. INTRODUCTION

1.1 Aims of the Experiment

The seasonal thermocline is the source of water which ventilates the permanent thermocline by direct advection along isopycnals. The regional and seasonal variability of this source has been the principal object of research in the Department of Regional Oceanography in recent years. To this end the SEA ROVER System (see Bauer et al., 1985, and below) was developed and used in a series of expeditions in the North Atlantic. In 1981 and 1983 surveys were made at the Polar Front and in the years 1981, 1983, 1984, 1985, 1986 and 1987 measurements were made along standard Long Sections. The first expedition in 1981 (NOA'81, "Poseidon" Cruise 76) is described in Bauer et al. (1985). This report describes the second expedition in 1983 (NOA'83, "Poseidon" Cruise 101).

The aims of the 1983 expedition were twofold. One was to collect data along standard Long Sections as a contribution to a data set illustrating the seasonal and regional variability in the seasonal thermocline. The second was to make a systematic synoptic-scale survey at the Polar Front.

In 1981 the SEA ROVER System measured profiles of temperature and conductivity and horizontal velocities at the sea surface and recorded navigation and meteorological data. In 1983 the system was enhanced to measure the downward shortwave radiation at 500 nm in the water and vertical profiles of the horizontal velocities.

1) **Long Sections**

The regional climate of the ocean boundary layer which serves as a link between the atmosphere and the interior of the ocean is not yet well understood. The reason for that is the failure of the too scarce coverage of hydrographic measurements, mainly based on station data, to resolve the regional, seasonal and interannual variations.

The data set is being used to study the system atmosphere - mixed layer - thermocline, for calculations of heat and fresh water budget and for investigation of seasonal cycles of various parameters for example, mixed layer depth, potential vorticity.

2) **Front Survey**

The mesoscale waveband in the spectrum of oceanic motion extends from the spectral peak of synoptic-scale motions (near the Rossby radius of deformation) to the spectral peak of microscale turbulence (at the Ozmidov scale). In the seasonal thermocline, the mesoscale waveband ranges from about 30 km to 30 cm. This spectral band includes internal waves and the enstrophy cascade of isopycnic turbulence and finestructure in hydrographic profiles. Mesoscale jets and fronts are a key phenomenon in these latter processes.

The aim of this part of the experiment was to survey the three-dimensional structure of thermoclinicity, baroclinicity, velocity and potential vorticity to a horizontal resolution of 10 nmi. Higher resolution would be available for the thermohaline and mass fields along the line of the sections.

Surveying mesoscale fronts with a rapidly moving ship seems to be the best strategy to minimize the difficulties of interpreting the structures caused by non-synoptic or poorly-resolving measurements.

The experiment should take place in a region where the relevant quantities show strong signals, that means in a region with the best signal-to-noise ratio. We therefore chose the North Atlantic Polar Front as a good test site for these studies.

1.2 Experimental design

For the experiment the full capabilities of the measurement system were used. The towed fish undulation in the form of a saw tooth wave should reach clearly the mixed layer and dive as deep as possible into the seasonal thermocline with a minimum wavelength to resolve the expected steep temperature gradients. The ship should move at full speed of about 5 m s^{-1} to improve synopticity and save time during measurements. The data should be recorded and processed continuously.

1) **Long Sections**

For the investigation of the long sections the ship followed along standard tracks whose choice had both technical and scientific reasons. They are the links between the front survey area at the Polar Front, the supply base at the Azores and the home port. They pass through the location of the Ocean Weather Ships to provide a comparison of the data with the long-term measurements at the Ocean Weather Stations. Repeated measurements along the same standard tracks on return trips and in different seasons and years should allow investigations about persistence of features and seasonal and interannual variations.

2) **Front Survey**

In 1981 a general survey pattern was designed to localize the synoptic-scale structures, meanders and eddies of the North Atlantic Polar Front and to find a region with high thermoclinicity. Then, focussing in on that region, a high resolution survey, to resolve the mesoscale structures and cut the front as many times as the remaining ship-time allowed, was made.

The analysis of the 1981 data set (Bauer et al., 1985) shows that the inhomogeneous data distribution due to the focussing strategy can lead to difficulties in interpreting the results of the survey and so it was felt that for 1983 a systematic synoptic-scale survey should be made to give homogenous data coverage and reduce problems due to asynopticity by making a single progressive sweep.

1.3 Experimental site and oceanographic conditions

Our Long Sections range from the Azores to about 55° N, from the anti-cyclonic Subtropical Gyre well into the cyclonic Subpolar Gyre, where the Polar Front is the boundary between these gyres, and from the Azores to the English Channel.

When the programme of Long Sections was first planned (1980) it was thought that both sections would intersect the streamlines of the North Atlantic Gyre (Dietrich, 1969). The mass transport across the Azores - Greenland section is concentrated in the region of the Polar Front otherwise known as the North Atlantic Current, between about 48° N and 52° N,

whereas the Azores - English Channel section was expected to cross the various branches of the recirculation between the Azores and the European continent (Dietrich et al., 1980). In the meantime work by Krauss (1986) and Sy (1987a and b) as part of the Kiel Sonderforschungsbereich "Warmwassersphäre des Atlantiks" has tended to revive the earlier picture of the Atlantic circulation of Helland-Hansen and Nansen (1926) and Iselin (1936) in which the North Atlantic Current water recirculates in the Subpolar Gyre and a second branch of the North Atlantic Current leaves the main branch at the Grand Banks and crosses the Atlantic passing south of the Azores as the Azores Current (see also Gould, 1985; Olbers et al., 1985). This means that our section Azores - Land's End lies within the slack triangular region between Scotland, the Grand Banks and Gibraltar.

Both sections cross the zero line of the net annual water flux resulting from precipitation minus evaporation (Baumgartner and Reichel, 1975).

Along the Azores - English Channel section the net annual heat flux through the surface is nearly zero while the Azores - Greenland section intersects the axis of maximum heat loss (Budyko, 1974).

The Azores - Greenland section follows the track of the long hydrocast section measured during the International Geophysical Year (Dietrich, 1969). A recent summary of the seasonal and regional variation along our sections can be found in the Isopycnic Atlas of the North Atlantic Ocean (Bauer and Woods, 1984) which was derived from the well-known Robinson-Bauer-Schroeder Atlas (1979). The general structure during July and August is a well-developed seasonal pycnocline with a shallow mixed layer.

Winter mixing reaches deeper than 150 m in the whole region we surveyed. That means that the water column in the depth range of the towed fish all lies within the seasonal pycnocline.

1.4 Sonderforschungsbereich 133 - "Warm Water Sphere of the Atlantic"

Our work including the investigation of large-scale structures in the seasonal thermocline as well as frontal structures can be seen in the context of the long running "Warm Water Sphere" cooperative research programme (Sonderforschungsbereich) funded by the Deutsche Forschungsgemeinschaft (German Research Council). The aim of this programme is to gain some

insight into the dynamics and thermodynamics of the North Atlantic, the transports of heat and mass from the western basin across the Mid-Atlantic Ridge into the eastern basin, and the recirculation in the subtropics.

Although many groups participate in this programme the interactions with the following groups are especially relevant to our work:

Satellite images of sea surface temperature at the Polar Front will help us to identify regions of strong thermoclinicity and give some hint of the time scales of the observed structures (Hardtke and Meincke, 1984). Surface fluxes after Isemer and Hasse (1985) based on Bunker's data will help us to interpret the large-scale variation of the seasonal thermocline.

From long sections with deep CTD-stations along the Mid-Atlantic Ridge (Meincke and Sy, 1983) the maximum depth of winter mixing can be estimated by the "thermoclinicity elbow" method (Woods, 1985). Drifter trajectories (Krauss and Meincke, 1982; Krauss and Käse, 1984) will be used to identify the seasonal catchment area of the water being advected through our area.

1.5 Publications and reports related to the 1983 expedition

Bauer, J. (1987) in his thesis deals with incorporation of low-salinity surface water into the North Atlantic Current water based on analysis of our expeditions in 1981 (Bauer et al., 1985), 1983 (this report) and 1984 (Stammer et al., 1988).

Bauer, J., J. Fischer, H. Leach, J. Woods (1985) in their report on our 1981 expedition describe the methods and data of that expedition and contains many important details not repeated here.

Bauer, J. and J.D. Woods (1984) used the North Atlantic part of the numerical atlas produced by M. Robinson, E. Schroeder and R. Bauer (1979) from NODC data to present the annual cycle of the hydrography on density surfaces. Monthly mean temperatures were combined with annual mean salinities to calculate pseudo-monthly mean densities.

The first part presented monthly mean maps of the distribution of pressure, temperature and salinity on various density surfaces.

Vertical sections in isopycnic coordinates were presented in part two. They follow the standard ship's tracks of the SFB-133 TP-B1: Azores - Greenland and Azores - English Channel.

Didden, N. (1987) describes a comprehensive investigation of the reliability and accuracy of measurements made using the acoustic Doppler current profiler.

Fiekas, V. (1987) combines the velocity field data from the 1983 expedition Polar Front survey with the hydrographic data to draw conclusions about the the ageostrophic effects.

Fischer,J. and A. Horch (1988) develop methods for correcting the radiation for various solar elevations back to the case of diffuse radiation for use in determing chlorophyll content.

Fischer, J., C. Meinke, P. J. Minnett, V. Rehberg and V. Strass (1985) give a detailed technical description of the mechanics, electronics and software of the Schleppfisch-system. This report includes also an operating manual for the use of the Schleppfisch (towed fish) and the basic CTD data processing for quick-look data. Although this is a description of the 1985 configuration of the system, it is still relevant for the 1983 state.

Fischer, J., H. Leach and J.D. Woods (1988) give a description of synoptic-scale structures at the North Atlantic Polar Front measured with the SEA ROVER system. This paper draws attention to the similarities between hydrographic data in the seasonal thermocline and sea surface currents. Derived quantities such as relative vorticity and spacing between isopycnals show significant correlations, thus allowing calculation of the isopycnic potential vorticity. This shows a similar distribution to the temperature on isopycnals.

Horch, A. (1984) is a technical report about the CTD-data processing and editing on the shipboard minicomputer "NOVA-4C". The second edition describes the state of the software in 1984, but includes the 1983 programs.

Horch, A. (1987) describes the analysis of the water turbidity data obtained from the radiometer mounted on the fish during the 1983 Polar Front survey.

Leach, H. (1984) describes the scientific navigation system based on an HP-1000 minicomputer, which was used in 1983 on board FS "Poseidon". This system is the basic tool for measuring currents by using both absolute and relative navigation. The second edition describes the state of the system in 1984, but the main concept remains unchanged.

Leach, H. (1986) used ship drift measurements from 1981 to calculate sea surface currents independently from the hydrographic data. By using the relative vorticity, which was derived from the objectively analysed current field, it was possible to calculate the surface streamfunction. Synoptic-scale meanders were the dominant features in the streamfunction and some similarities with the thermohaline structures are described. The method used in the analysis of the 1981 data has been used to analyse the 1983 data as described in this report.

Stammer, D. (1986) describes the variability of isopycnic potential vorticity in the North Atlantic based on atlas data and on the data from the Long Sections of our expedition in 1981 and 1983.

Stammer et al. (1988) is a compendium of all the SEA ROVER Long Sections and is in preparation still.

2. INSTRUMENTATION - THE SEA ROVER

An overview of the SEA ROVER System is given in Fig. 2.1.

2.1 The IFM towed fish system during NOA'83

Hydrographic data (CTD) and downward radiation were measured by instruments mounted on a towed depth-controlled fish, which is described in detail by Fischer et al. (1985) and Bauer et al. (1985). The main component of this system is the underwater vehicle including hydraulics unit, sensors for the fish attitude and the scientific payload. The fish is controlled by a microprocessor deck unit, which also writes the scientific data onto magnetic tape (raw data archive) and to the data monitor (section 2.5), new in 1983.

The scientific payload was a CTD-unit, with two sensor pairs for temperature and conductivity and one pressure gauge, and the new radiometer described in section 2.2. The resolution and accuracy of these sensors are specified in Table 2.1 as given by the manufacturers. Thermometers and conductivity cells were mounted in pairs on either side of the fish's nose, the pressure gauge was inside the fish directly fixed to the CTD-unit, and the radiometer was mounted on top of the fish (Fig. 2.2). The data were digitized with 16 bit (15 bit plus sign) resolution for the CTD-variables and 12 bit for the radiometer data. The interval between successive data cycles was 62.5 milliseconds (CTD) and 125 milliseconds for radiation.

A subsample (one cycle per second) of the data was converted to physical units to allow a preliminary quality check of the incoming data stream. The fish was towed on an unfaired 10 mm single core towing cable, which had a nominal breaking strain of 60 kN. All signal transfer to and from the underwater unit and the current supply was carried along this cable.

During operational mode the fish followed a saw-tooth track under automatic control. The parameters determining the undulations were upper and lower turning depth and diving rate, all chosen by the operator. Only during deployment and recovery the fish was manually controlled.

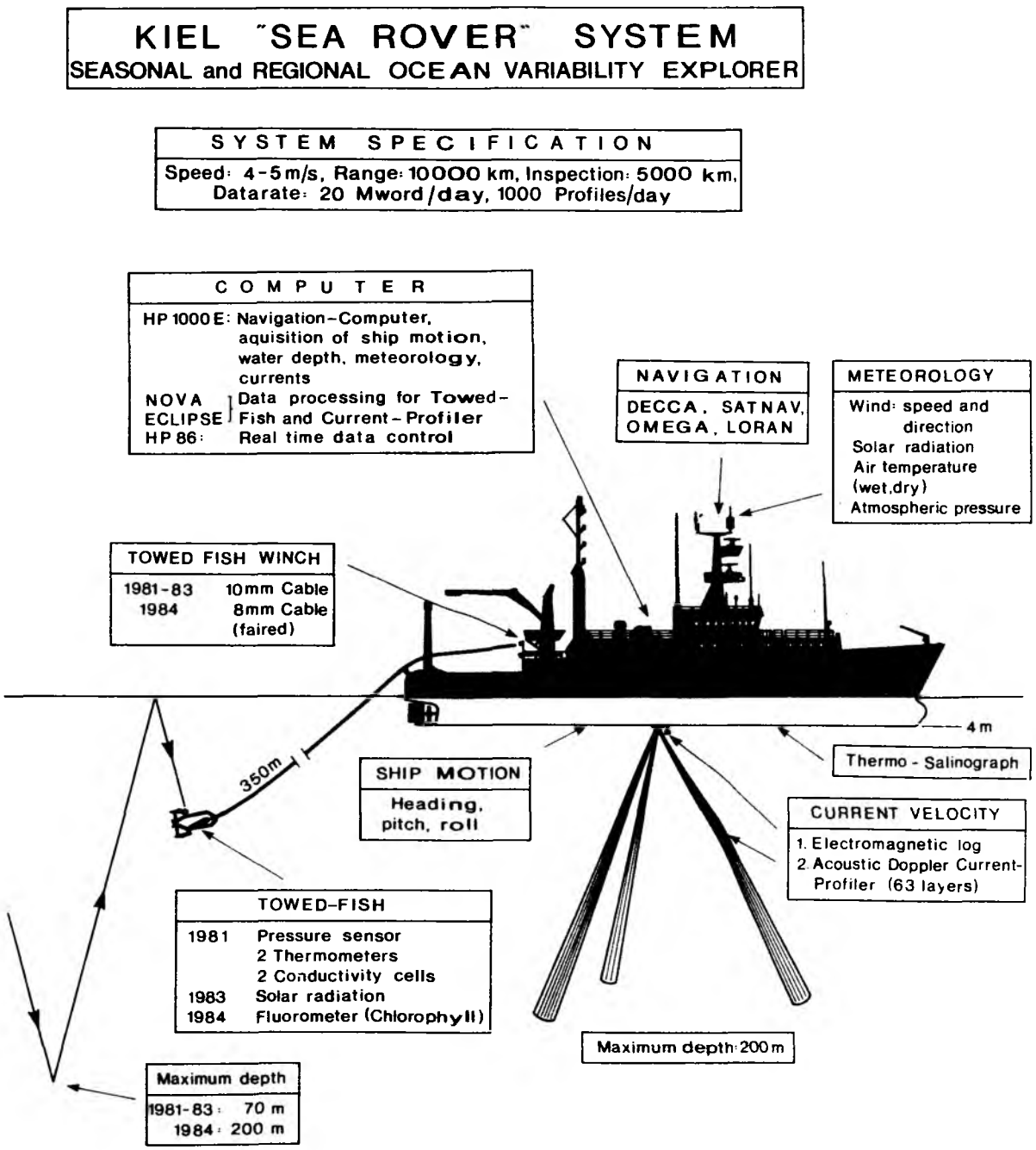

Fig. 2.1: Schematic diagram of the SEA ROVER Systems.

Table 2.1: Table of sensor specification (CTD and radiometer)

PARAMETER	SPECIFICATION	
PRESSURE	Principle	: Strain-gauge pressure cell
	Range	: 0 - 600 dbar
	Resolution	: ± 0.01 dbar
	Accuracy	: 0.25 % of range
TEMPERATURE	Principle	: Platinum resistance
	Range	: -2 - +40 °C
	Resolution	: 0.001 °C
	Accuracy	: ± 0.005 °C
CONDUCTIVITY	Principle	: Symmetric electrode cell
	Range	: 5 - 55 mS/cm
	Resolution	: 0.001 mS/cm
	Accuracy	: ± 0.005 ms/cm
RADIATION at λ = 500 nm	Principle	: Photodiode with bandpass filter ($\Delta\lambda$ = 2 nm)
	Range	: 0 - 5 V corresponding to 0 - 910 W/m² for a "standard-radiation spectrum"
	Resolution	: 0.001 V
	Accuracy	: ± 0.001 V

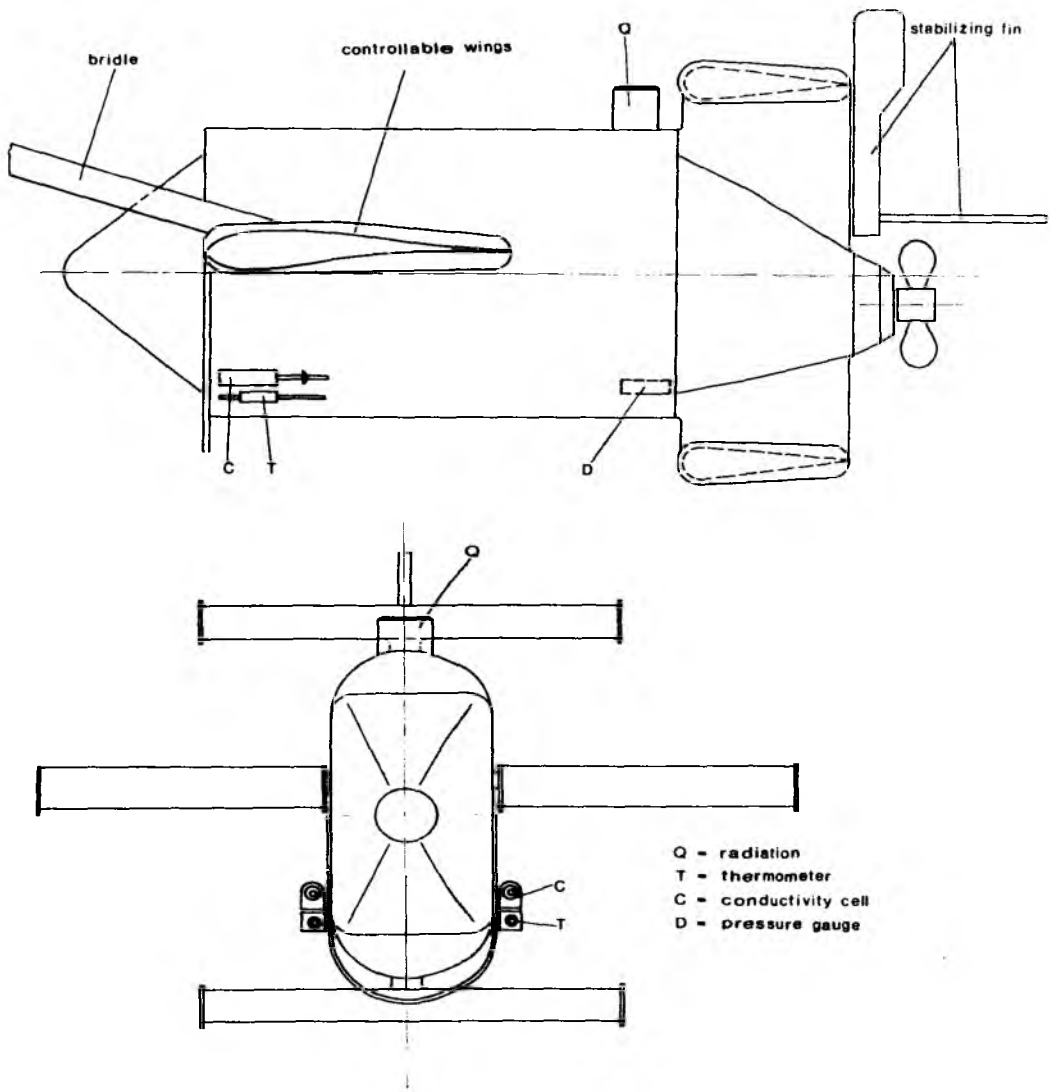

Fig. 2.2: Front and side view of the towed fish, showing the main components of the fish and the scientific sensor configuration during the experiment NOA'83.

2.2 The radiometer

In addition to the CTD the fish was fitted in 1983 for the first time with a radiometer sensitive to monochromatic radiation at 500 nm (bandwidth 4 nm) coming from above. Its specifications are shown in Table 2.1. This instrument was manufactured by Q-Instrument, Laestedet 29, DK 2670 Goere Strand, Denmark, in collaboration with the Institut for Fysik Oceanografi, Haraldsgade 6, DK 2200 Copenhagen, Denmark. The instrument uses a PIN-diode and amplifier with an output range of 0 - 5 V. The analogue voltage was digitized using a 12 bit A/D-converter.

Although the instrument was delivered with a calibration in quanta m^{-2} s^{-1} it was decided to recalibrate it using both the radiometer on board "Poseidon" and the radiometer on the roof of the Institute. These gave the calibration of the instrument as a function of the global radiation:

$$E_d/[W\ m^{-2}] = 5.064587 + 181.0201 \cdot E_d/[V]$$

with a correlation coefficient of 0.99997. This calibration is justified and shows a good correlation because the irradiance at 500 nm remains a constant fraction of the total irradiance except for very low solar elevations.

The temperature dependance of the output signal of the radiometer was investigated in a calibration tank for the temperature range 8 - 18 °C. This gave the following dependance:

$$I_{offset}/[mV] = - 13.118 - 0.263 \cdot T/[°C]$$

with a correlation coefficient of 0.994. The offset was negative and therefore the measured values had to be increased by the amount given by the formula to obtain the true output voltage.

Further details of the radiometer are given in Horch (1987).

2.3 The "Poseidon" scientific navigation system

The NOA'83 expedition was the second expedition in which the "Poseidon" scientific navigation system (Leach, 1987) was used to collect and store navigation data. The system is based on a Hewlett-Packard HP1000 mini-computer to which many of the ship's navigational instruments are interfaced as shown in Figure 2.3. During this cruise the computer was running under a version of the RTE-MIII operating system with 128K memory. This allowed a maximum of seven partitions which in turn limited the number of programs which could run in parallel to seven. Seven tasks could be performed in real-time:

1. the acquisition of satellite-navigation positions from the Magnavox MX1105 (program SATN2),
2. the integration of the ship's position relative to the water using the Colnbrook electromagnetic log (program EML03),
3. displaying the navigational information in alphanumeric and graphic form on the system's graphic terminals (program PLOT4).
4. transferring the navigation data from the memory buffer to disc (program KEPL2)
5. acquisition of meteorological data (program METØ3)
6. acquisition of data from the acoustic Doppler current profiler (program DCPX6)
7. transferring the current profiler data to disc (program DCPK2) or tape (program DCPKT).

The navigation data and the current profiler data were transferred from disc to tape two or three times a day as necessary using the programs NAVDT and DCPDT respectively.

During the first two sections (B101, B102) the current profiler data were averaged in real-time and stored in the two-minute file on disc, before being transferred to tape (programs DCPK2 and DCPDT). Starting with the third section (B103) on 29.6.83 (day 180) the raw data were written directly to tape (program DCPKT).

Spot values of all the available navigational parameters were printed out every two minutes.

Fig. 2.3: Block diagram of "Poseidon" Scientific Navigation System as used in NOA'83.

The electromagnetic log was calibrated between Lisbon and the Azores on 21st June 1983 (day 172) using a drifting radar-buoy with a sail centred at the depth of the log (ca. 4.5 m). The fore-aft and port-starboard components were calibrated separately. The details of the method used are contained in Leach (1984). This was the fourth set of coefficients obtained which were accordingly stored in a file named #KAL4.

2.4 The Doppler current profiler

During the NOA'83 expedition the acoustic Doppler current profiler (ADCP) was used for the first time to continuously measure current profiles from the ship underway. The measurements are based on the fact that acoustic energy transmitted in narrow beams downward through the water column is scattered by minute particles which are assumed to drift with the local current. The Doppler frequency shift of the back-scattered energy is proportional to the component of velocity parallel to the beam. Using acoustic pulses transmitted by a three-beam transducer the Doppler frequency measurements of the range-gated return signals provide profiles of the relative velocity between transducer and scattering volume as a function of distance from the transducer.

The main components of the Ametek Straza DCP 4400/115 acoustic Doppler current profiling system installed on RV "Poseidon" are a 115 kHz three-beam transducer, a junction box for the generation of the transmit signal and a microprocessor and signal processing unit which is interfaced with a Hewlett Packard HP85. The HP85 provides operational control of the microprocessor and acquires frequency shift data of the return signal from the signal processor. The data are transferred in real-time via a serial interface to a HP1000 computer, merged with navigational data, time, roll and pitch and then stored on magnetic tape.

The transducer was flush mounted with the hull in a midship well at 4 m depth. The three beams of 5° width are tilted 30° from the vertical and separated by 120° in the azimuth, one of the beams being nominally aligned with the ship's forward direction. The pulse repetition rate is 1 s, but the serial data transfer reduces the average profile sampling rate to one profile every 2.5 s. The frequency is measured in 63 sequential time intervals selectable between 1.6 ms and 19.2 ms, corresponding to vertical

depth bins between approximately 1 m and 12.8 m. We chose a bin size of 4.8 ms (3.15 m) thus covering a depth range of 200 m. The pulse width was chosen equal to the bin width resulting in an effective vertical resolution of twice the bin width. For a single acoustic pulse (ping) a data cycle consists of 64 Doppler frequencies for each of the three beams (63 depth bins and the bottom bin), the ADCP operating parameters, water temperature measured at the transducer head, ship heading with a 0.3° resolution, roll and pitch (not synchronized with the outgoing pulse) and additional information from the ship's navigation system.

The ADCP measures water velocity relative to the moving ship. Mean absolute current profiles were derived only between pairs of Transit satellite fixes in irregular intervals ranging between 25 minutes and 2 hours. In shallow water (continental shelf, English Channel, see Fig. 3.2) bottom tracking wss used to derive the ship velocity relative to the ground.

2.5 Real-time monitoring

A real-time monitor system based on an HP86 desk-top computer was derived to control the data quality and to obtain real-time information about the spatial structures of various parameters. The system was linked to the microprocessor control unit, which transferred one full data cycle per second during the downward phase of the undulation. The data cycle comprises conductivity, temperature and depth in physical units, the corresponding salinity and density and raw radiation data. One profile (all variables) every hour was stored on a diskette to be plotted afterwards (after 4 hours), a print-out of the hourly values at the turning depths was used to monitor the large-scale structures (for the long sections) and time series of temperature and pressure on isopycnals (real-time plots) were used to control the frontal survey.

3. THE EXPERIMENT

The NOA'83 expedition had two major scientific objectives, firstly, to collect a data set which would contribute to the investigation of the large-scale variability and the seasonal cycle of the upper ocean and, secondly, to obtain a data set for investigating the dynamics of the synoptic scale at the North Atlantic Polar Front.

In both parts of the experiment, the fish was towed at a speed of 8 to 9.5 knots, with the nominal turning depth set to 10 m and 70 m and a ascent/descent rate between 0.8 m/s and 1.2 m/s. According to these values the horizontal resolution was about 750 m between profiles of the same orientation. A typical example of the track and the pitch- and roll-angles is given in Figure 3.1. From the data sampling rate, 16 cycles per second for the CTD (mainly MS38) and 8 radiation values per second, the mean vertical resolution was 6 cm and 12 cm respectively. The raw data were archived in blocks of 512 words, containing 72 data cycles followed by a trailer with information about time and orientation of the profiles. The data format is listed in Table 3.1.

3.1 The Long Sections

The Long Sections along which measurements were made in 1983 are shown in Figure 3.2 and listed in Table 3.2. The temporal distribution is shown in Figure 3.3. The cruise began, for organizational reasons, in Lisbon and the first section B101 was thus from Lisbon to the Azores. However, during this section a series of technical difficulties with the towed fish resulted in very little data being collected.

The standard section Azores – OWS "C" – 55° N, B102 northbound, and B103/120 southbound, was laid east of Chancer Bank (43° N, 29° W) in 1983. The southbound section was interrupted for the Polar Front Survey (see below). During the first two sections, B101 and B102, the Doppler current profiler data were averaged over 2-minute intervals in real-time on the HP1000 and only starting with section B103 were the raw data written onto tape.

The final section of the cruise was B121 from the Azores via OWS "R" towards the English Channel. This section was made at the same time of year as the first, outbound section, B101, of the 1981 expedition (see Bauer et al., 1985).

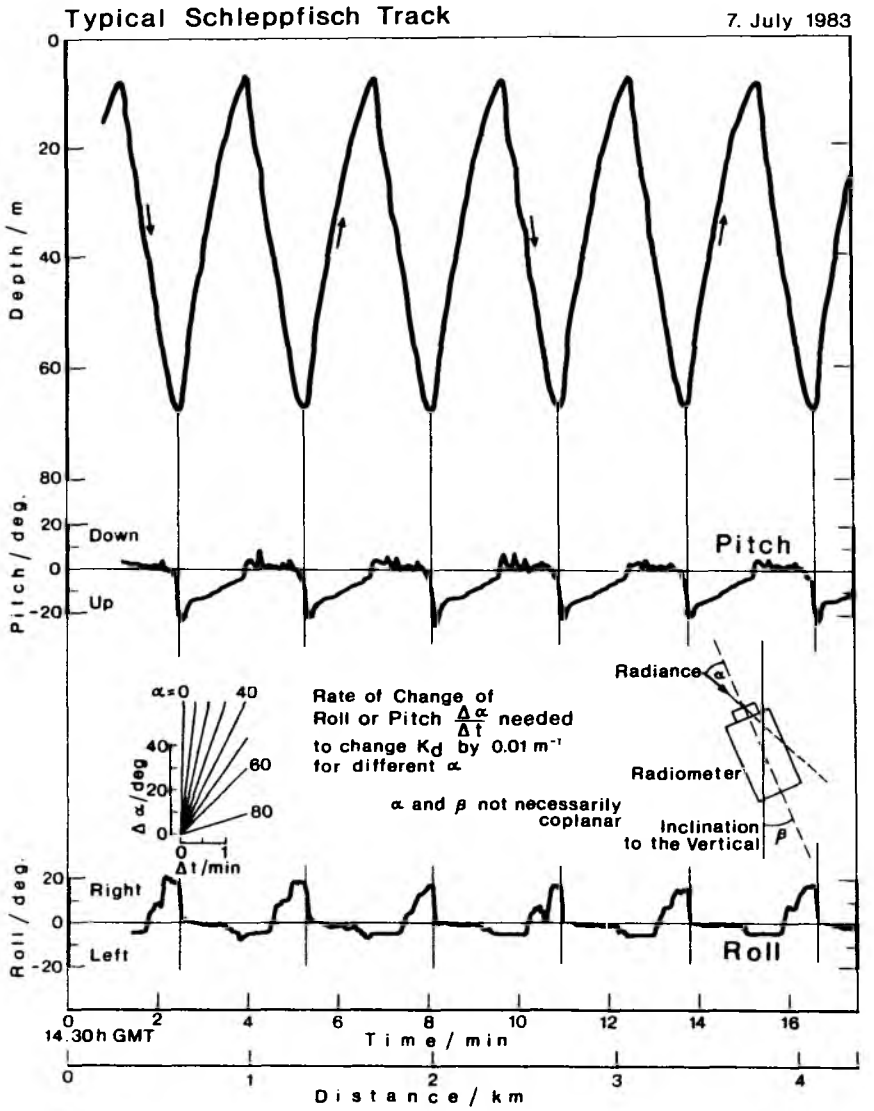

Fig. 3.1:

Time series of the towed fish undulations and the pitch- and roll-angles. Time was also converted to distance by assuming a constant towing speed of 8 knots.

Table 3.1: Schleppfisch Controller - Format of Magnetic Tape Data Storage

TAPE DRIVES : Kennedy 9000-1
NUMBER OF TRACKS : 9
FORMATTER : NRZI, synchronous, read after write
PARITY : ODD
BUFFER SIZE : 2048 bytes
TAPE BLOCK SIZE : 1024 bytes
TAPE BLOCK FORMAT : -

Word no.	Variable	Resolution
1	PRESSURE	0.1 dbar
2	TEMPERATURE 1	0.001 K
3	CONDUCTIVITY 1	0.002 mS/cm
4	IRRADIANCE	-
5	FLUORESCENCE	-
6	TEMPERATURE 2	0.001 K
7	CONDUCTIVITY 2	0.002 mS/cm
8 - 504 are a further 71 cycles of words 1-7		
505	DATE	
506	TIME: HOUR	
507	TIME: MINUTE	
508	TIME: SECOND	
509	(WATER DEPTH)	
510	UP/DOWN FLAG 0 = ASCENDING PROFILE 1 = DESCENDING PROFILE	
511,512	set to 0	

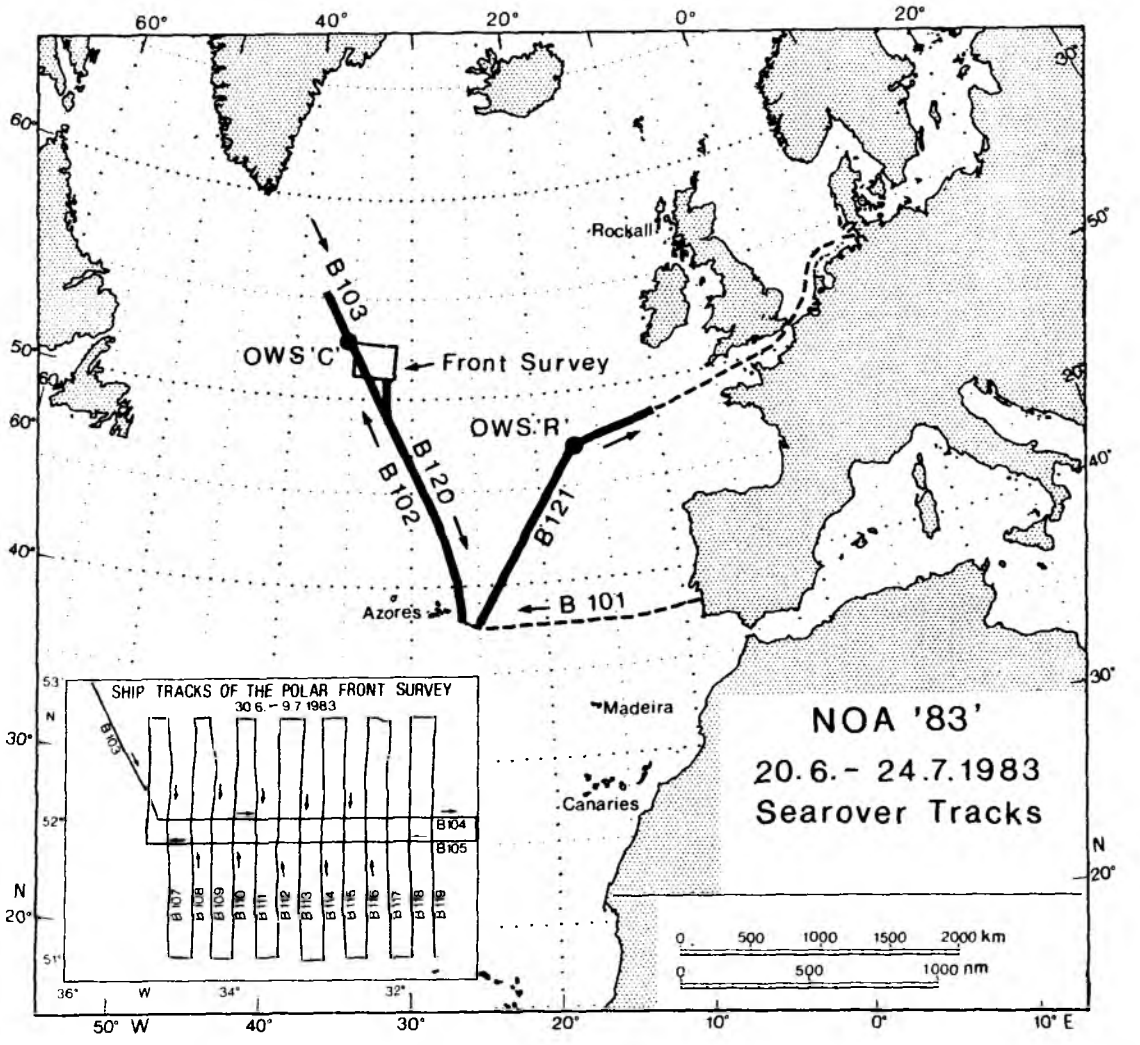

Fig. 3.2: Map of the eastern North Atlantic showing the position of the Long Sections.

Table 3.2: List of all NOA'83 SEA ROVER sections with start and end time, start and end position, and the nominal ship's heading.

Section		Start of Section Day No.	Time (GMT)	Longitude (W)	Latitude (N)	End of Section Day No.	Time (GMT)	Longitude (W)	Latitude (N)	Heading (°T)
B101		171	13:30	09 23.17	38 05.20	175	07:50	25 36.91	37 42.15	265
B102		175	18:30	25 40.31	37 41.90	180	17:20	37 28.00	54 49.93	335
B103		180	17:20	37 28.00	54 49.93	181	14:31	34 51.31	52 00.75	155
B104		181	14.31	34 51.31	52 00.75	182	06:22	30 59.83	51 59.85	90
B105	M	182	06:22	30 59.83	51 59.85	182	07:26	30 59.73	51 50.75	180
	Z	182	07:26	30 59.73	51 50.75	183	01:01	35 01.00	51 50.36	270
B106		183	01:01	35 01.00	51 50.36	183	06:36	34 59.44	52 43.48	360
B107	Z	183	06:36	34 59.44	52 43.48	183	07:28	34 44.30	52 43.31	90
	M	183	07.28	34 44.30	52 43.31	183	19:17	34 43.99	51 00.56	180
B108	Z	183	19:17	34 43.99	51 00.56	183	20:27	34 28.42	51 00.23	90
	M	184	20:27	34 28.42	51 00.23	184	08:27	34 24.74	52 44.28	360
B109	Z	184	08:27	34 24.74	52 44.28	184	09:09	34 13.87	52 42.00	90
	M	184	09:09	34 13.87	52 42.00	184	19:57	34 12.47	50 59.75	180
B110	Z	184	19:57	34 12.47	50 59.75	184	21:09	33 55.41	50 59.56	90
	M	183	21:09	33 55.41	50 59.56	185	09:35	33 57.61	52 45.39	360
B111	Z	185	09:35	33 57.61	52 45.39	185	10:33	33 42.59	52 45.44	90
	M	185	10:33	33 42.59	52 45.44	185	23:05	33 39.42	51 00.79	180
B112	Z	185	23:05	33 39.42	51 00.79	186	00:07	33 24.57	51 00.12	90
	M	186	00:07	33 24.57	51 00.12	186	13:01	33 24.35	52 43.52	360
B113	Z	186	13:01	33 24.35	52 43.52	186	14:05	33 07.57	52 43.06	90
	M	186	14:05	33 07.57	52 43.06	187	02:05	33 07.32	50 59.92	180
B114	Z	187	02:05	33 07.32	50 59.92	187	03:03	32 52.48	51 00.08	90
	M	187	03:03	32 52.48	51 00.08	187	14:31	32 48.62	52 41.76	360
B115	Z	187	14:31	32 48.62	52 41.76	187	15:25	32 34.45	52 40.76	90
	M	187	15:25	32 34.45	52 40.76	188	03:05	32.34.11	51 00.04	180
B116	Z	188	03:05	32 34.11	51 00.04	188	04:00	32 20.05	50 59.80	90
	M	188	04:00	32 20.05	50 59.80	188	15:27	32 19.96	52 42.89	360
B117	Z	188	15:27	32 19.96	52 42.89	188	16:23	32 04.41	52 42.75	90
	M	188	16:23	32 04.41	52 42.75	189	03:49	32 02.83	51 00.03	180
B118	Z	189	03:49	32 02.83	51 00.03	189	04:49	31 47.94	50 59.95	90
	M	189	04:49	31 47.94	50 59.95	189	16:07	31 47.10	52 43.21	360
B119	Z	189	16:07	31 47.10	52 43.21	189	17:09	31 31.81	52 42.79	90
	M	189	17:09	31 31.81	52 42.79	190	04:55	31 30.29	50 59.25	180
B120		190	11:45	31 49.93	51 28.22	190	12:51	32 00.12	51 20.95	220
						191	06:29	32 00.02	48 35.85	180
						193	00:21	27 36.96	42 47.41	150
						194	03:51	26 07.58	38 36.14	165
B121		197	12:06	24 56.86	37 53.36	200	11:16	16 59.71	47 00.41	35
						201	16:40	10 41.52	48 15.60	70

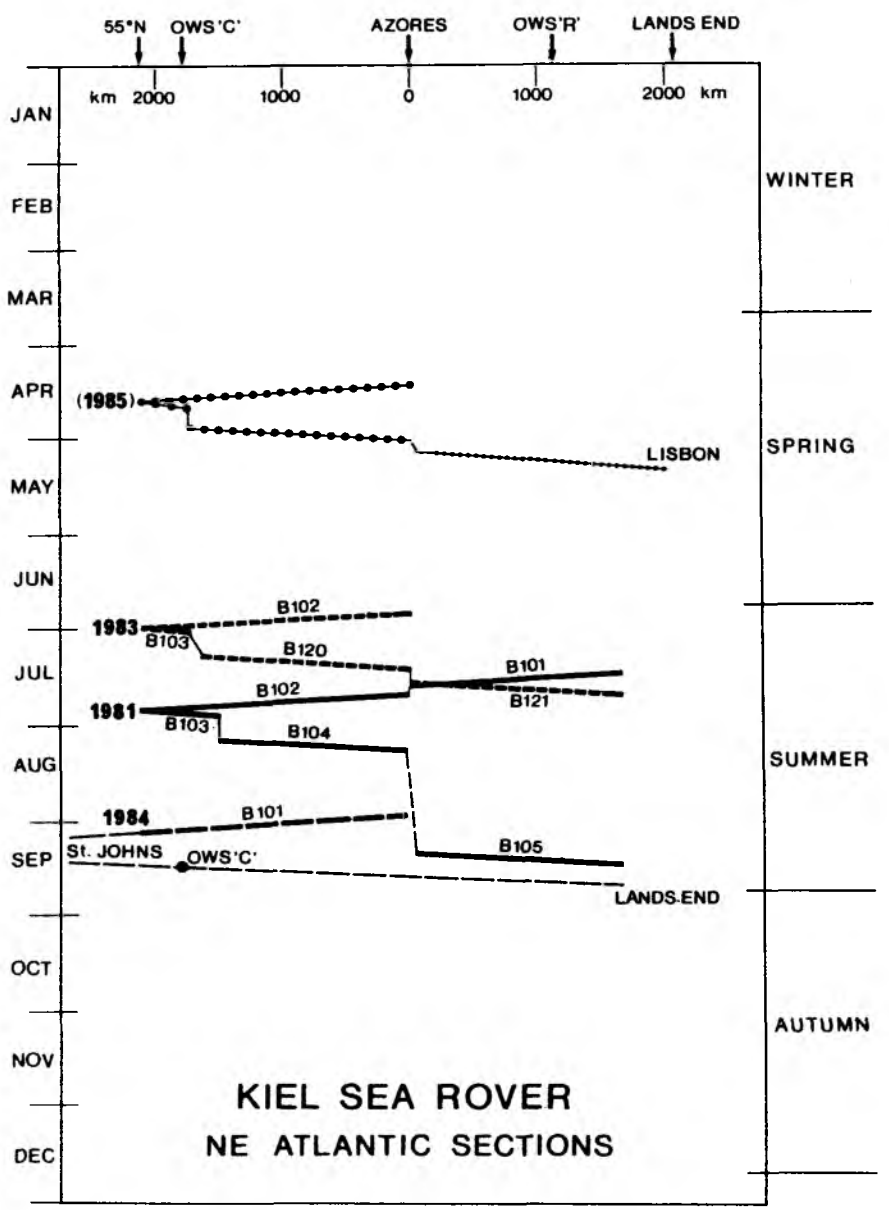

Fig. 3.3: Space-Time diagram of the SEA ROVER Long Sections showing the 1983 expedition in relation to the other expeditions.

Section B102 was subsequently repeated at essentially the same time of year in 1986 (see Figure 3.3).

3.2 The Polar Front Survey

The area for the survey was determined during the section B102 northbound from the Azores. To avoid the difficulties experienced with analysing the 1981 data a very regular survey pattern was used so that areas of very different data density would not arise.

The area chosen lay between 51° N and 52°45' N and between 35° W and 31° W. First, two east-west sweeps were made to determine the position of the meander structure and then a series of north-south legs with a spacing of 10 nmi (Fig. 3.4). This spacing was chosen as the roughly hourly-spaced satellite fixes would also give an average resolution of about 10 nmi for the absolute current measurements along the ship's track. The area surveyed in the available 9 days, 30th June – 9th July, was thus 275 km east-west by 200 km north-south.

Immediately following the survey on 9th July a section of 3 CTD dips to 1000 m depth was made straddling the main front in the SE of the survey area. Details are given in Table 3.3.

The bottom topography (Fig. 3.5) shows that the SW of the survey area lay over flat bottom and the NE of the survey area overlapped onto part of the Mid-Atlantic Ridge SE of the Gibbs Fracture Zone.

Table 3.3: List of CTD stations during NOA'83

Station number	Longitude (W)	Latitude (N)	Start and End Day/Time (GMT)
1	31°30.00'	51°00.00'	190/0508 - 190/0600
2	31°39.00'	51°14.00'	190/0739 - 190/0837
3	31°47.88'	51°27.63'	190/1010 - 190/1109

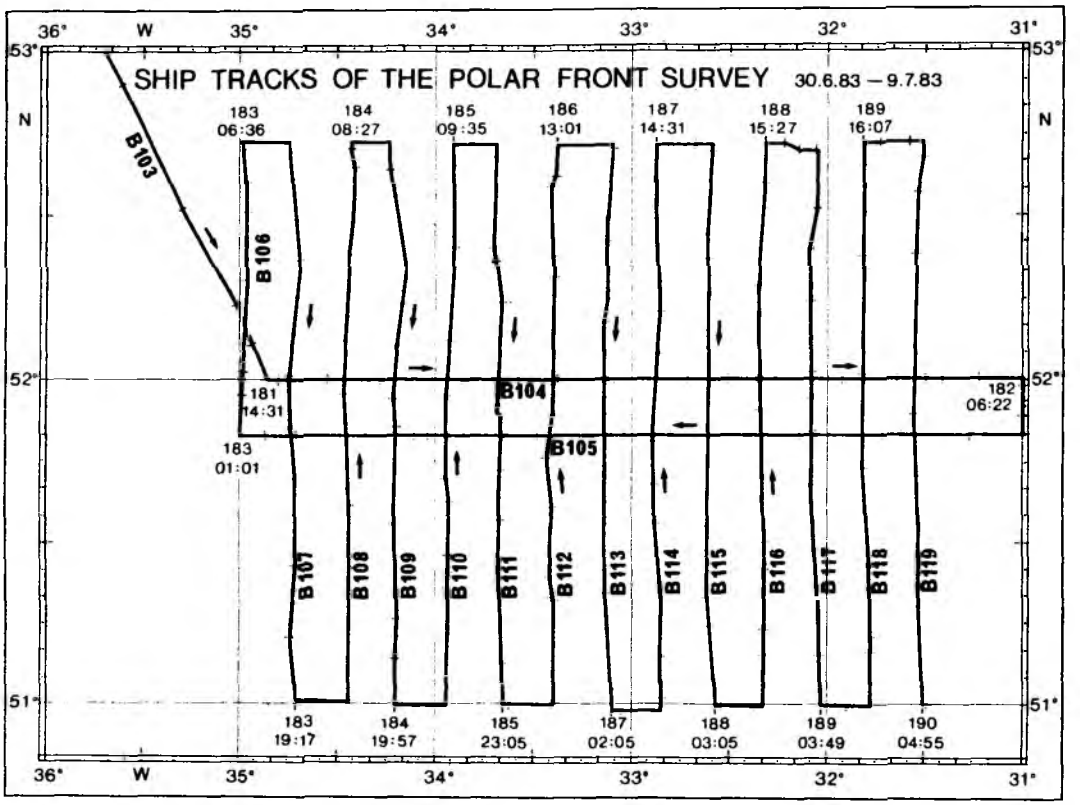

Fig. 3.4: Ship's track during the Polar Front survey, giving the days (181 = 30th June, 190 = 9th July) and times at significant points.

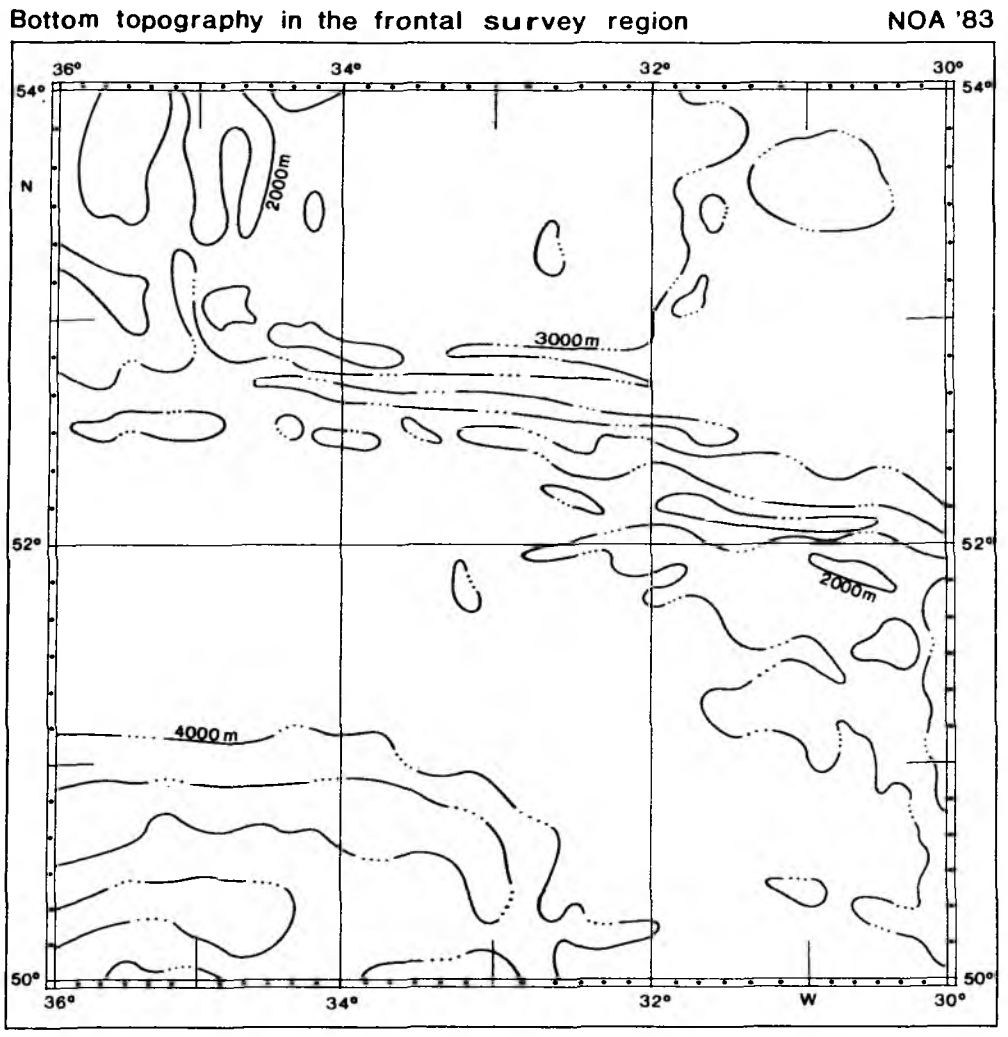

Fig. 3.5: Bottom topography in the area of the Polar Front survey.

4. PROCESSING AND REDUCTION OF HYDROGRAPHIC AND OPTICAL DATA

The data processing followed the sequence illustrated in the flow diagram (Fig. 4.1).

4.1 Raw data recording: CTD-data and optical data

The CTD and radiation data were stored in a digitized form (16-bit words) on magnetic tapes in a format given in Table 3.1. The vertical resolution was 6 cm for the CTD- and 12 cm for the radiation data. Each file contains 4 hours of raw data.

4.2 Navigation data recording and correction

On the navigation computer a permanent random access file was arranged with 720 records, one for each 2-minute interval of the day. This file was updated every two minutes with the current navigation data (see also section 2.3). Absolute and relative navigation data stored in this file were transferred twice a day to magnetic tape for archiving and further processing. Before merging the navigation data with the CTD data, a correction for errors in the data (e.g. bad satellite fixes, transmission errors) was applied according to Horch (1984).

4.3 First processing - Editing the raw data

Before the raw data were converted into physical units a time constant correction was applied to the temperature data. Empirical tests (Bauer et al., 1985) have shown, that a time constant, $\tau = 85$ ms, was appropriate to minimize the mismatch between the response of the thermometers and the conductivity cells. Then the raw values of the CTD data were converted into physical units using the calibration coefficients in Table 4.1.

Salinities were calculated using the PSS-78 (Lewis and Perkin, 1978) algorithm and afterwards filtered with a median-filter (Sy, 1985) with a 5-cycle window to remove any residual spikes. The data were than averaged over 5 cycles and density was calculated from the reduced data set, which has a vertical resolution of about 30 cm.

DATA PROCESSING FLOW DIAGRAM

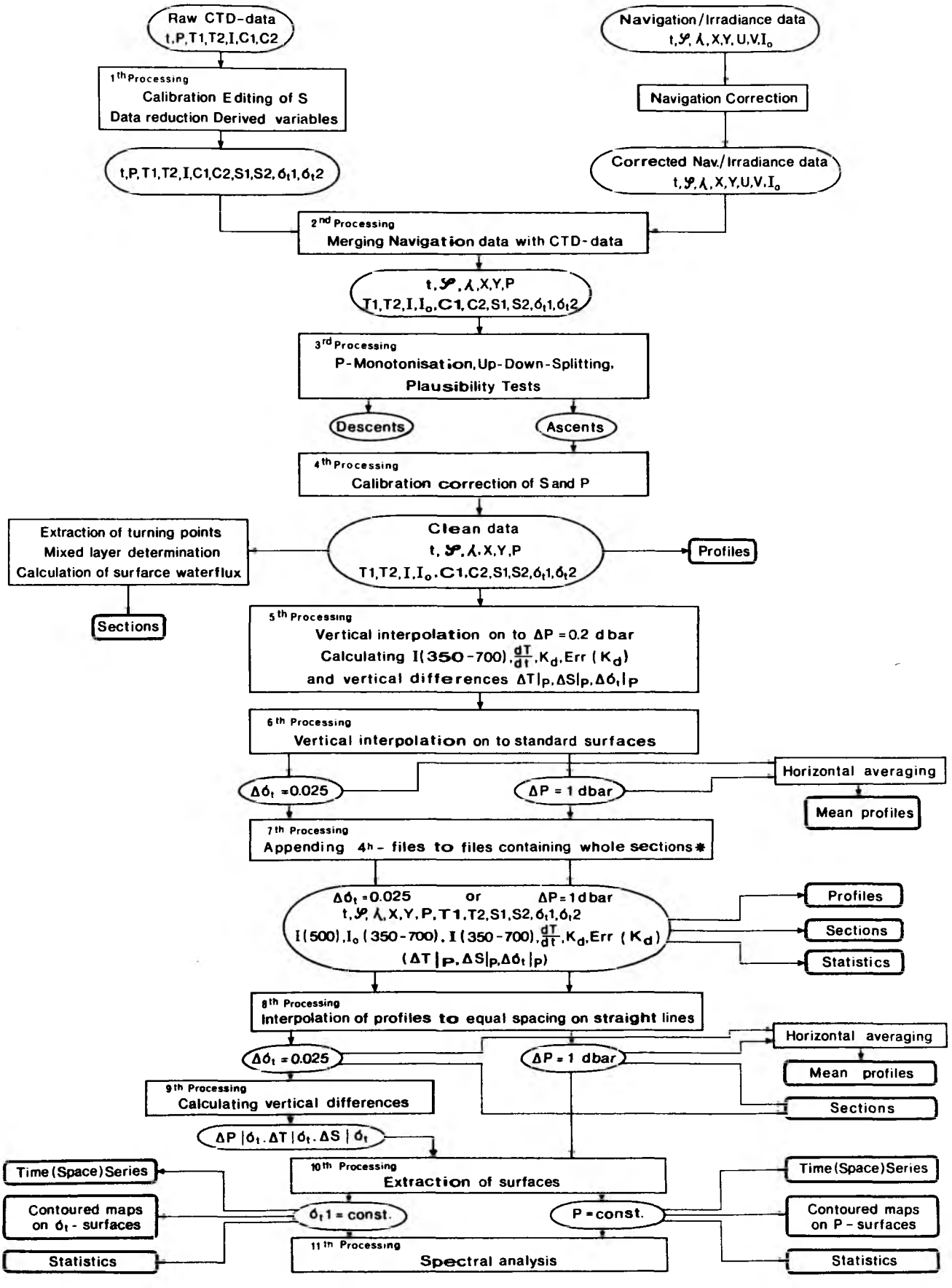

Fig. 4.1: Flow diagram of the processing of the hydrographic data from NOA'83

Table 4.1:

1. Coefficients for calibration of sensor MS38 and MS39

$$y = a_0 + a_1 x + a_2 x^2$$

x: raw data value y: calibrated variable

MS38	a_0	a_1	a_2
P	$-.3054922 \times 10^3$	$.3798940 \times 10^{-1}$	$-.6430963 \times 10^{-7}$
T Sensor 1	$-.2444710 \times 10^2$	$.2428303 \times 10^{-2}$	$.8774922 \times 10^{-10}$
T " 2	$-.2482918 \times 10^2$	$.2421992 \times 10^{-2}$	$.2031399 \times 10^{-9}$
C " 1	$-.2644104 \times 10^2$	$.3399403 \times 10^{-2}$	$.3781363 \times 10^{-8}$
C " 2	$-.2702130 \times 10^2$	$.3460328 \times 10^{-2}$	$.2303073 \times 10^{-8}$
RA	0.0	1.0	0.0

MS39	a_0	a_1	a_2
P	$-.3326914 \times 10^3$	$.4045241 \times 10^{-1}$	$-.1451173 \times 10^{-6}$
T Sensor 1	$-.2532271 \times 10^2$	$.2438172 \times 10^{-2}$	$-.1819694 \times 10^{-9}$
T " 2	$.1689166 \times 10^2$	$-.1100183 \times 10^{-2}$	$.2502351 \times 10^{-1}$
C " 1	$-.2736481 \times 10^2$	$.3452988 \times 10^{-2}$	$.2507046 \times 10^{-8}$
C " 2	$-.2553159 \times 10^2$	$.3249933 \times 10^{-2}$	$.3663812 \times 10^{-8}$
RA	0.0	1.0	0.0

2. Coefficients for calibration of sensor MSØ2

$$y = a_0 + a_1 x + a_2 x^2$$

$$x = \tan\left(0.5\pi(1-N/32768)\right)$$

N: raw number y: calibrated variable

MSØ2	a_0	a_1	a_2
P	$.2952524 \times 10^4$	$-.1902166 \times 10^4$	$-.1696181 \times 10^1$
T	$.1608203 \times 10^2$	$-.1152992 \times 10^2$	0
C	$.2050144 \times 10^{-1}$	$.1132899 \times 10^{-1}$	0

3. Coefficients for calibration correction of salinity

$$S_c = a_0 + a_1 S$$

S: CTD-salinity S_c: corrected salinity

	a_0	a_1
S Sensor 1	.650518656	.980137944
S Sensor 2	.728637278	.974995434

4. Pressure calibration correction

$P_c = P + a_0$

P_c: corrected pressure value

P : CTD-Pressure

a_0: 0.6×10^4 Pa

4.4 Second processing - Merging fish and navigation data

In this stage the data from the towed fish and the corrected navigation data were combined using the time information in both data. The interval between successive data cycles was then 0.3125 sec and the time was explicitly stored in each cycle. Additionally the short-wave radiation from the ship's radiometer was included in the data cycle.

4.5 Third processing - Pressure monotonization and up/down-splitting

Systematic differences in the pitch and roll angles during the descending and ascending parts of the fish track made it necessary to separate the data into descents and ascents (Leach et al., 1985; Bauer et al., 1985) Data cycles which were not monotonous in pressure were eliminated within this stage and after substituting obviously incorrect data by preceeding values, the clean profiles were stored in separate files.

4.6 Fourth processing - Salinity and pressure correction

To improve the absolute accuracy of the CTD-salinities water samples (taken every 4 hours) were analysed with a Guildline Salinometer and then used for the final calibration of the CTD-salinities. Within the same routine a temperature dependent pressure correction, which was determined during NOA'81 (Bauer et al., 1985) was also applied.

4.7 Fifth processing - Interpolation to depth levels for attenuation

In order to determine the attenuation from the vertical radiation gradients, the data were interpolated to depth levels 0.2 m apart. This interval was chosen to maintain the initial vertical resolution. From these data the attenuation K_d, the error in K_d, the total short-wave radiation I (350 - 700 nm) and the resulting heating rate $\frac{dT}{dt}$ were derived. The attenuation $K_d(z)$ at 500 nm is defined as

$$K_d(z) = \frac{d}{dz} \left(\ln E_d(z) \right) \qquad (4.1)$$

and the vertical gradient of the logarithmic radiation profile $E_d(z)$ was

obtained by a linear regression over a 5 m depth interval (26 data points). K_d represents the mean attenuation over the corresponding depth interval (Horch, 1987). Due to the smoother appearance of the ascending fish track only these profiles were used for the further processing stages. In order to calculate heating rates, the radiation values at 500 nm had to be converted into total short-wave radiation between 350 and 700 nm. This required four processing stages:

Firstly, a calibration of the temperature dependent offset of the raw radiation data was carried out (Horch, 1987), see also section 2.2.

Secondly, the raw values E_d (500,z) were converted into fractional parts of the surface value E_d (500,0), where E_d (500,0) was obtained from the meteorological system of FS "Poseidon" according to

$$E_d\ (500,0)\ [V] = a + b\ I_o\ [W/m^2] \qquad (4.2)$$

with I_o = global radiation from "Poseidon" sensor, a = 0.02783, b = 0.005524, obtained by a linear regression.

Thirdly, the transformation of the monochromatic radiation into the total short-wave radiation was carried out by using the empirical formula from Morel and Højerslev (1979):

$$E_d\ (350\text{–}600,z)\ \% = A(z) \cdot [E_d\ (500,z)\ \%]^{B(z)} \qquad (4.3)$$

with A(z), B(z) depth dependent parameters listed in Horch (1987).

Fourthly, the fractional parts E_d (350–700,z) % were then converted into W/m^2 by using formula (4.2). The heating rate was then calculated from the vertical radiation gradient by linear regression

$$\frac{dT}{dt} = \frac{1}{\rho c_w} \frac{d}{dz} E_d\ (350\text{–}700,z)$$

with ρ the density and c_w the specific heat of water.

4.8 Sixth processing - Interpolation to depth and σ_t-levels

In this processing stage the data were interpolated to standard depth and density intervals 1.0 m and 0.025 kg m^{-3} apart. The end products were stored in separate files for depth and density orientated data.

4.9 Seventh processing - Combining 4-hour files to section files

In this stage the files containing 4 hours of data were combined to longer files for the sections listed in Table 3.2.

4.10 Eighth processing - Interpolation to constant horizontal spacing

To compare nominally parallel sections and data from previous experiments it was necessary to interpolate the originally irregular spaced data to constant horizontal spacing. For the front experiment the sections were projected onto straight lines combining the end position of the sections with an horizontal spacing of 800 m, which was close to the original profile separation. The southern boundary was 51° N and the reference latitude was 52° N, the distance between the legs was 10 nmi. The long sections were projected onto loxodromes, defined by the positions listed in Table 4.2.

Table 4.2: Points defining loxodromes onto which Long Section data are projected

Section: Azores - OWS 'C' - 55° N		
37°50.00' N 26°00.00' W	—	52°45.00' N 35°30.00' W
Section: Azores - OWS 'R'		
37°40,00' N 24°40.00' W		47°00.00' N 17°00.00' W
Section: OWS 'R' - Land's End		
47°00.00' N 17°00.00' W		48°40.00' N 10°00.00' W

4.11 Ninth processing - Calculation of thickness

The spacing between isopycnals (thickness), which is one component of isopycnic potential vorticity, was calculated for density intervals of $\Delta\sigma_t$ = 0.1 kg m^{-3} and stored within the data cycle centred on the σ_t-interval together with the salinity difference over the same interval. Within the same routine the distance of the isopycnals relative to a chosen density surface (σ_t = 26.5 kg m^{-3}) was determined.

4.12 Tenth processing -Reorganisation of data from profiles to surfaces

In order to obtain horizontal (isopycnic) maps of the various parameters the profile orientated data were reorganized into files containing all data on distinct surfaces of constant depth or density. This processing stage was the basis for investigating the horizontal structures of the Polar Front survey.

4.13 Objective analysis

Horizontal maps of the frontal survey were obtained by objectively interpolating the data onto a 15 km x 15 km grid, which was also used for mapping the velocity data. The objective analysis method used here was the same as for the experiment NOA'81 (Bauer et al., 1985). Briefly, the method works as follows (for detailed information see Fiekas, 1987). Firstly, the two-dimensional auto-correlation function (acf) of a scalar field was calculated and smoothed. Then the raw acf was multiplied by a conical taper to assure the weighting function was zero after 8 grid points. Negative values were also set to zero. The resulting weighting function was then used in a successive-correction objective analysis scheme.

4.14 Deep CTD dips

Three deep CTD profiles (0 - 1000 m) were recorded at the Polar Front. Processing of these data followed the scheme described in Sy (1985) and Fiekas (1987). The raw data (CTD) were sampled at a rate of 16 cycles per second and a vertical resolution of about 6 cm (lowering rate 1 m/s). Initially stored in analogue form the data were later converted into digital 16-bit words stored on magnetic tape.

After a temperature time-constant correction (τ = 85 ms) the raw data were transformed into physical units using a laboratory calibration. Then salinity was derived and spikes were removed by using a 9-point median filter. Averaging over 9 data points completed this processing stage.

A plausibility test was then used to eliminate any residual inconsistencies in pressure, temperature and salinity, where maximum allowable differences between successive data points were 1.0 dbar, 0.1 K and 0.1 for salinity.

Finally a 15 data point median filter was applied to salinity and afterwards a 3-point median was used to smooth both the temperature and salinity. From these data σ_t was derived and the profiles were then monotonized with respect to σ_t and interpolated to standard depths (10 m apart).

5. PROCESSING AND REDUCTION OF CURRENT DATA

The acoustic Doppler current profiler (ADCP) was first added to the Sea-Rover system in 1983 and the various stages of processing of the data will therefore be discussed here in detail. A flow diagram of the data processing is shown in Figure 5.1.

5.1 Raw data acquisition

As described in section 2.3, the raw ADCP data, Doppler frequencies, were transferred to the HP1000 navigation computer and the raw values in semi-decoded form (0.5 Hz with 871 Hz offset) were written on tape along with information about the navigation and roll and pitch of the ship. The form of the data cycle is shown in Table 5.1. Due to the necessity of buffering the raw data (548 bytes at 9600 bit s^{-1} every second) on arrival at the HP1000, thus making synchronization difficult, and due to the other activities of the HP1000 it was only possible to write every second or third raw data cycle to tape.

5.2 First processing: Calculation of the relative ship's velocities

For this processing stage the separately measured Doppler frequencies for each of the three beams and each bin in each beam were available. Using the speed of sound these frequencies were converted to relative ship velocities for each depth level using the corresponding bins from each beam and taking the temperature dependance of sound speed into account. Firstly the ship's velocity components, v_f (forward component), v_p (port component) and v_z (vertical component) were calculated. Then the horizontal velocity components were transformed into velocities east (u_r) and north (v_r) using the ship's heading H,

$$\underset{\sim}{v}_r = \begin{pmatrix} u_r \\ v_r \end{pmatrix} = \begin{pmatrix} \sin H & -\cos H \\ \cos H & \sin H \end{pmatrix} \begin{pmatrix} v_f \\ v_p \end{pmatrix} .$$

The mean velocity profiles along with the mean and standard deviation of roll, pitch and heading, averaged over two minutes were stored in so-called day-files of 720 records, one for each 2-minute period of the day. A second day-file contains standard deviation profiles of horizontal velocities u_r,

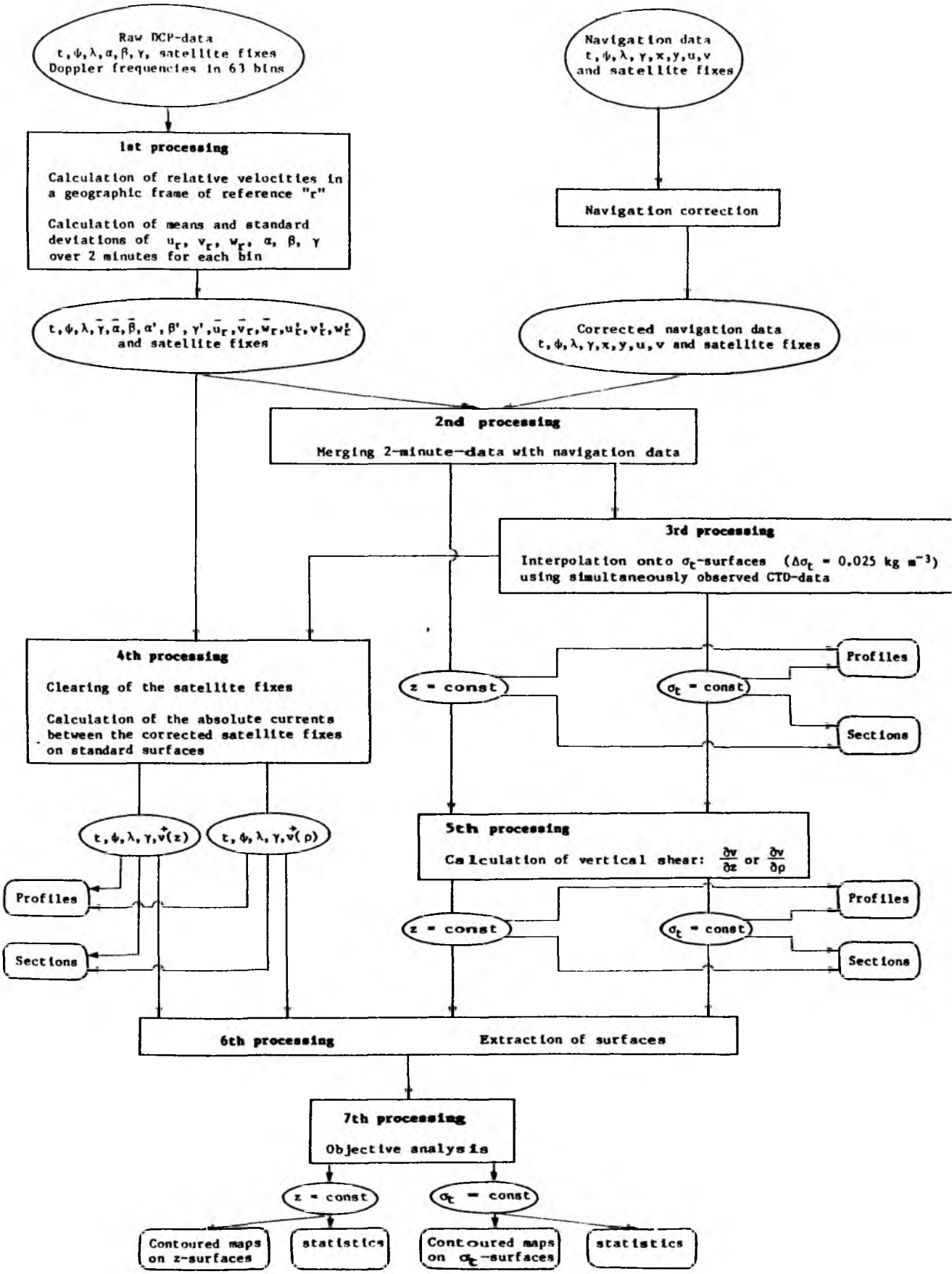

Fig. 5.1: Flow diagram of the processing of the acoustic Doppler current profiler data from NOA'83.

Table 5.1: Raw DCP data cycle format

Integer Word	Content	Units
1	Code	number
2	Time	centiseconds
3	Time	seconds
4	Time	minutes
5	Time	hours
6	Date	day of year
7	Date	year
8	Heading (direct)	0.1 deg
9	Longitude Decca	deg
10	Longitude Decca	0.1 millideg
11	Latitude Decca	deg
12	Latitude Decca	0.1 millideg
13	Longitude Satnav1	deg
14	Longitude Satnav1	0.1 millideg
15	Latitude Satnav1	deg
16	Latitude Satnav1	0.1 millideg
17	Roll	0.1 deg
18	Pitch	0.1 deg
19	Water-depth(Echo-sounder)	metre
20	Standard deviation (roll)	0.1 deg
21	Standard deviation (pitch)	0.1 deg
22	Standard deviation (heading)	0.1 deg
23	Satfix day of year	
24	Satfix time	minutes + 60xhours
25	Satfix time + quality	seconds + 100xquality
26	Satfix Longitude	deg
27	Satfix Longitude	0.1 millideg
28	Satfix Latitude	deg
29	Satfix Latitude	0.1 millideg
30	Heading (via DCP)	0.1 deg
31	Profile transmit pulse width	code 8-14
32	Profile range bin size	code 17-21
33	Operating mode	code 24-28
34	Blanking period	code 32-39
35	GPS time	hours
36	GPS time	minutes
37	GPS time	seconds
38	GPS velocity East	milliknots
39	Profile delay	code 73-79
40	GPS velocity North	milliknots
41	Profile cycle time	code 88-90
42	EM-Log voltage S1 (thwartship)	mV
43	EM-Log voltage S2 (longship)	mV
44		
45	Resets	code 121-122
46	Track count	code 128-139
47	GPS number of satellites NS	
48	Profile detection threshold	code 144-151
49	GPS quality indicator QI	0, 2 or 3
50	GPS Longitude	10**-8 deg
51	GPS Longitude	deg
52	GPS Longitude	10**-4 deg
53	GPS Latitude	10**-8 deg
54	GPS Latitude	deg
55	GPS Latitude	10**-4 deg
56	Ping-to-ping tracking gain loop	code 208-215
57	Intra-ping loop gain	code 216-223
58	Data select	code 248-249
59	Water temperature	Celsius
60	Water depth (DCP)	metre
61	N1 % good Beam 1	
62	N2 % good Beam 2	
63	N3 % good Beam 3	
64	NP number of pings averaged	
65-128	Datawords with frequencies Beam 1	bin 0-63
129-192	Datawords with frequencise Beam 2	bin 0-63
193-256	Datawords with frequencies Beam 3	bin 0-63

Although represents the status of early 1987 the changes since 1983 have been essentially additions to the format.

v_r and of percentage of signal returns above the 4dB signal to noise threshold in all three beams. Using this averaging procedure the data volume was reduced by a factor of 48.

5.3 Second processing: Merging the DCP-data with the corrected navigation data

The navigation data from the HP1000 were collected in 2-minute dayfiles and corrected as described in section 4.2; the ship's drift as measured by the EM-log was distributed uniformly between the satellite-fixes so that continuous estimates of absolute positions were available every 2 minutes without discontinuities following the fix-update.

In the second processing stage the corrected absolute positions from the navigation dayfiles were used to replace the positions from dead-reckoning in the DCP dayfiles.

5.4 Fourth processing: Calculation of absolute currents

The planned third processing stage, the interpolation of the relative velocities onto standard σ_t-surfaces, was not carried out because the various errors in the DCP-data were generally bin-oriented and in order to exclude bad layers particularly at the top of the profiles it was felt to be better to maintain the depth-oriented structure of the data and if need be combine these with depth-oriented data from the fish.

As a preparation for the fourth processing the satellite fixes were checked for their quality and some removed so that no interval of less than 25 minutes between fixes was used for the calculation of the absolute currents. The method of calculating the absolute currents used was as follows.

1) To calculate the distance $\underset{\sim}{x}_{DCP}$ that the acoustic current profiler had moved relative to one of the 63 layers the relative ship velocity $\underset{\sim}{v}_r$ during the period $\tau = \sum \Delta t_i$ was integrated

$$\underset{\sim}{x}_{DCP} = \int_{t_1}^{t_2} \underset{\sim}{v}_{\tau}\,(t)dt = \sum \underset{\sim}{v}_{\tau_i}\,\Delta t_i$$

2) The distance $\underset{\sim}{x}$, the ship's drift between the dead-reckoning position $\underset{\sim}{x}_{DCP}$ and the absolute position of the second fix is then a measure of the mean current $\underset{\sim}{v}$ during the integration period τ.

$$\underset{\sim}{v} = \frac{\underset{\sim}{x}}{\tau} = \frac{1}{\tau}\left(\underset{\sim}{x}_{SAT} - \underset{\sim}{x}_{DCP}\right)$$

where $\underset{\sim}{x}_{SAT}$ is the distance between the two fix positions.

3) This procedure was repeated for each of the 63 layers thus giving a profile of the absolute current as a function of depth.

5.5 Fifth processing: Calculation of vertical shear

Whereas the calculation of absolute currents requires knowledge of the absolute motion of the ship the calculation of the shear can be made simply by vertically differentiating the data from the second processing stage, the relative ship velocities. This was carried out as the fifth processing stage.

5.6 Sixth and seventh processing: Extraction and objective analysis of surfaces

In these processing stages the absolute current data or the shear data from selected surfaces were sought then objectively analysed as discussed in Leach (1986) and Bauer et al. (1985). Details of the analysis of these data will be discussed below in chapter 7.

6. DATA - LONG SECTIONS

The data from the expedition will be illustrated with measured, and to a lesser extent, derived quantities. This and the following chapter are designed to document the nature of the data collected; scientific analysis of the results will be presented elsewhere (for example Fiekas (1987), Horch (1987)) and a comprehensive documentation of the data from the Long Sections is being prepared as a Compendium of Sea Rover Long Sections 1981-87 (Stammer et al., 1988) which will include the data from this expedition in a form enabling comparison with the results of the other expeditions in this series.

6.1 Section plots

In this section plots of various parameters as sections along the leg B102, Azores - OWS 'C' - 55° N, are shown.

The general nature of the hydrographic situation is well illustrated by the temperature of σ_t surfaces, 0.1 kg m^{-3} apart, shown in Figure 6.1. Between 38° N and 55° N the surface temperature (highest isopycnal) drops from 18 °C to 8 °C. Particularly apparent is the relatively uniform hydrography up to about 45° N followed by a series of 3 structures with scales of 200 - 300 km before the Polar Front itself at 52°30' N. The Subarctic Water also shows a relatively uniform character. The cold water centred at about 46°30' N seems to be associated with a cyclonic eddy judging by the acoustically measured current vectors along this section shown in Figure 6.2. The strong thermohaline features at about 48°30' N and 50°30' N seem to be associated with stronger currents. The Polar Front at 52°30' N manifests itself in strong eastward flow at this latitude.

Because the attenuation of solar irradiance can only be measured during the hours of daylight the long section of this parameter is not continuous (Fig. 6.3, where the attenuation together with the surface salinity is shown). However, the general increase of the attenuation and therefore of the turbidity of the water from south to north can be seen. Also apparent is the broad-scale maximum value in the region of the Polar Front (around km 1500), although on the northbound section B102 (Fig. 6.3a) there is a smaller-scale maximum at km 1100 for example. Also conspicuous in the section B102 is the sharp front in the attenuation at km 350 corresponding to a front in the salinity.

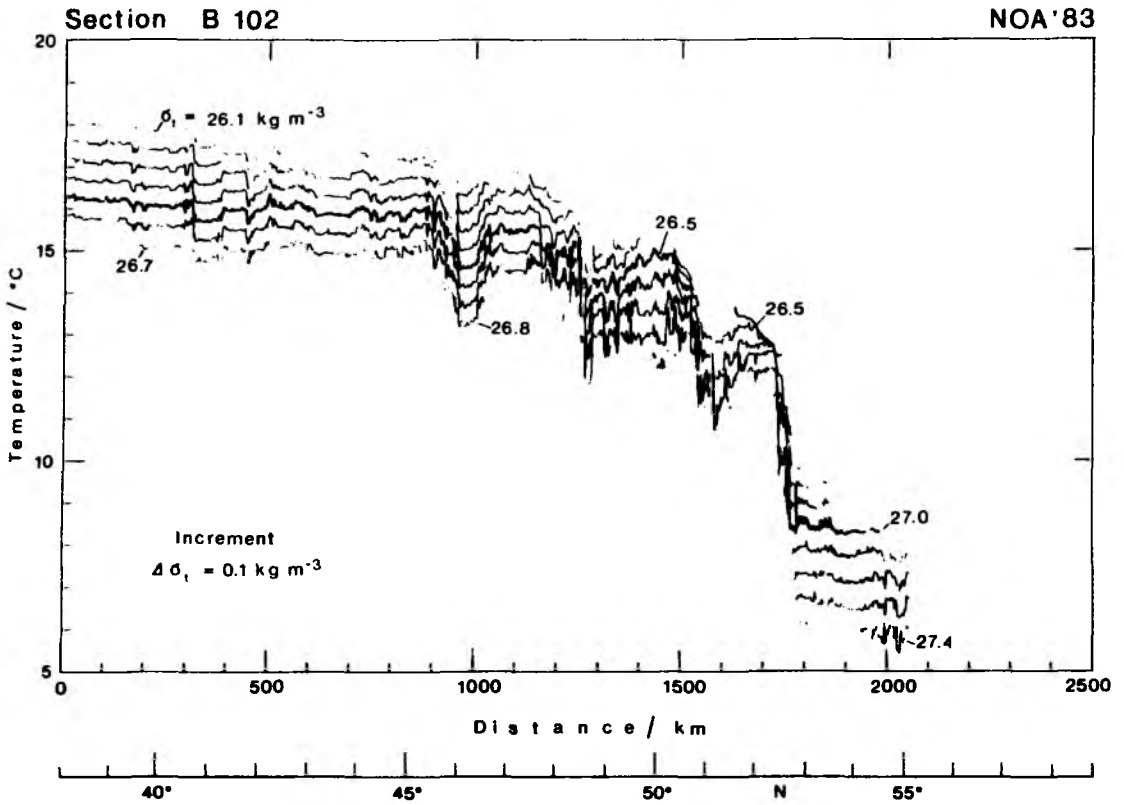

Fig. 6.1: The temperature on standard isopycnals along the section B102 from the Azores via OWS 'C' to 55° W.
The isopycnal increment is 0.1 kg m^{-3}.

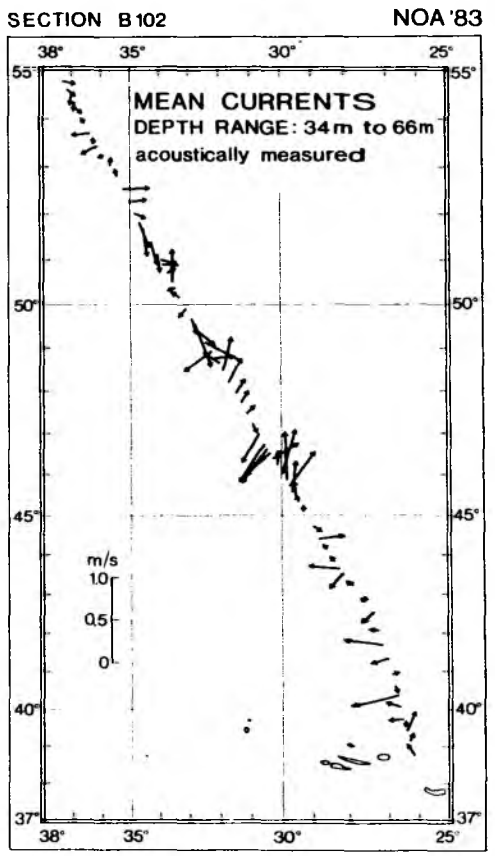

Fig. 6.2: Acoustically measured currents along the section B102 averaged over the depth range 34 - 66 m. Note the eddy at 46°30' N and the Polar Front jet at 52°30' N.

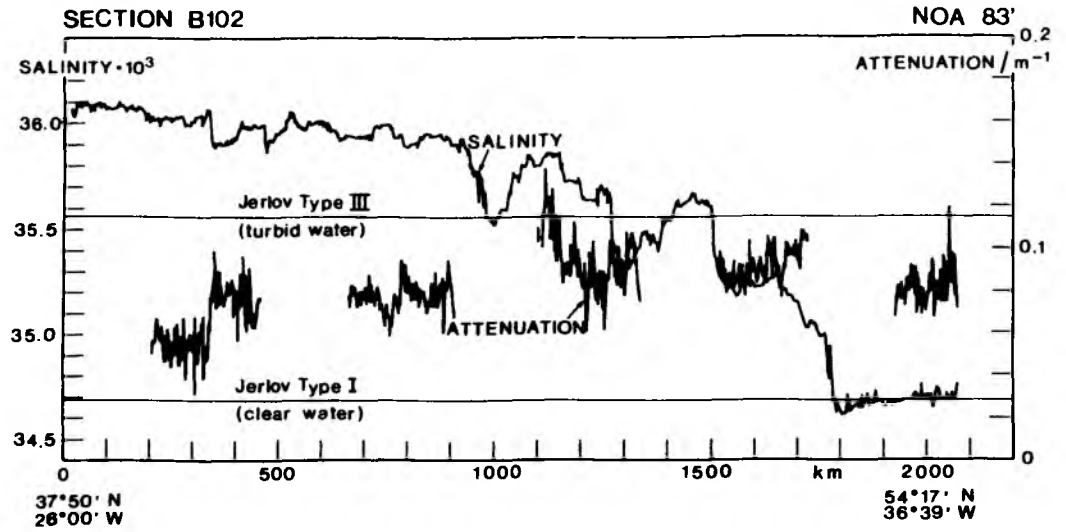

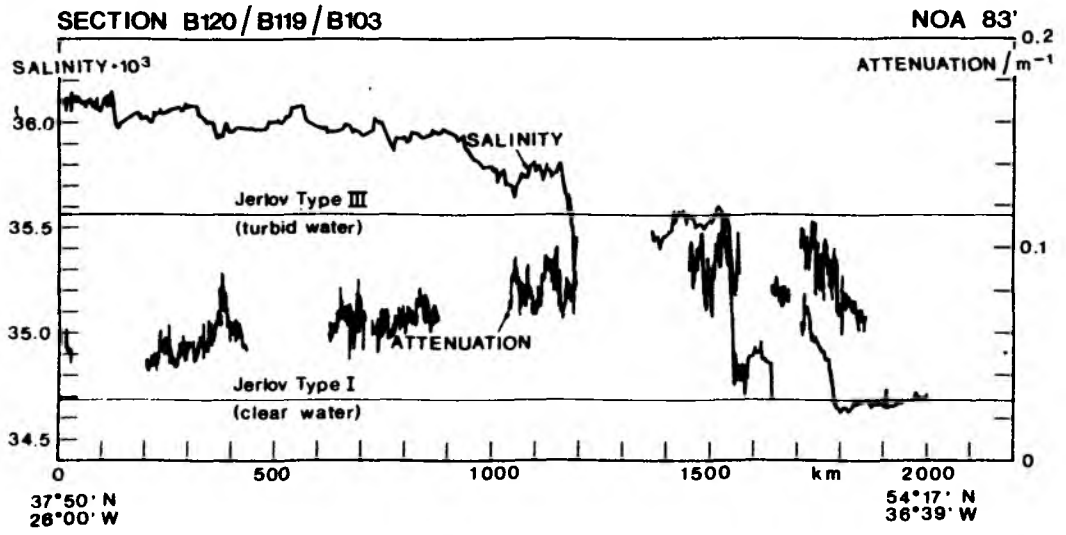

Fig. 6.3: Salinity at the upper turning point of the fish track (ca. 10 m depth) and the mean attenuation of the upper 40 m of the water column for a) section B102, b) sections B120, B119 and B103 combined.

6.2 One degree averages

For the sake of comparing the data from expedition to expedition and quantifying the variability the means and standard deviations for each degree of latitude of the temperature, salinity and density as a function of depth and the temperature and salinity as a function of density were calculated (Fig. 6.4). As in the section plots (Fig. 6.1) the hydrographically quiescent regions south of 45° N and north of 53° N contrast sharply with the region of increased variability between 45° N and 53° N.

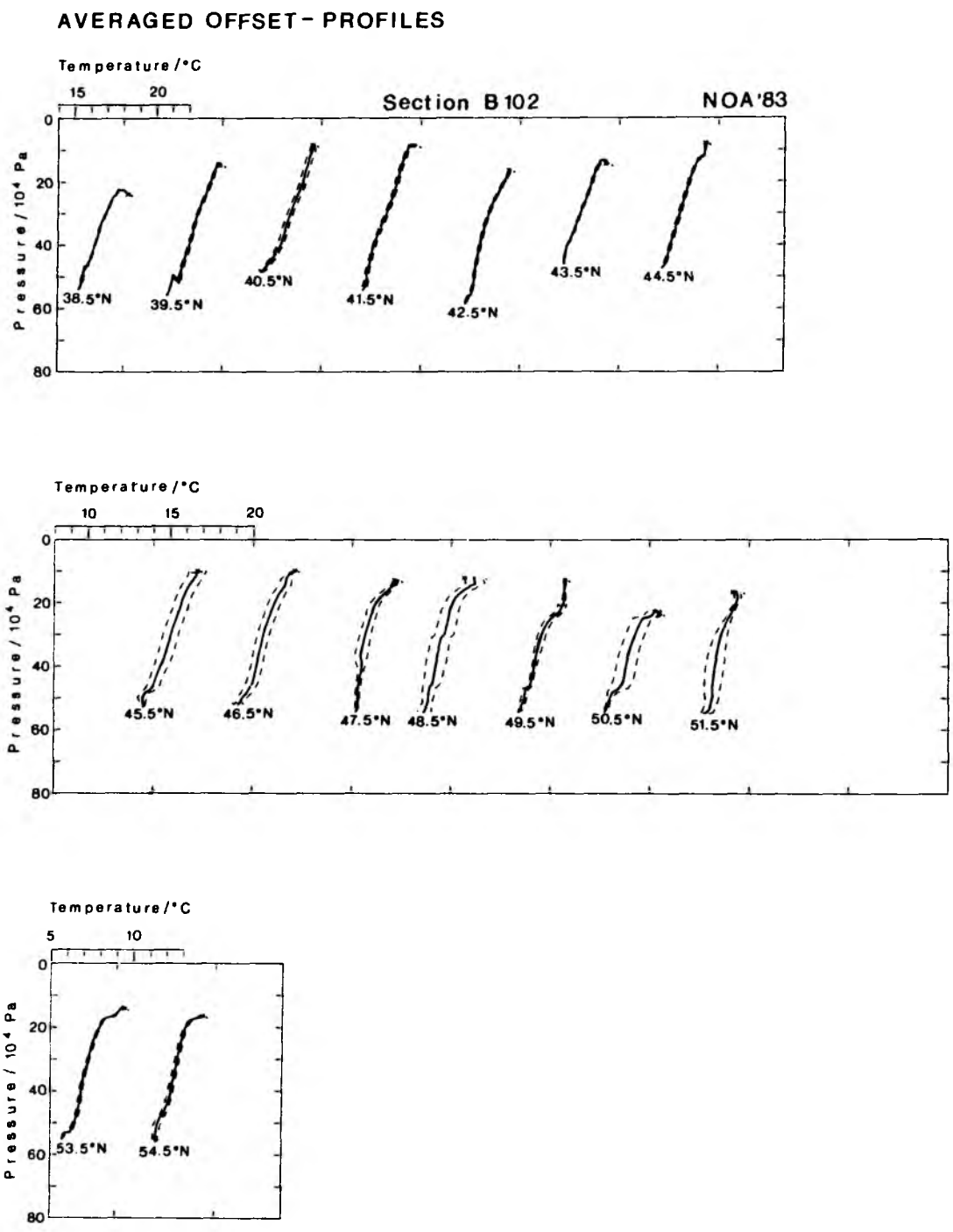

Fig. 6.4 a) Offset profiles showing means and standard deviations over each degree of latitude of temperature as a function of depth.

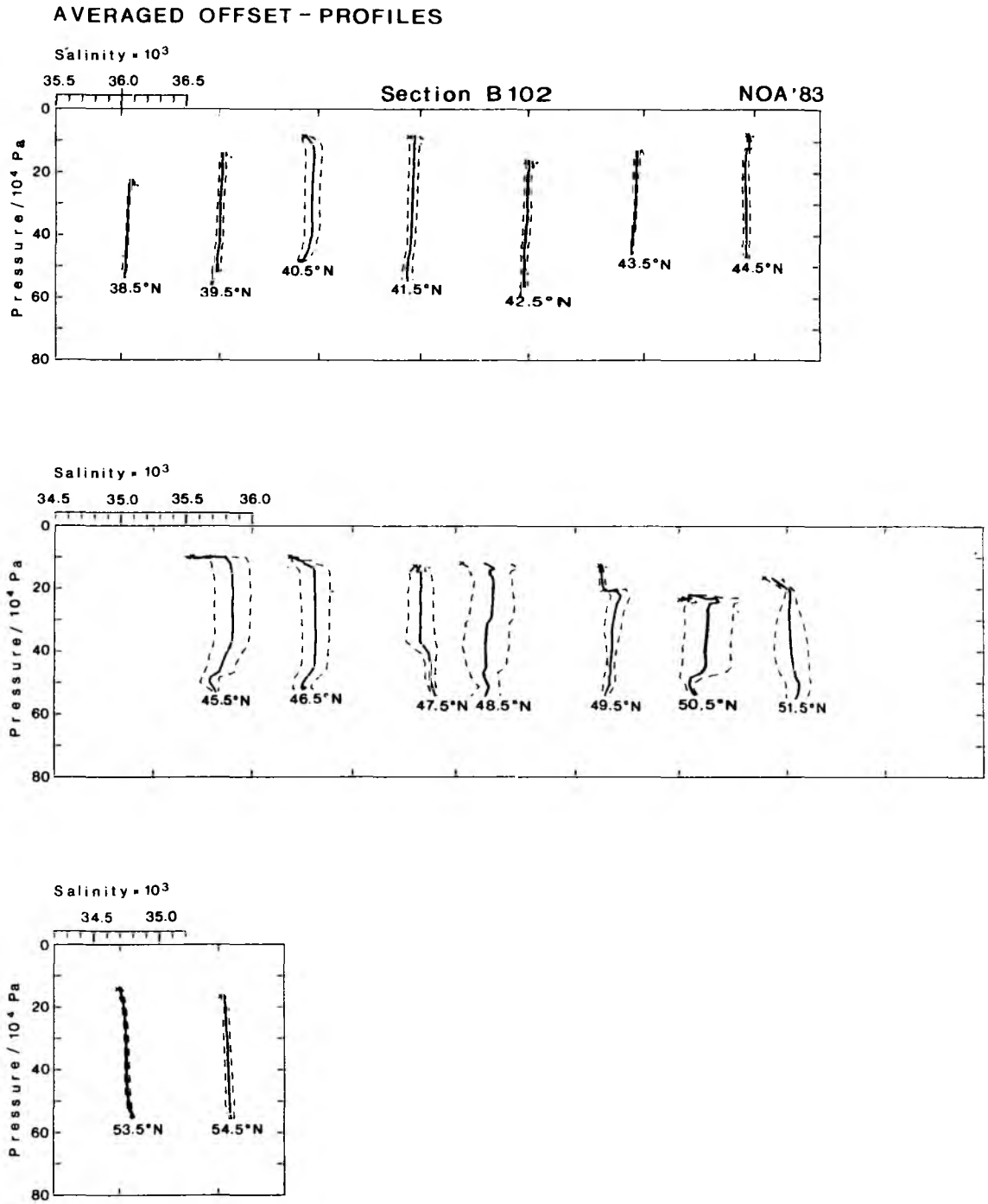

Fig. 6.4 b): Offset profiles showing means and standard deviations over each degree of latitude of salinity as a function of depth.

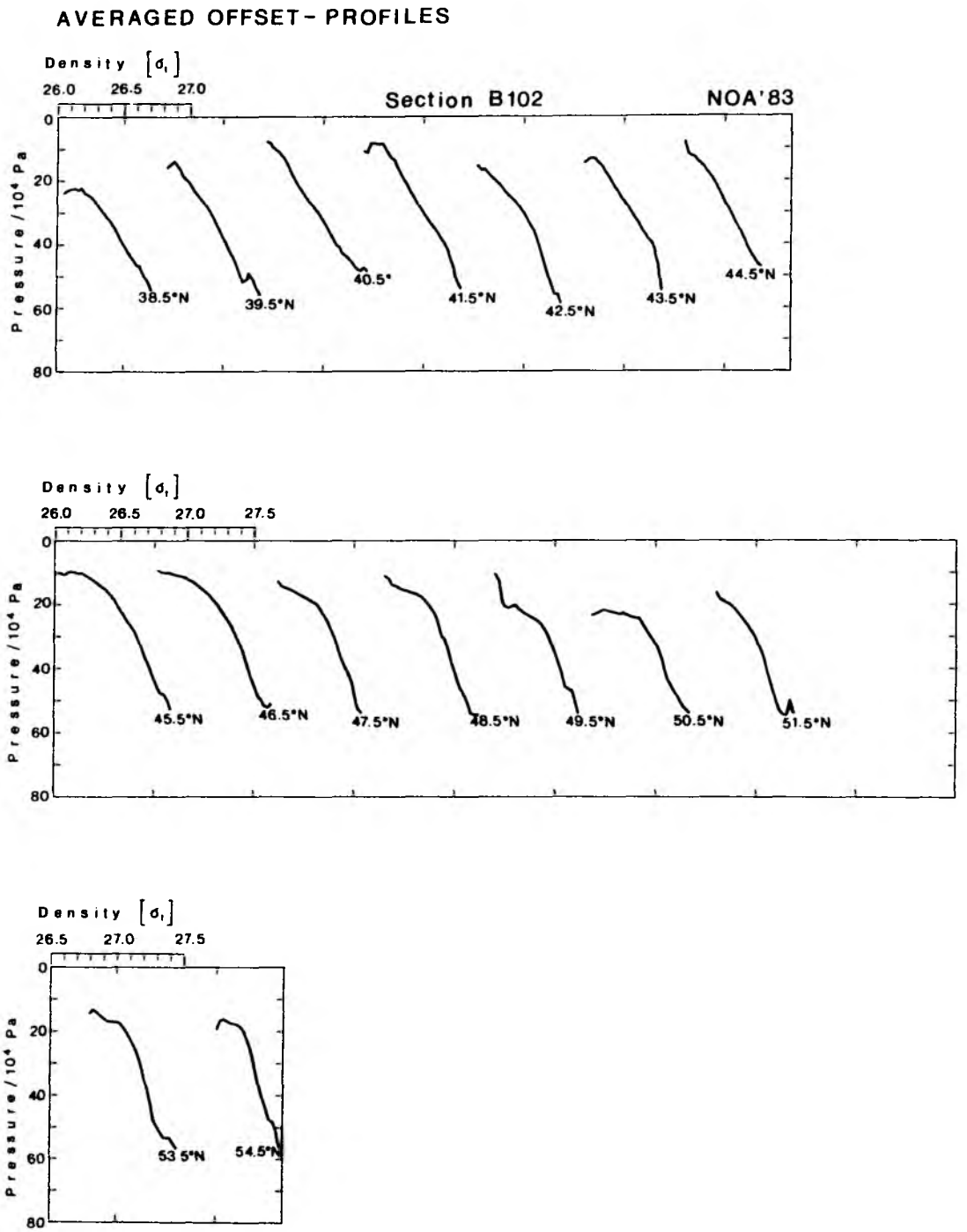

Fig. 6.4 c): Offset profiles showing means and standard deviations over each degree of latitude of density as a function of depth.

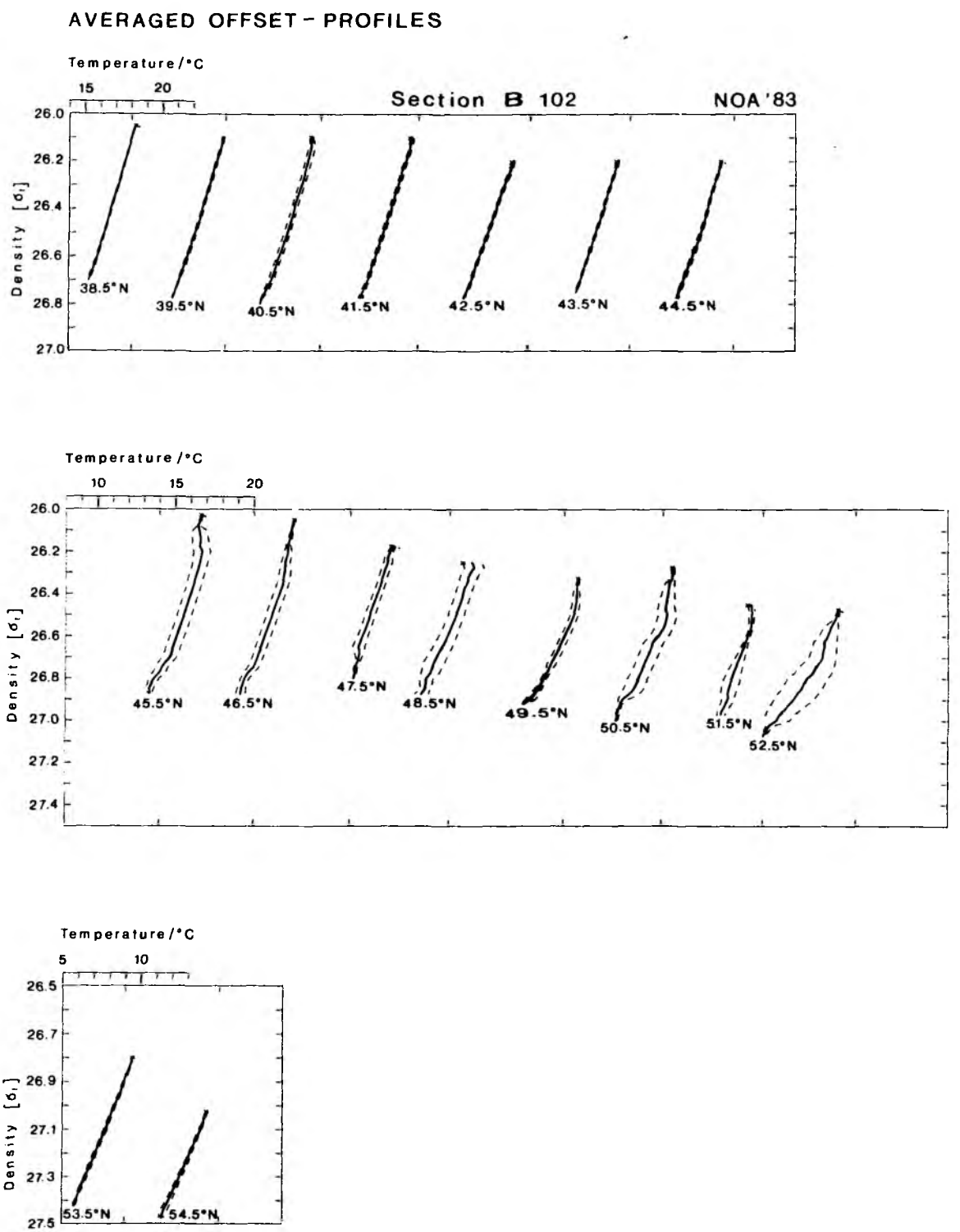

Fig. 6.4 d): Offset profiles showing means and standard deviations over each degree of latitude of temperature as a function of density.

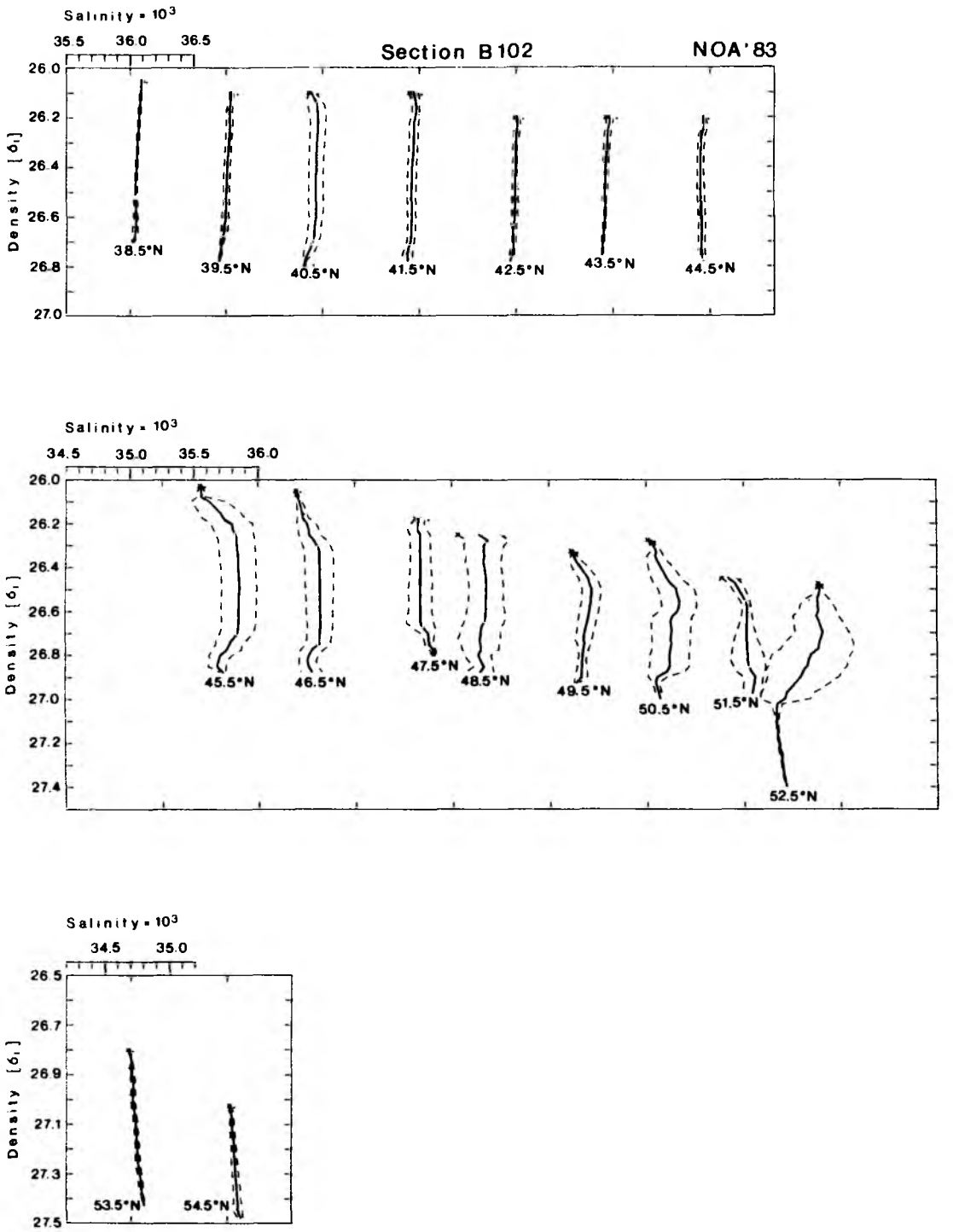

Fig. 6.4 e): Offset profiles showing means and standard deviations over each degree of latitude of salinity as a function of density.

7. DATA - FRONT SURVEY

In this chapter plots of the data from the Polar Front Survey are presented. The first section shows horizontal distributions in the form of maps, the second section shows the data along selected legs of the survey and the third section presents the data in statistical form.

7.1 Maps

In this section maps of the distribution of various parameters within the area of the Polar Front Survey are presented. The survey consisted of two east-west legs and then a series of north-south legs working from west to east (see Fig. 3.4). The general hydrographic situation is best typified by the distribution of temperature on the density surface σ_t = 26.85 kg m^{-3} (Fig. 7.1). In the NW of the area the front is seen with a strong gradient. From here it curves round to the SE and the isotherms fan out and the gradient thus weakens. In the SE of the area the front is seen again to be sharp. In the NE of the area an isolated warm water feature is apparent. Although its isotherms are not closed within our area, some other parameters (see below) show a tendency to closed isolines and satellite images (Viehoff, 1987) show that this feature is indeed a warm eddy. The depth of the isopycnal σ_t = 26.85 kg m^{-3} (Fig. 7.2) shows the same broad features as the thermohaline structure with a strongly baroclinic band in the NW of the area and in the SE corner. The structure near the warm eddy is less clear cut but shows a weak relative depth maximum here. The spacing between the isopycnals σ_t = 26.8 and 26.9 kg m^{-3} (Fig. 7.3) shows a large positive anomaly in the regions of warm water (see Fig. 7.1) in the W and SE of the area, the zero anomaly isoline corresponding very roughly to the 11 °C isotherm. The area of below average thickness anomaly corresponds to the cold water in general. The warm eddy in the NE of the area is typified by a weak but identifiable local maximum in the spacing anomaly.

As discussed in Chapter 3 above, the leg spacing for the survey was chosen to be 10 nmi so that a quasi-homogeneous and isotropic distribution of satellite fixes would arise enabling current vectors to be calculated with roughly isotropic resolution. This was successful as the position of the fixes (Fig. 7.4) shows. The raw current vectors calculated on the one hand using the electromagnetic (EM) log data (Fig. 7.5) and on the other

hand the acoustic Doppler current profiler (DCP) data (Fig. 7.6) show broad similarities; a band of strong currents starting in the NW corner of the area curves round to the south and becomes less distinct; another area of strong eastward currents is apparent in the SE of the area and an anticyclonic feature can be seen in the NE of the area. It will not escape the reader that the bands of strong currents are closely associated with the thermoclinity and baroclinity maxima.

Due to difficulties experienced with the DCP data during legs B107 and B109 (heavy swell from SW) it was decided to leave these out of the objective analysis of the currents. The observed currents were objectively analysed, then the vorticity, streamfunction and divergence-free currents were calculated as described in Bauer et al. (1985) and Leach (1986). Figures 7.7 - 7.16 show in pairs the various stages of this analysis for the EM-log data and for the DCP data in parallel. Although both sets of maps show a broadly similar velocity field structure the DCP data for the depth range 22 - 38 m show a stronger cut-off anticyclone in the central southern part of the area.

Although it is only possible to calculate absolute currents between satellite fixes, the relative measurements from the DCP can in theory give information about the vertical current shear with any chosen resolution. In practice however the acoustic data are relatively noisy and need to be averaged or filtered to obtain a clearer picture. In this particular case the shear data were filtered in the vertical (using a binomial filter) and then blocked together to give a resolution of 40 min, corresponding to about 10 km. These shear values were then objectively analysed onto a grid and processed like the current vectors, first calculating the vorticity shear, then the vertical derivative of the streamfunction by solving the Poisson-equation and finally the divergence-free shear (the shear of the divergence-free velocity). Even after this procedure the shear field for the depth range 56 - 91 m showed a fairly rough nature (Fig. 7.17) and only by taking an even larger depth range, 56 - 122 m, did this quantity become smoother. The shear field shows generally the same structure as the velocity field. Typical values of the shear in the frontal jet are about $1 \cdot 10^{-3}$ rad s^{-1} which corresponds geostrophically to 1.0 kg m^{-3}/100 km. Comparing this with the density anomaly at 60 m depth (Fig. 7.19) shows that this measured shear is probably rather larger than would be expected from

the baroclinicity. The shear data are discussed in greater detail in Fiekas (1987).

The rather noisy nature of the acoustic data and the poor vertical resolution of the reliable shear data together with particular difficulties in the upper bins make it impossible to look at the measured shear in the region of the anticyclonic eddy in the NE of the area where the hydrographic data suggest a baroclinicity reversal (Figs. 7.20 - 7.22). The density field at 15 m (Fig. 7.20) shows the feature as a density maximum, implying cyclonic positive shear; the density field at 30 m (Fig. 7.22) shows a rather confused situation and the density field at 45 m (Fig. 7.22) shows the feature as a density minimum, implying anticyclonic positive shear. The other principal features of the mass field do not show changes of sign of this sort as a function of depth.

The weighted confidence limits (see section 8.3, Bauer et al. (1985) and Leach (1986)) for selected quantities are shown in Figs. 7.23 - 7.26. From these figures it can be seen that the weighted confidence limits for the depth of an isopycnal are about 0.2 m and for the spacing of two isopycnals about 0.1 m. The vorticity has weighted confidence limits of about 2 rad Ms^{-1} over much of the area and the streamfunction limits of $0.5 \cdot 10^3$ m^2 s^{-1}.

The maps of the attenuation at 15 and 20 m depth are shown in Figures 7.27 and 7.28. Since the SE of the area was surveyed during the nights no data are available there. In general water with higher turbidity is found in the W and SE of the area, in the region of the anticyclone and in a narrow band in the central eastern part of the area. Apart from this band there is a clear correlation of higher turbidity with the warmer water.

7.2 Sections

Here selected sections from the survey are shown to illustrate the detailed structure of the Polar Front. Fig. 7.29 shows sections of temperature, salinity and pressure in density coordinates, the depth of isopycnals, the N^2-structure and the north-south velocity component along the east-west section B105. The thermohaline structure shows the warm water in the west up to km 60 and the cold water in the east, km 110 - km 230. Between km 60 and 110 appears a frontal region with thermohaline anomalies and east of km 230 there also appears a more disturbed region again. The mass field

shows a broad baroclinic zone centred at about km 100. The N^2-distribution shows a jump in the depth of N^2-maximum at about km 90 and the velocity component shows a maximum southward velocity in excess of 50 cm s^{-1} at km 90 and 40 m depth.

The remaining sections shown below are north-south sections. Leg B109 (Fig. 7.30) in the west of the area is illustrated with the parameters σ_t (y,z); attenuation, K_d (y,z); T (y, σ_t) and the normalized spacing $H'(y, \sigma_t)/\bar{H}^y$. The thermohaline structure shows the main Polar Front at km 165 and also a thermohaline anomaly between km 40 and 60. The surface attenuation maximum at km 125 is on the right-hand side of the baroclinic zone (looking downstream) associated with the Polar Front. The attenuation maximum at km 25 in 30 - 40 m depth is also on the right-hand side of a frontal structure judging by the depth of the isopycnal σ_t = 26.85 kg m^{-3} and the current measurements (Fig. 7.2, Fig. 7.5 - 7.16). The thermohaline anomaly between km 40 and 60 is perhaps an advective feature.

Leg B116 (Fig. 7.31) in the east of the area is illustrated with the parameters σ_t (y,z), K_d (y,z) and T (y, σ_t). The thermohaline structure shows the main Polar Front at the south end of the section and the warm anticyclone at the north end of the section. The attenuation shows generally higher values in the region of the anticyclone with particularly high values at the edges. The streak of higher attenuation seen in the maps (Figs. 7.27, 7.28) in the east of the area is seen in this section at about km 115.

7.3 Statistics

Histograms of the isopycnal temperature and salinity distribution from the front survey are shown in Figures 7.32 and 7.33. Three principal water masses are apparent, the warm, salty water of the west and SE, the cooler, fresher water of the central part of the area, and the cold, still fresher water of the NW. The water of the anticyclone appears on the lower isopycnals as small water mass on the cooler, fresher side of the main warm water mass.

The T-S diagram for the 3 deep CTD dips straddling the front is given in Fig. 7.34.

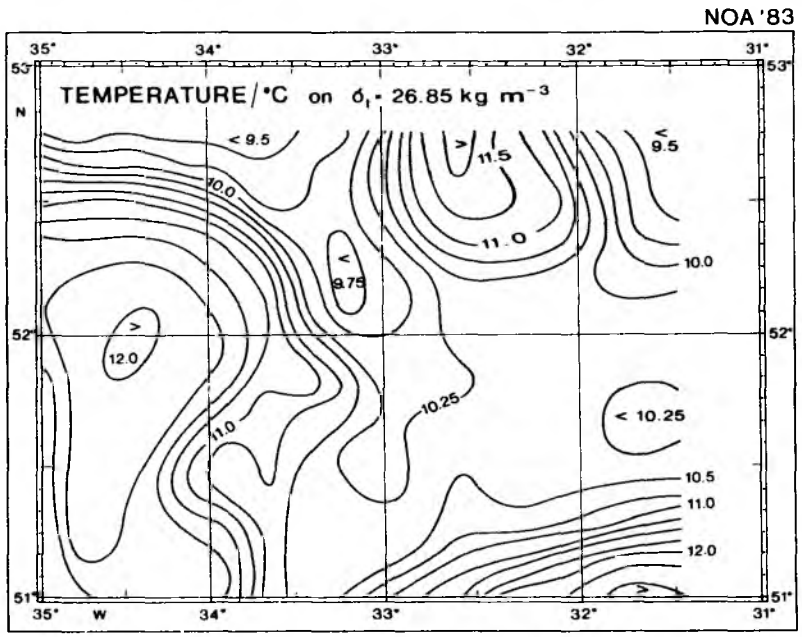

Fig. 7.1: Temperature on the density surface σ_t = 26.85 kg m^{-3}. Contour interval 0.25 K.

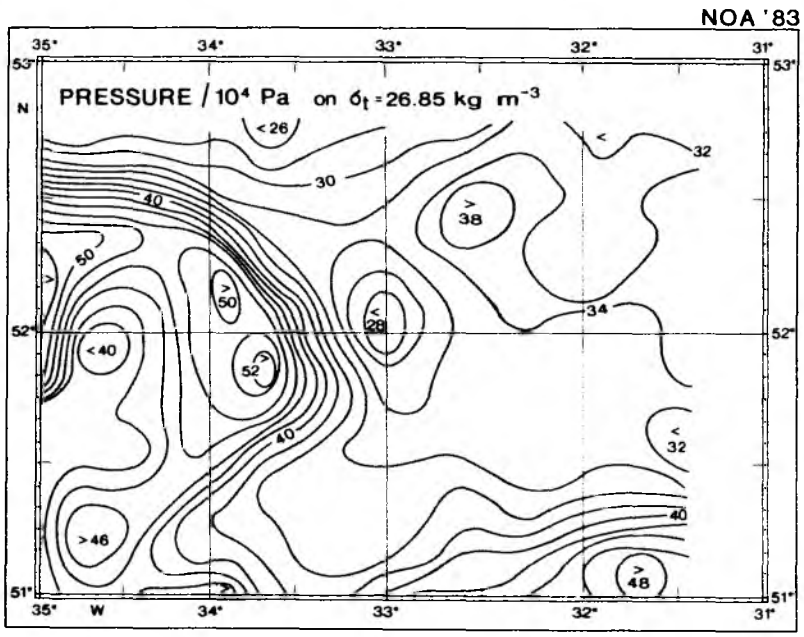

Fig. 7.2: Depth of the density surface σ_t = 26.85 kg m^{-3}. Contour interval 2 m.

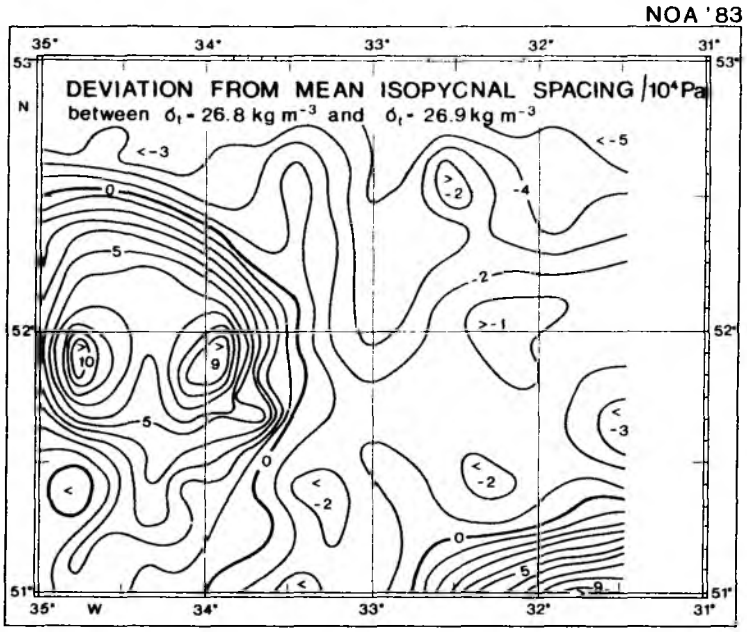

Fig. 7.3: Spacing between the isopycnals σ_t = 26.8 and 26.9 kg m^{-3}. Contour interval 1 m.

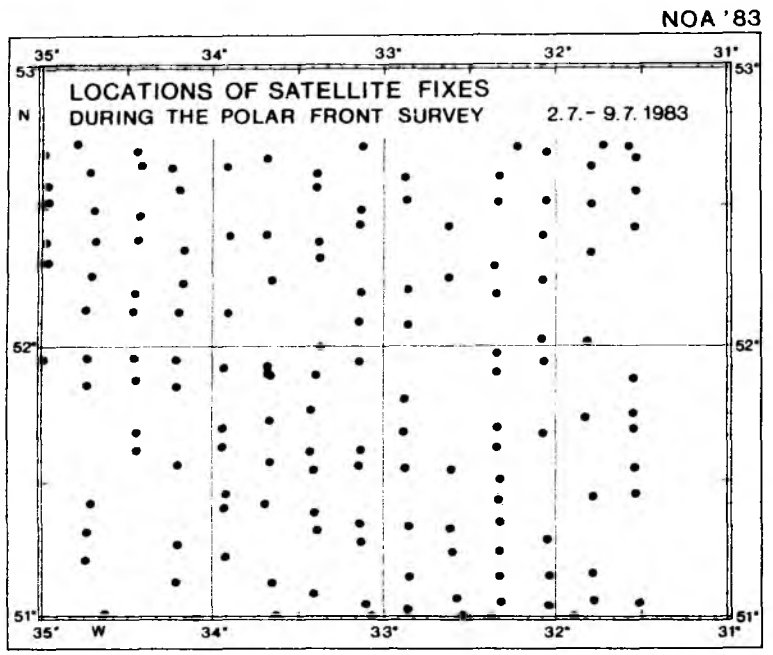

Fig. 7.4: Position of satellite fixes during the Polar Front survey.

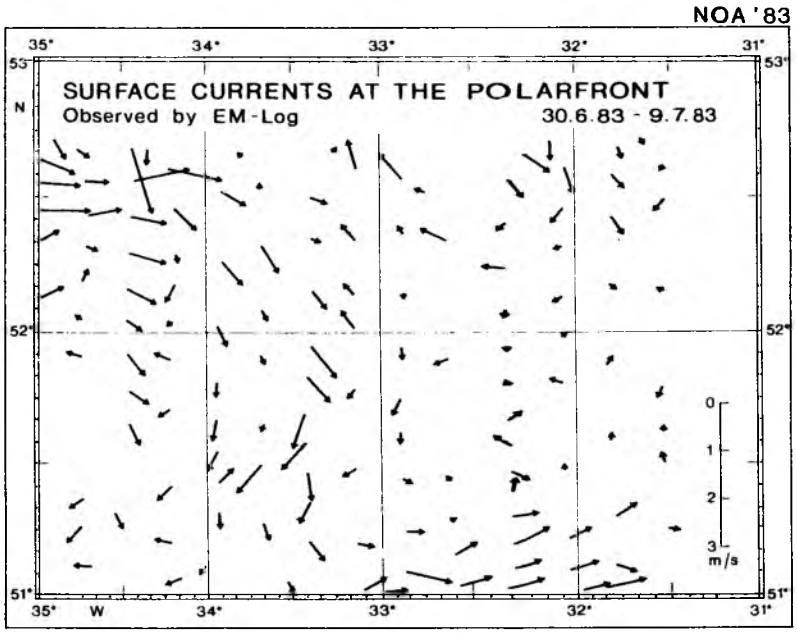

Fig. 7.5: Surface currents at the Polar Front measured using the EM-log.

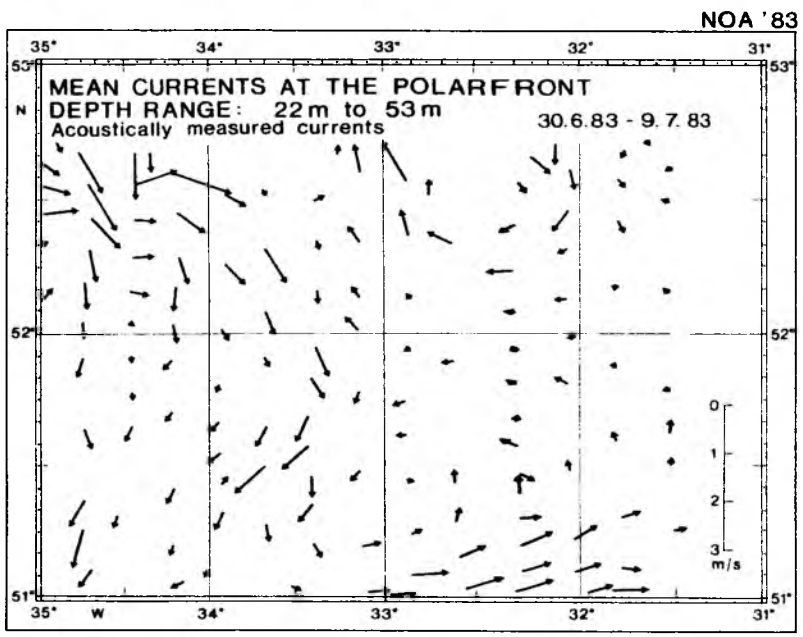

Fig. 7.6: Currents at the Polar Front averaged over the depth range 22 m to 53 m measured with the acoustic Doppler current profiler.

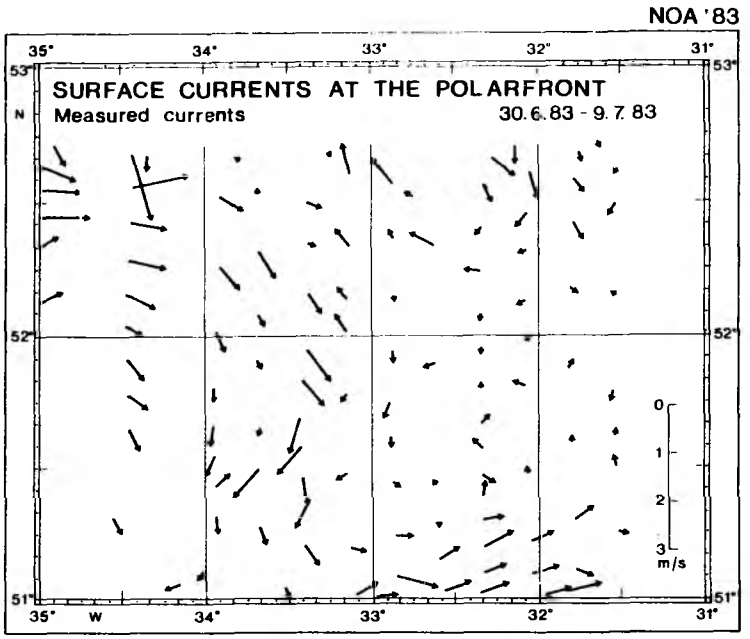

Fig. 7.7: Measured surface currents at the Polar Front used in the objective analysis.

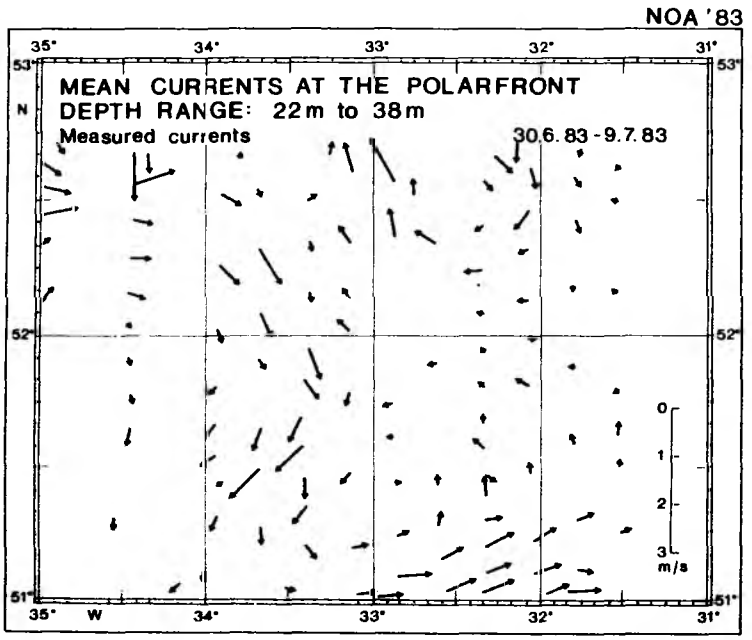

Fig. 7.8: Measured currents for the depth range 22 - 38 m used in the objective analysis.

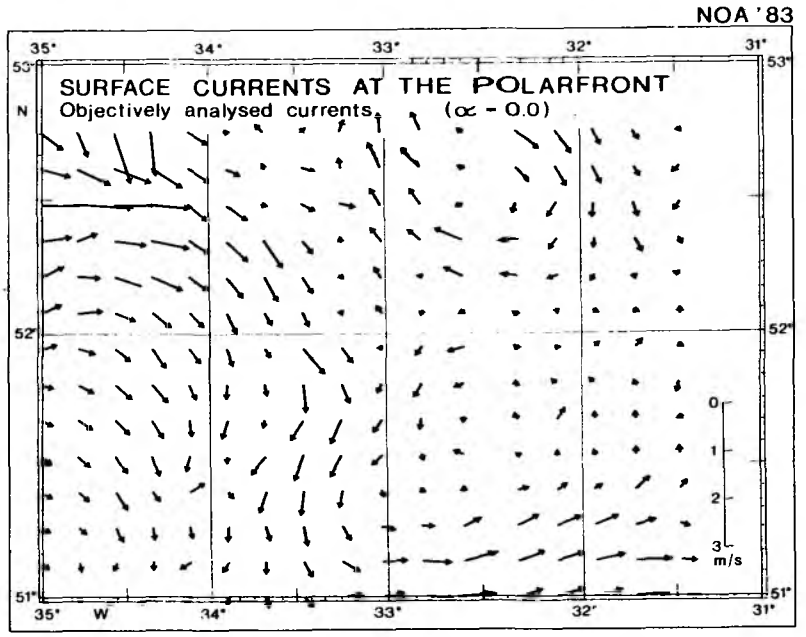

Fig. 7.9: Objectively analysed surface currents.

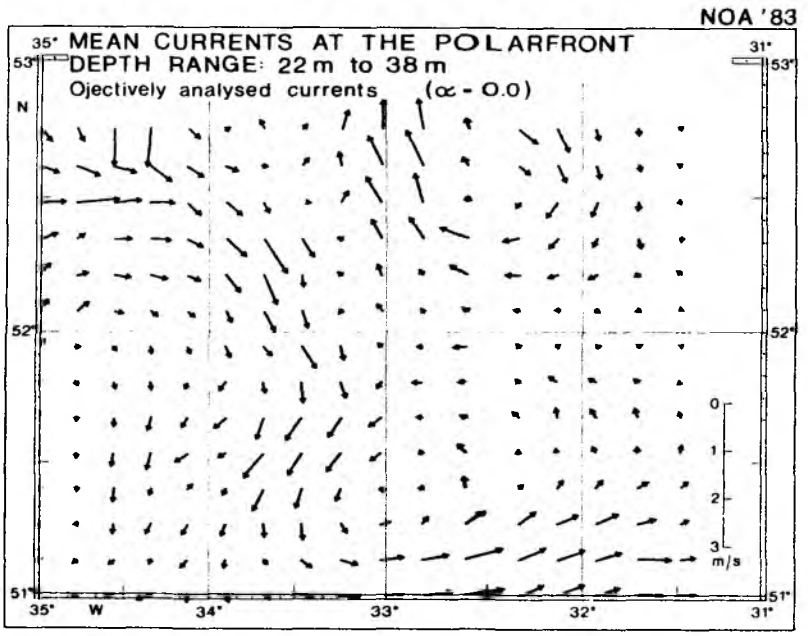

Fig. 7.10: Objectively analysed currents for the depth range 22 - 38 m.

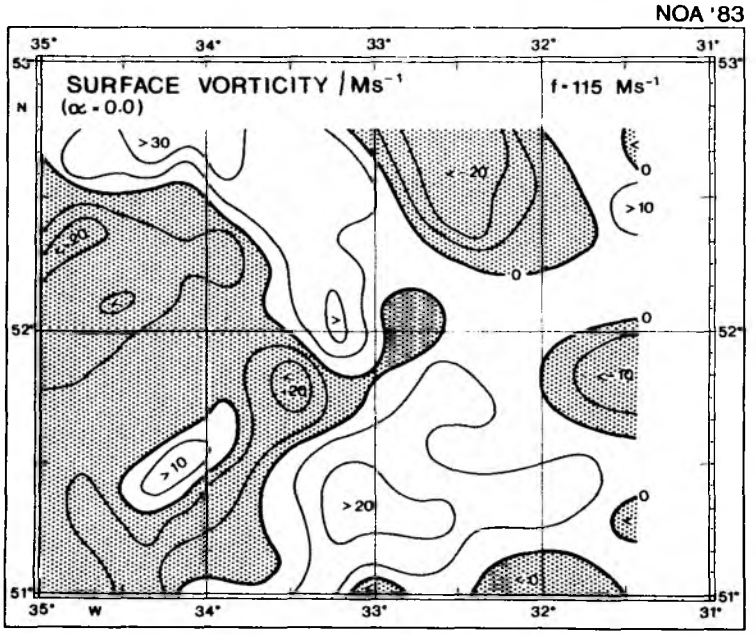

Fig. 7.11: Vorticity calculated from objectively analysed surface currents. Contour interval 10 rad Ms^{-1}.

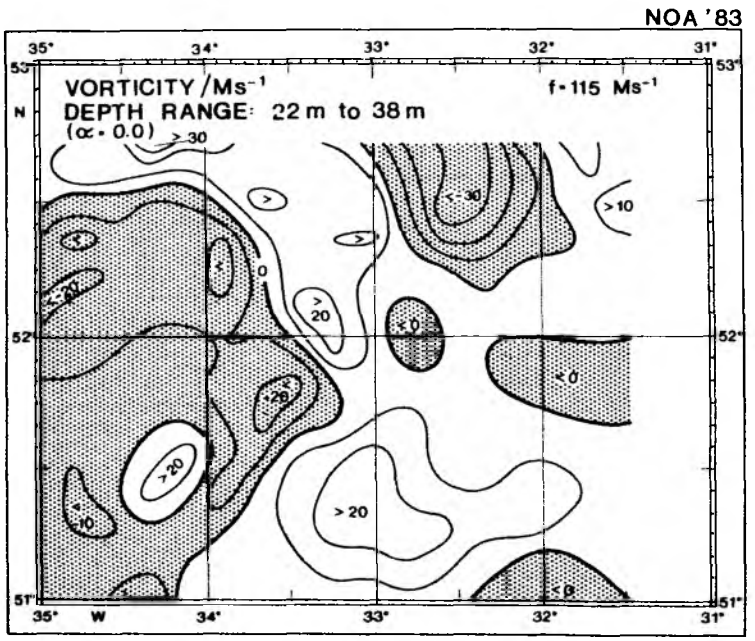

Fig. 7.12: Vorticity for the depth range 22 - 38 m. Contour interval 10 rad Ms^{-1}.

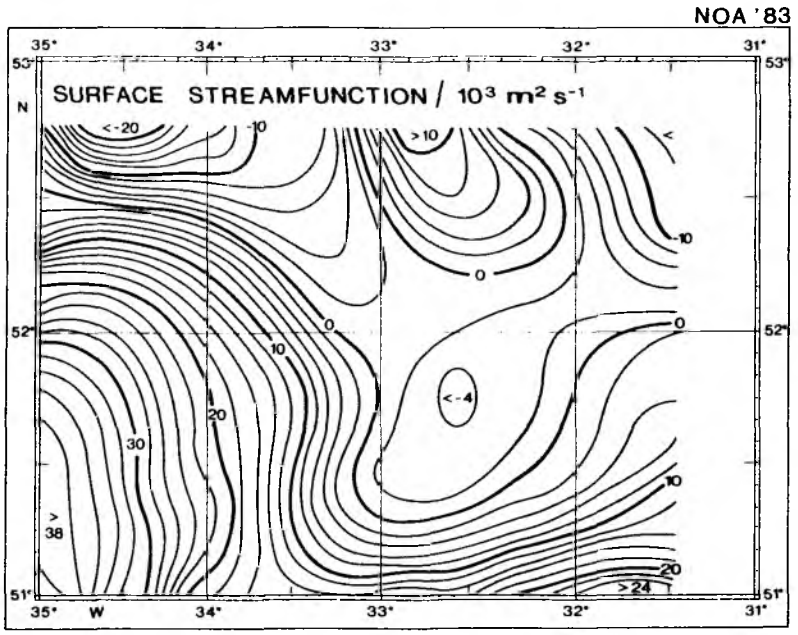

Fig. 7.13: Streamfunction calculated from surface currents. Contour interval $2 \cdot 10^3$ m^2 s^{-1}.

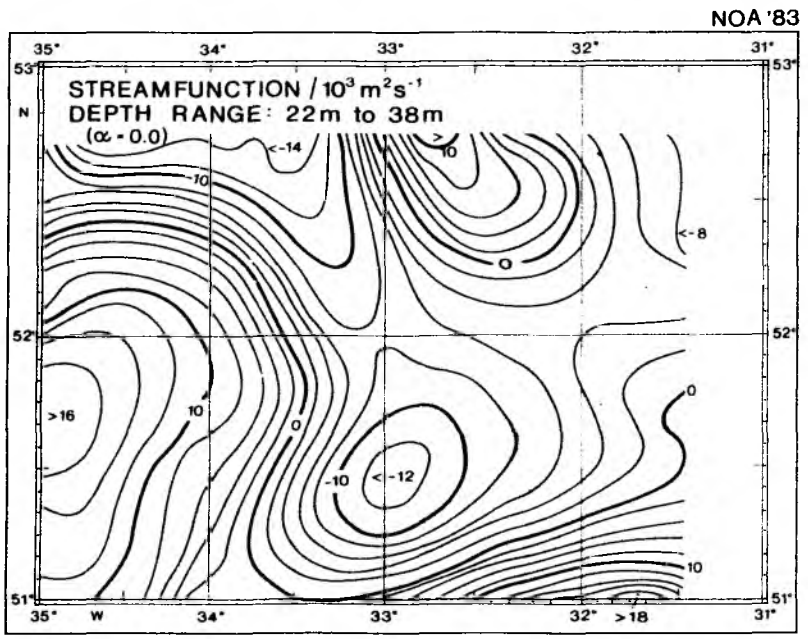

Fig. 7.14: Streamfunction for the depth range 22 – 38 m. Contour interval $2 \cdot 10^3$ m^2 s^{-1}.

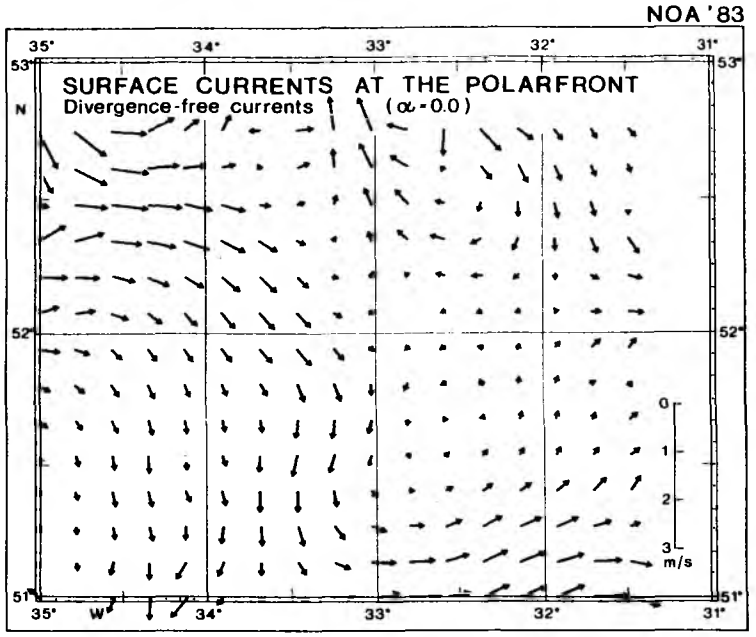

Fig. 7.15: Divergence-free currents calculated from surface streamfunction.

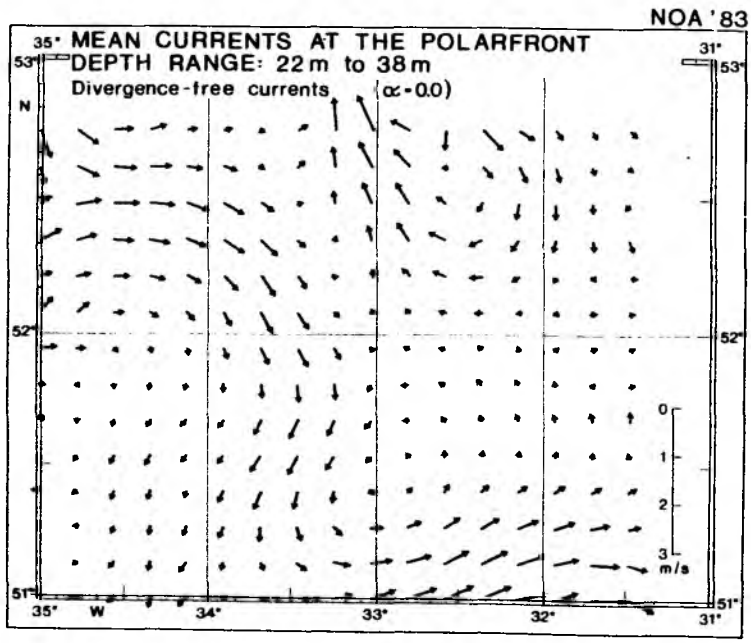

Fig. 7.16: Divergence-free currents for the depth range 22 - 38 m.

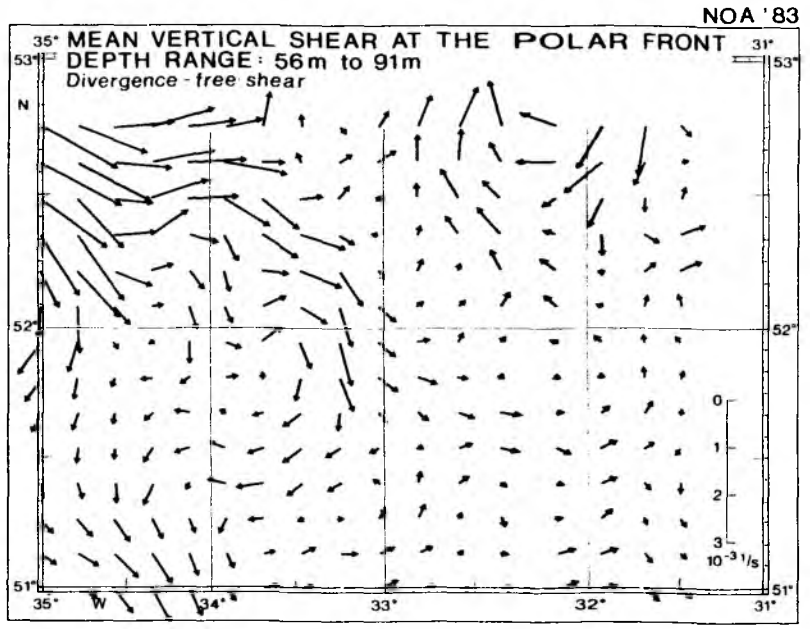

Fig. 7.17: Mean acoustically measured shear of the divergence-free current over the depth range 56 - 91 m.

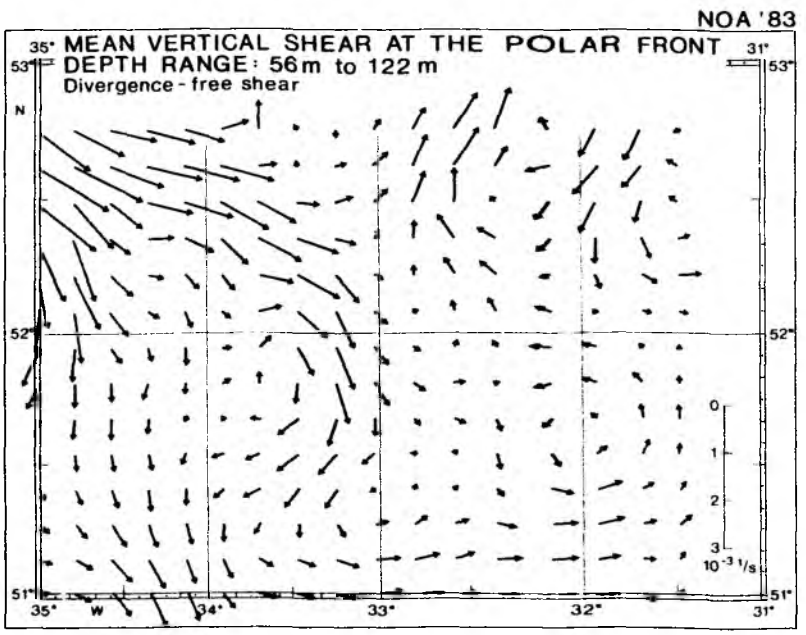

Fig. 7.18: Mean acoustically measured shear of the divergence-free current over the depth range 56 - 122 m.

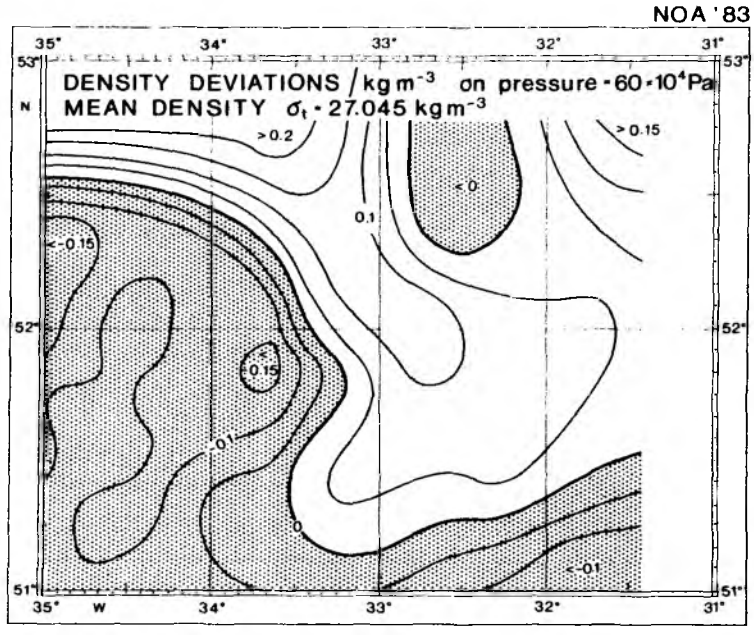

Fig. 7.19: Equivalent density anomaly at 60 m depth calculated from the vertical gradient of the streamfunction derived from acoustically measured shear. Contour interval 0.05 kg m^{-3}.

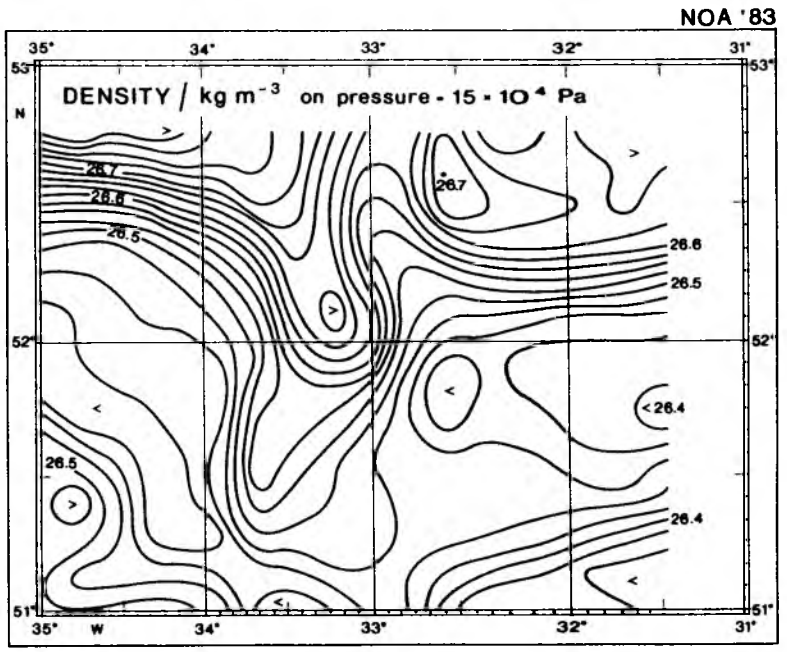

Fig. 7.20: Density at 15 m depth. Contour interval 0.025 kg m^{-3}.

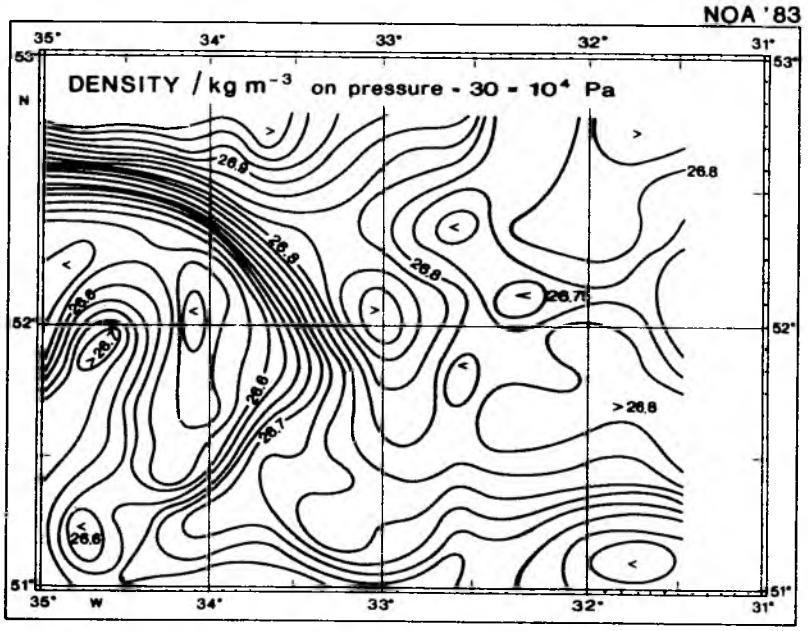

Fig. 7.21: Density at 30 m depth. Contour interval 0.025 kg m^{-3}.

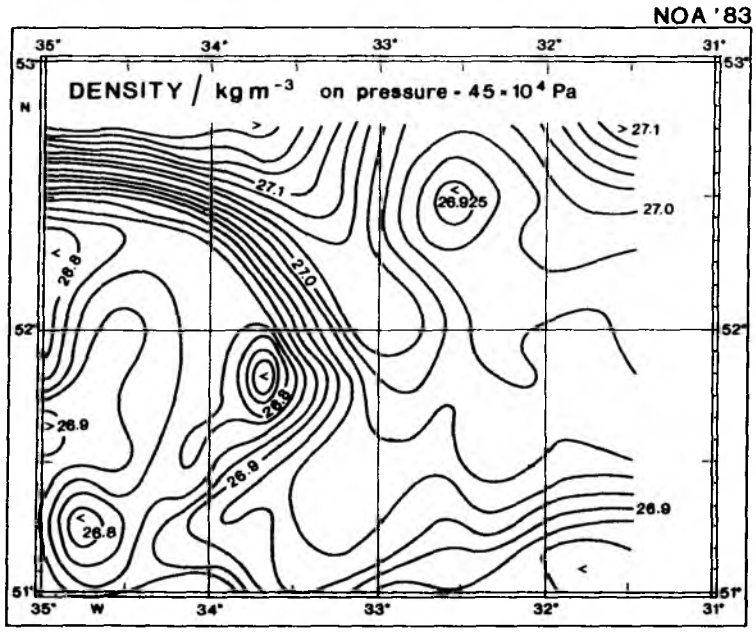

Fig. 7.22: Density at 45 m depth. Contour interval 0.025 kg m^{-3}.

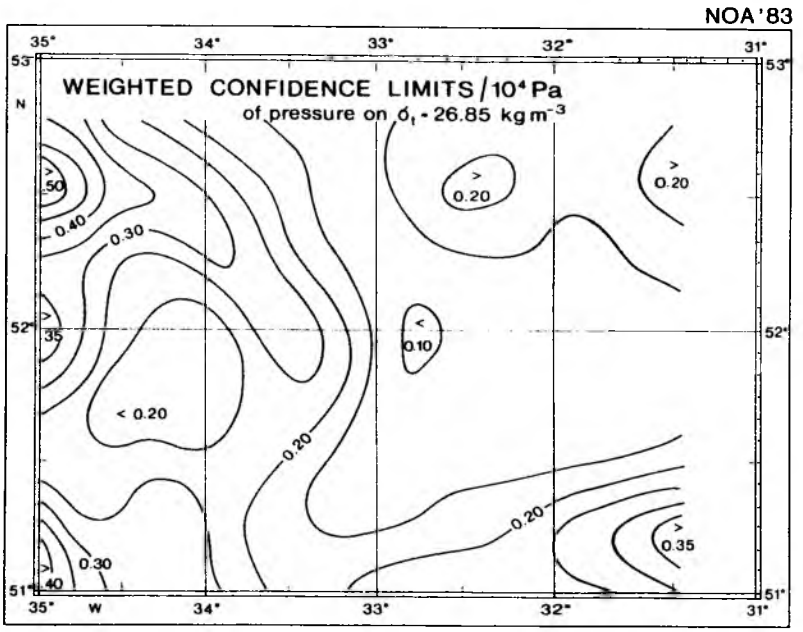

Fig. 7.23: Weighted confidence limits of the depth of the isopycnal, σ_t = 26.85 kg m^{-3}.
Contour interval 0.05 m.

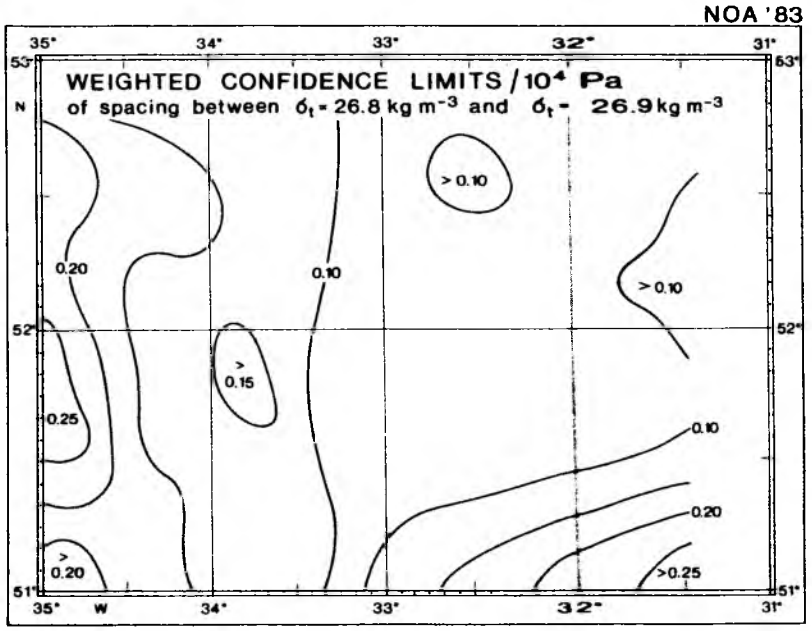

Fig. 7.24: Weighted confidence limits of the spacing between isopycnals σ_t = 26.8 and 26.9 kg m^{-3}.
Contour interval 0.05 m.

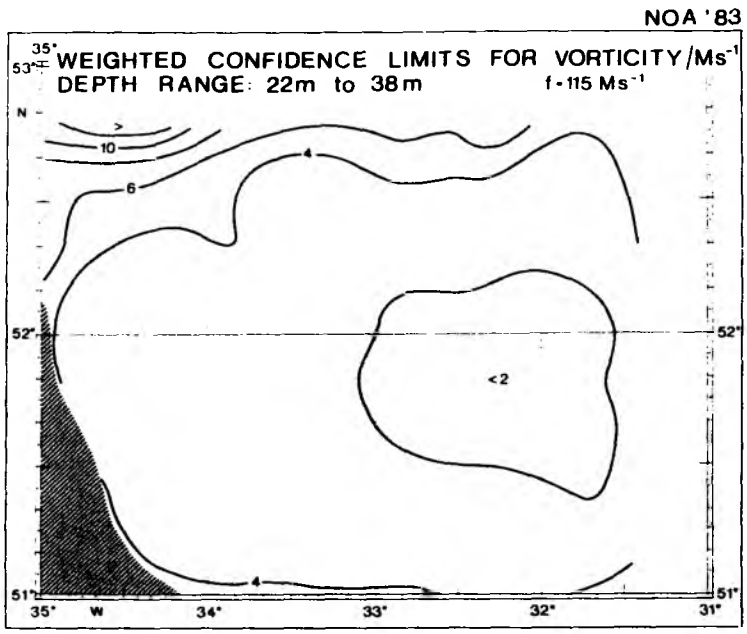

Fig. 7.25: Weighted confidence limits for vorticity in the depth range 23 - 38 m.
Contour interval 2 rad Ms^{-1}.

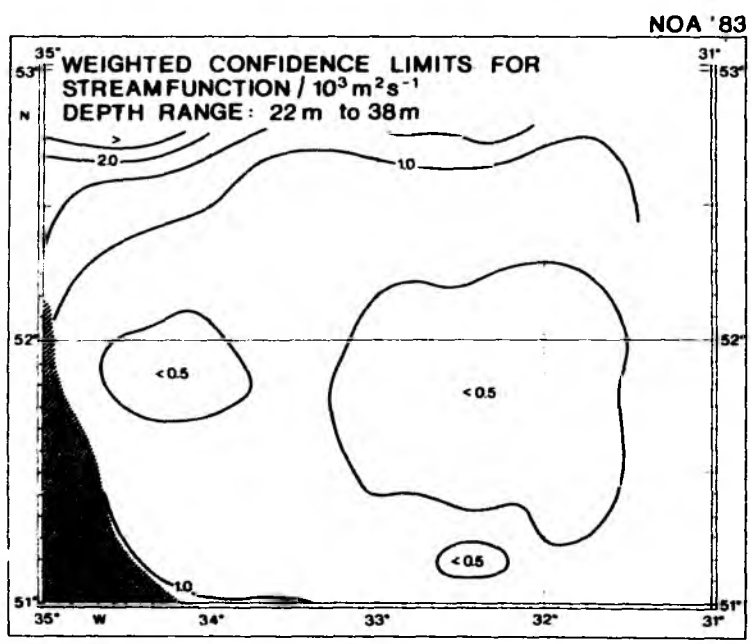

Fig. 7.26: Weighted confidence limits for the streamfunction for the depth range 22 - 38 m.
Contour interval $0.5 \cdot 10^3 m^2 s^{-1}$.

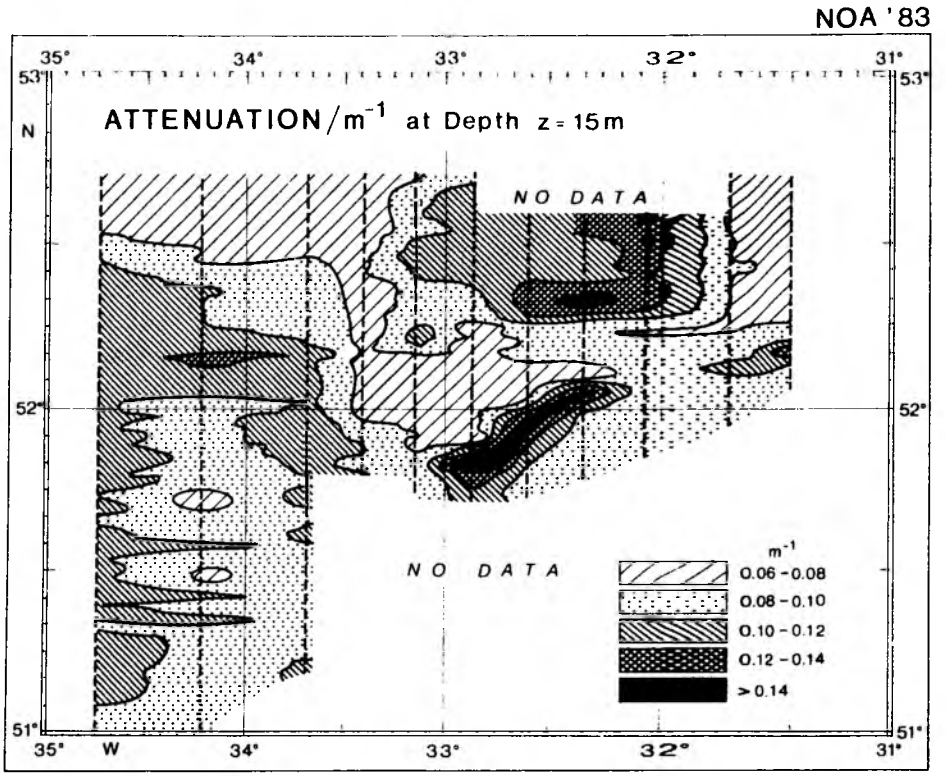

Fig. 7.27: Attenuation of downward irradiance at 15 m depth. Contour interval 0.02 m^{-1}.

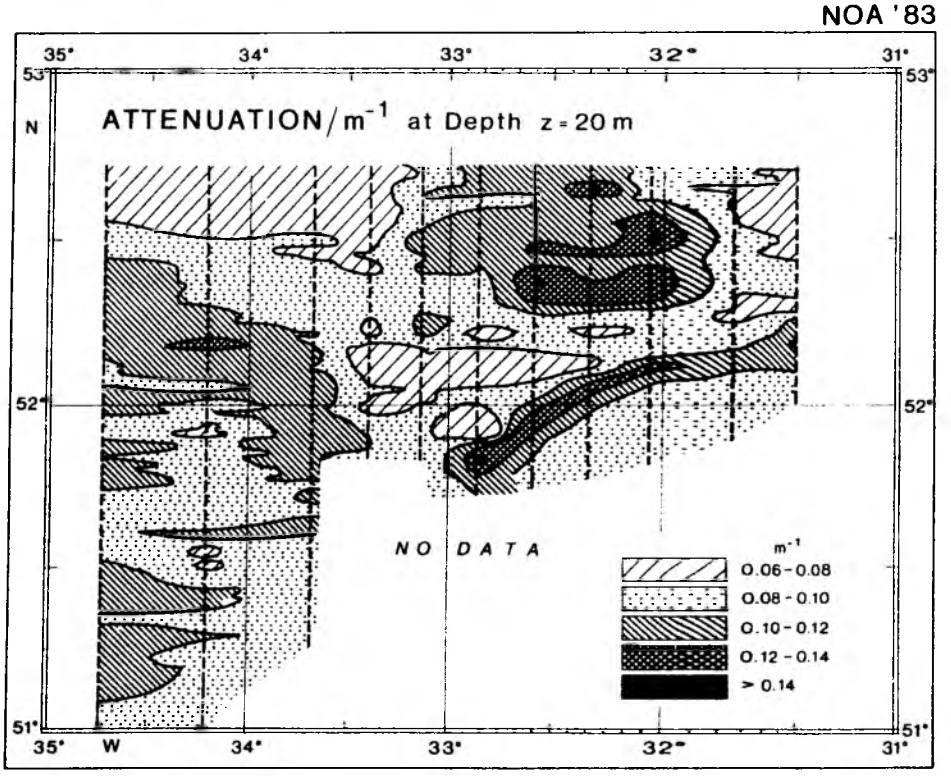

Fig. 7.28: Attenuation of downward irradiance at 20 m depth. Contour interval 0.02 m^{-1}.

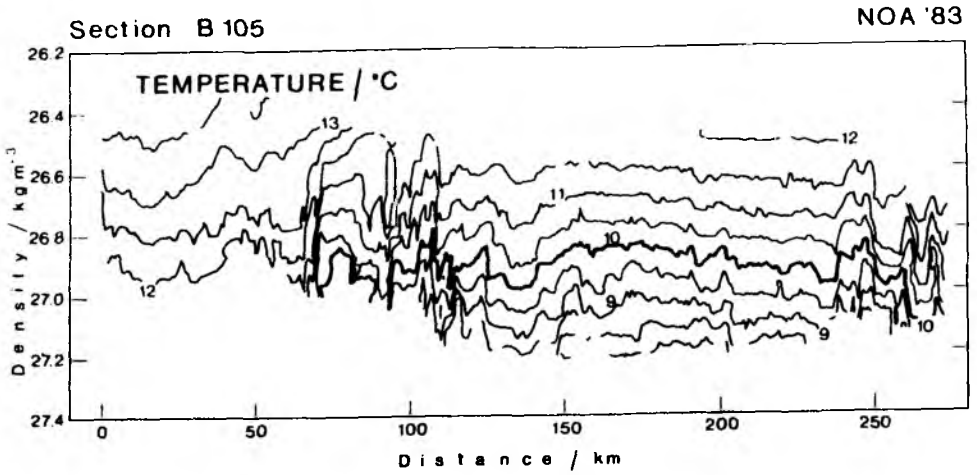

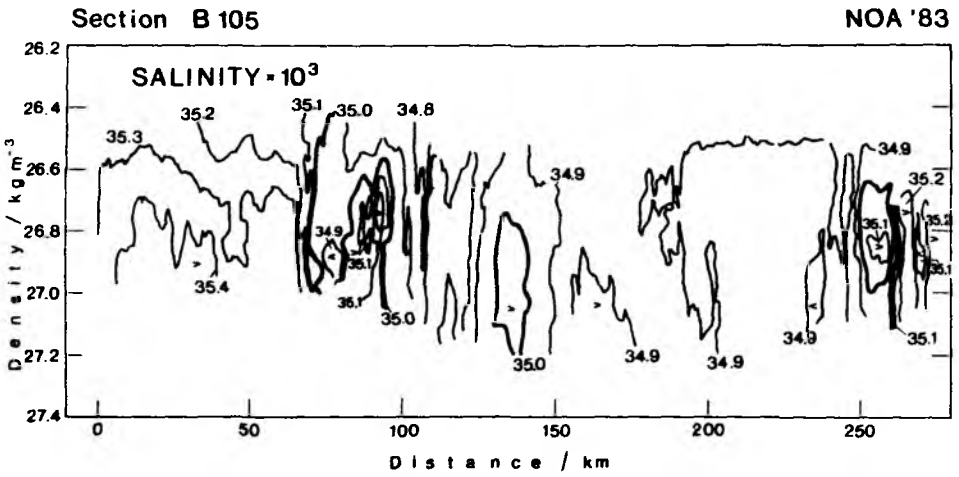

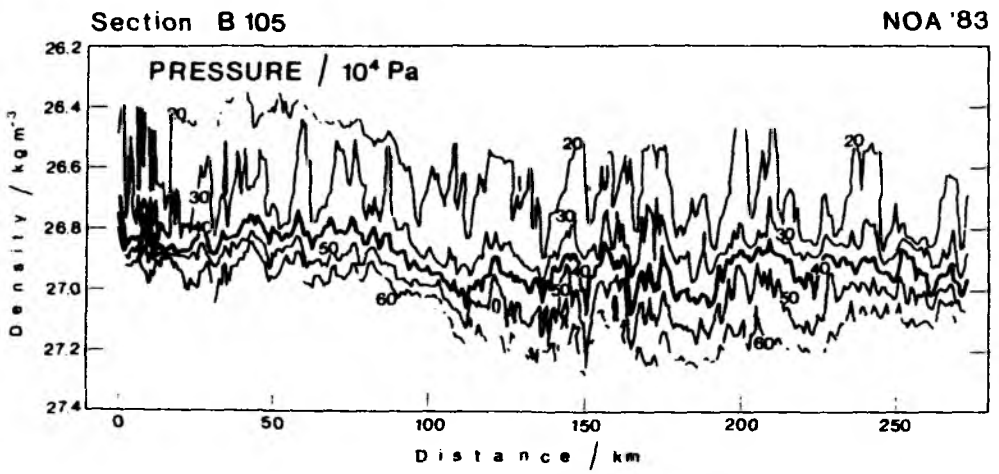

Fig. 7.29: Section B105 showing sections of a) temperature, b) salinity and c) depth in density coordinates.

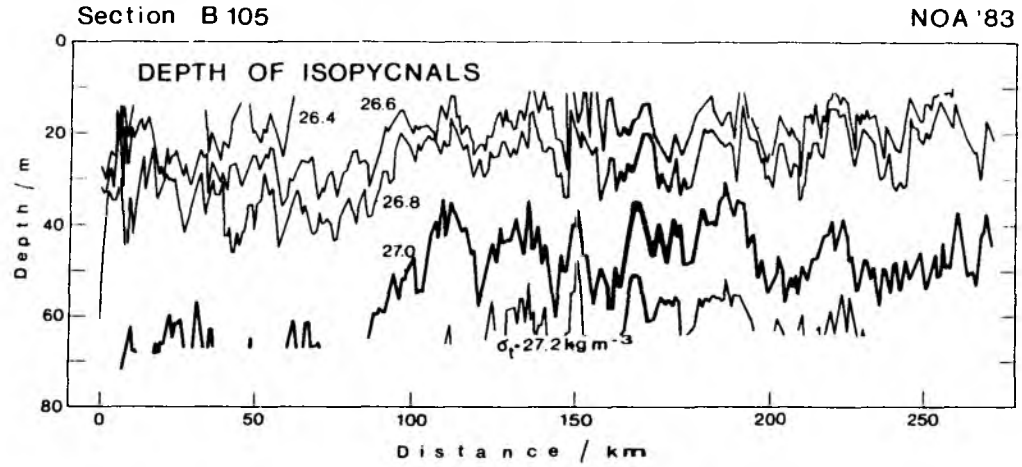

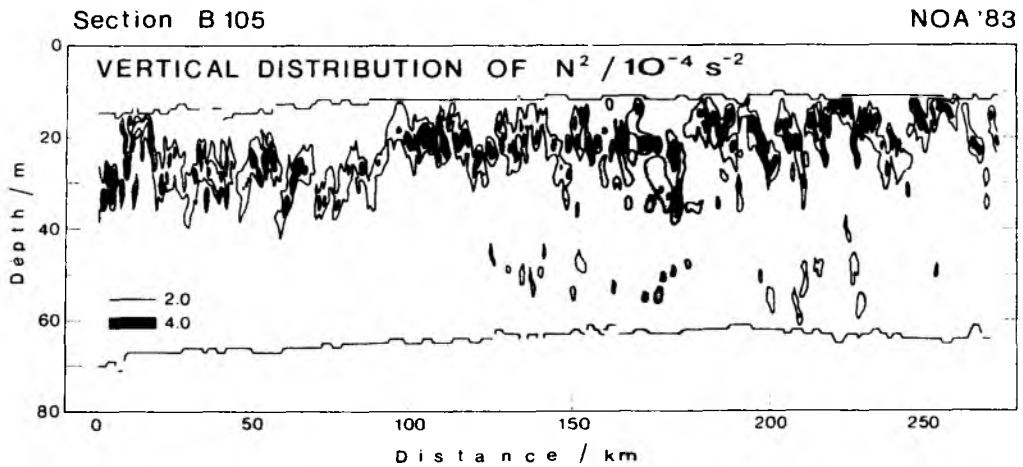

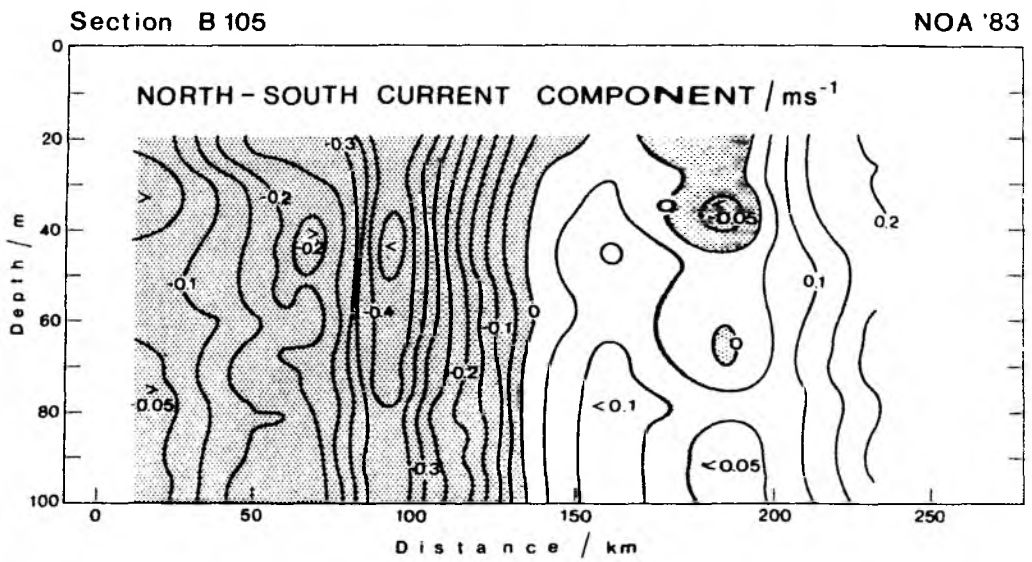

Fig. 7.29: Section B105 showing sections of d) isopycnals, e) N^2 and f) velocity component perpendicular to the section in depth coordinates.

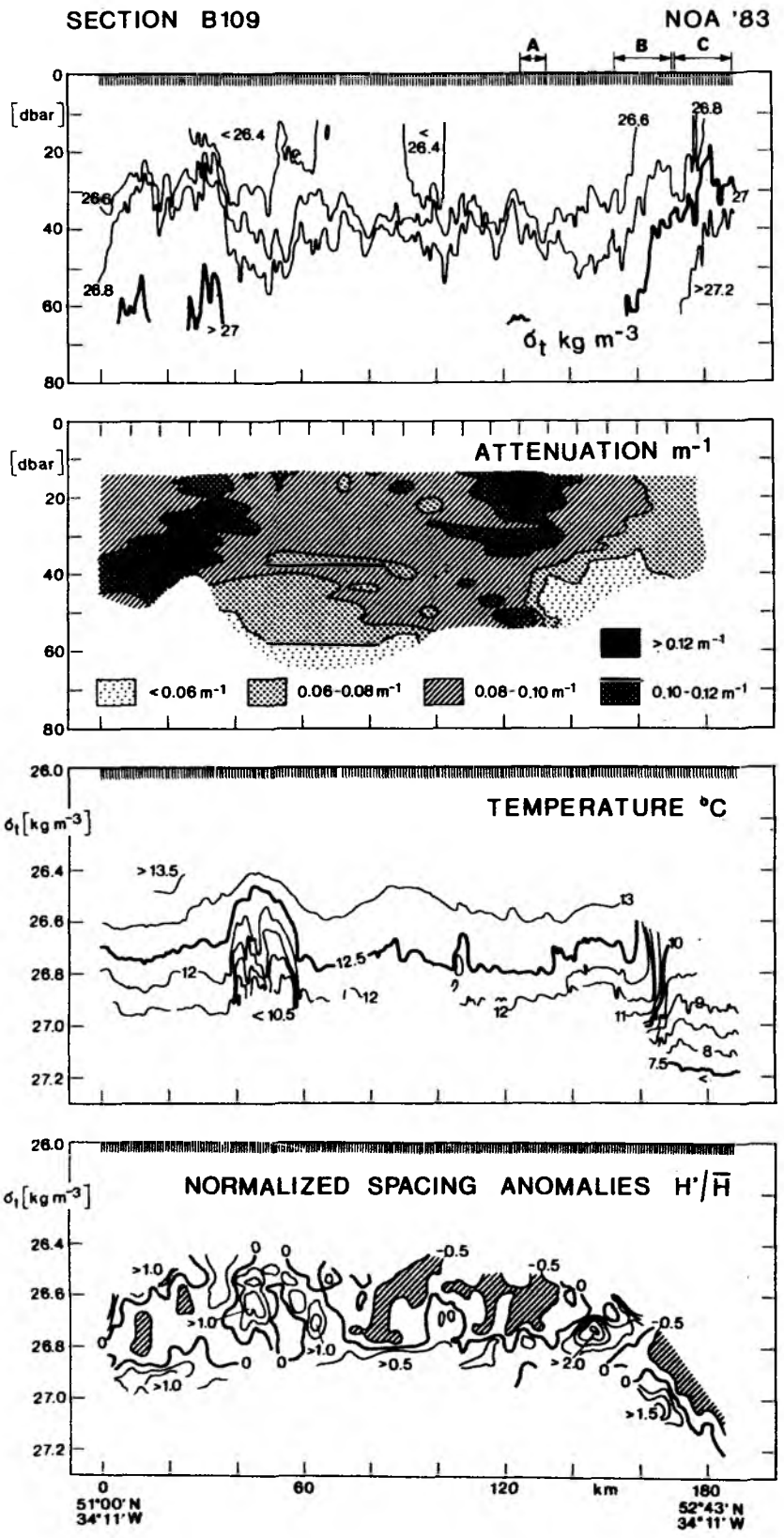

Fig. 7.30: Section B109 showing density and attenuation as functions of depth and temperature and normalized isopycnal spacing as functions of density.

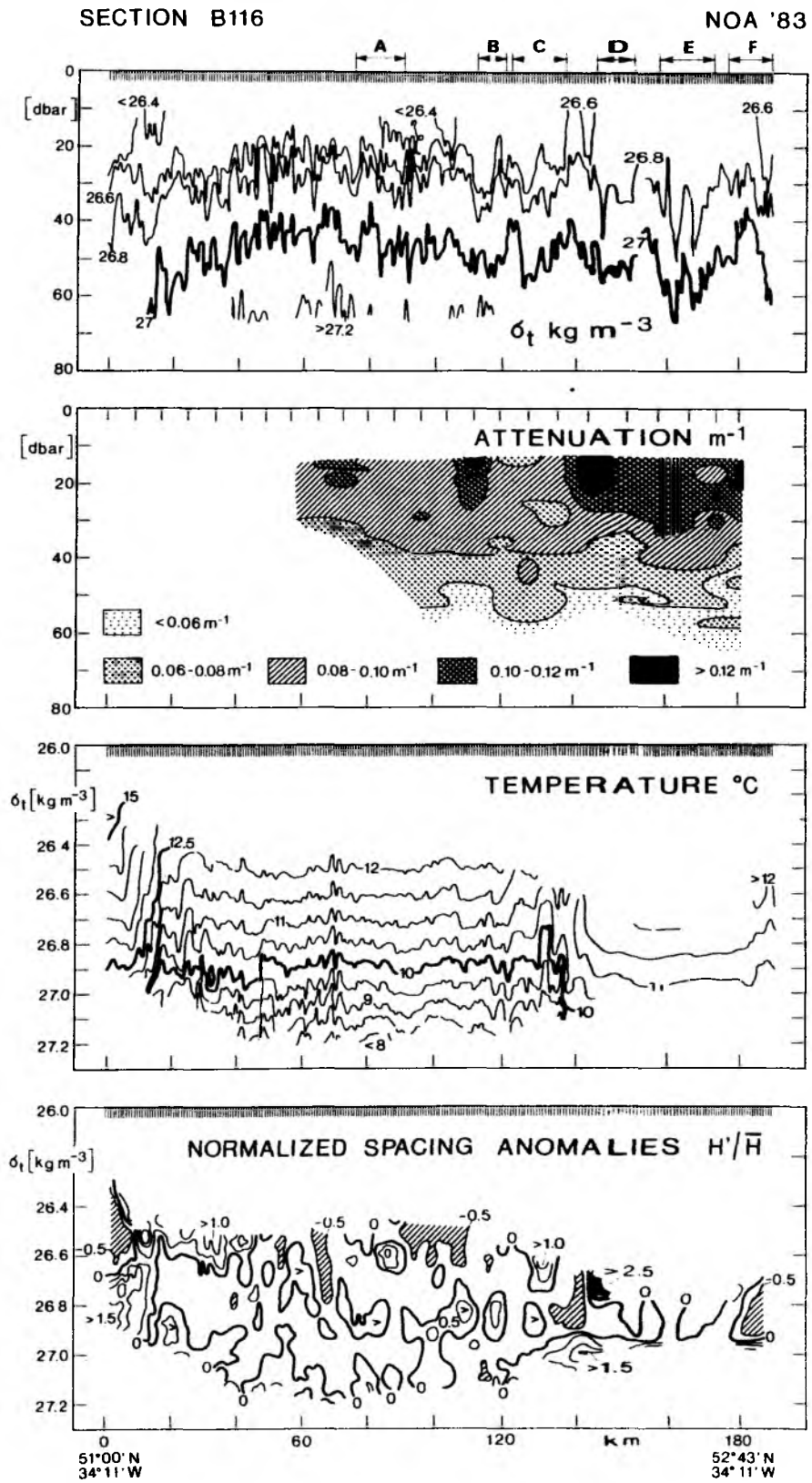

Fig. 7.31: Section B116 showing density and attenuation as functions of depth and temperature as a function of density.

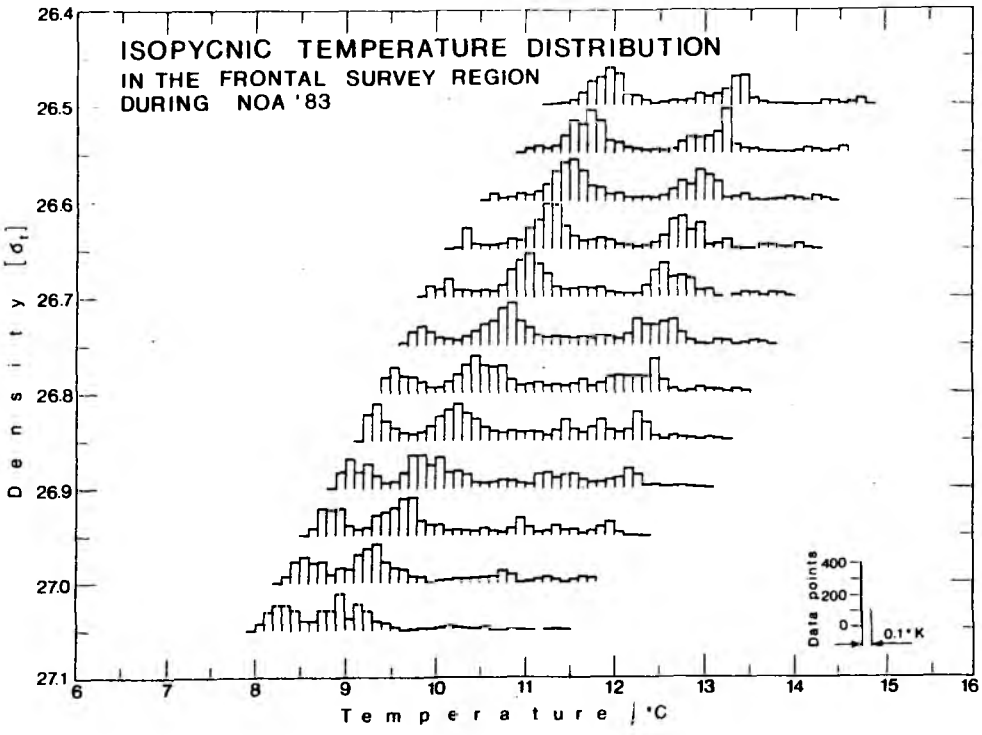

Fig. 7.32: Histograms of temperature on isopycnals for the Polar Front survey.

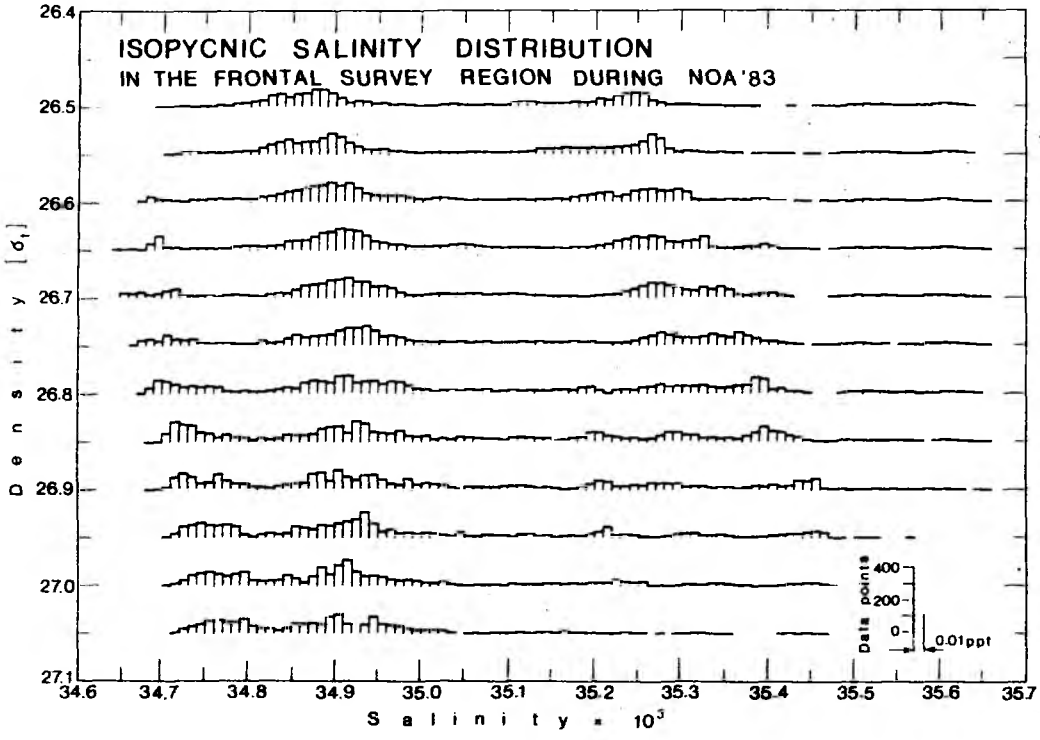

Fig. 7.33: Histograms of salinity on isopycnals for the Polar Front survey.

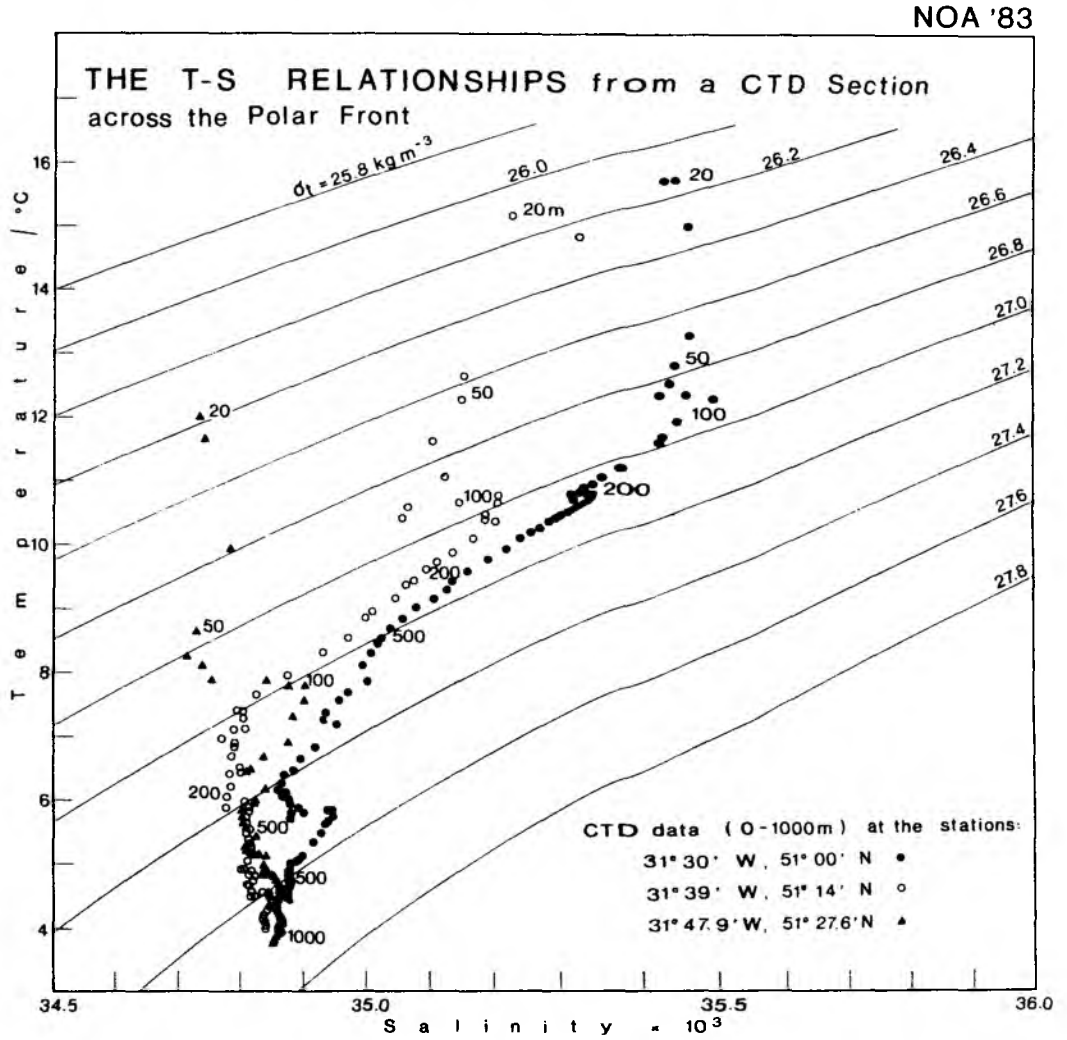

Fig. 7.34: T-S-diagram for the three deep CTD stations.

8. ANALYSIS OF ERRORS OF HYDROGRAPHIC AND OPTICAL DATA

8.1 Measurement errors and corrections applied during data processing

The sources of inaccuracies in the CTD-data were electronic noise (random errors) and more important the characteristic response of the sensors to rapidly changing field and the inaccuracies involved in the laboratory calibration of the sensors (both errors being systematic). Another important source of inaccuracy was the heat flow, especially in the thermometers and the pressure gauge. Since the applied corrections have been described in detail by Bauer et al. (1985) only deviations from the previous experiment (NOA'81) will be discussed in detail.

The resolution given by the manufacturers listed in Table 2.1 were reduced by altering the original 16-bit digitalization to 15 bit plus sign to 2 mK, 0.002 mS/cm and 0.02 dbar for the thermometers, conductivity cells and the pressure gauge, respectively.

Pressure

The most severe error sources for pressure were caused by rapid temperature changes of the surrounding water (inside the fish), calibration inaccuracies and the dynamic pressure due to high towing speeds. These errors sum up to $\varepsilon_p = \pm 1.6$ dbar (Bauer et al., 1985).

Temperature

Calibration inaccuracies of the thermometers were small (2 mK rms error) compared with those introduced by the response time. A time constant correction from (τ = 85 ms) was only used to reduce the mismatch between the different response of thermometers and conductivity cells. Laboratory tests revealed a true time constant for the thermometers of τ = 120 ms, a value which was supported by the manufacturer. The absolute accuracy of temperature is therefore limited by the difference in the used and true time constants to about $\varepsilon_T = 0.02$ K in the region of the strongest vertical temperature gradients (0.5 K/m).

Conductivity

The main source of error in the conductivity signal is due to calibration inaccuracies ($\varepsilon_c \approx 5$ µS/cm). It was assumed, that the temperature effect

was negligible and any fouling by drifting material does not occur (the differences between both conductivity cells remain fairly constant during the expedition). We did not try to correct the conductivity itself, but the salinity as described below.

Salinity

To improve the absolute accuracy of the CTD—salinities, they were corrected by means of accurately analysed water samples (accurate to about $0.002 \cdot 10^{-3}$). The correction parameters were determined by linear regression and are given in Table. 4.1. In order to test the influence of the later processing stages, which were non-linear (median filter), a numerical error analysis of the derived quantities as salinity and density was carried out (Bauer et al., 1985).

8.2 Numerical estimates of uncertainties in derived quantities

Derived quantities such as salinity and density were influenced by the different time response of thermometers and conductivity cells and the various non-analytical stages of the data processing. Inaccuracies, introduced by this processing scheme can only be tested numerically by applying an error test as described by Bauer et al. (1985). By using the appropriate input parameter, namely a diving speed of 1 m/s and a set of synthetic input profiles (Fig. 8.1) we have derived the error profiles shown in Figure 8.2. The top row of this figure shows the error profiles before the median filtering, and the bottom row the final error profiles. Maximum errors were observed at the top of the seasonal thermocline with $\varepsilon_T < 3$ mK, $\varepsilon_S < 0.005 \cdot 10^{-3}$ and $\varepsilon_{\sigma_t} < 0.003$ kg/m^3. This result shows, that these errors can be neglected compared with those errors discussed above, and the accuracy in density can be estimated by using $\varepsilon_S = 0.02 \cdot 10^{-3}$, $\varepsilon_T = 0.02$ K to be less than $\varepsilon_{\sigma_t} = 0.01$ kg/m^3.

According to Bauer et al. (1985) the error in isopycnic spacing should be smaller than 5 % of the true spacing.

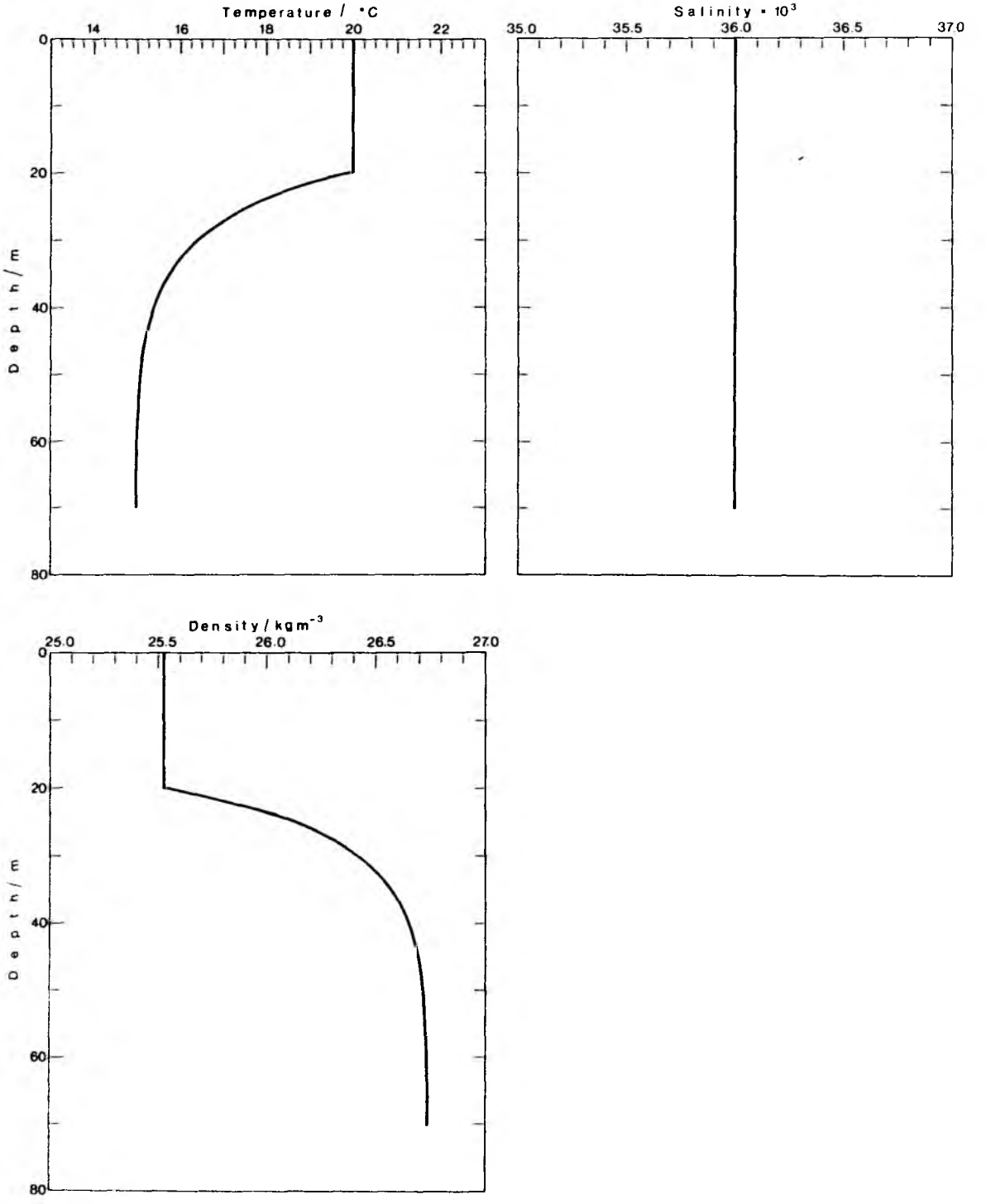

Fig. 8.1: Synthetic profiles of temperature, salinity and density for the numerical estimation of errors in the CTD data processing.

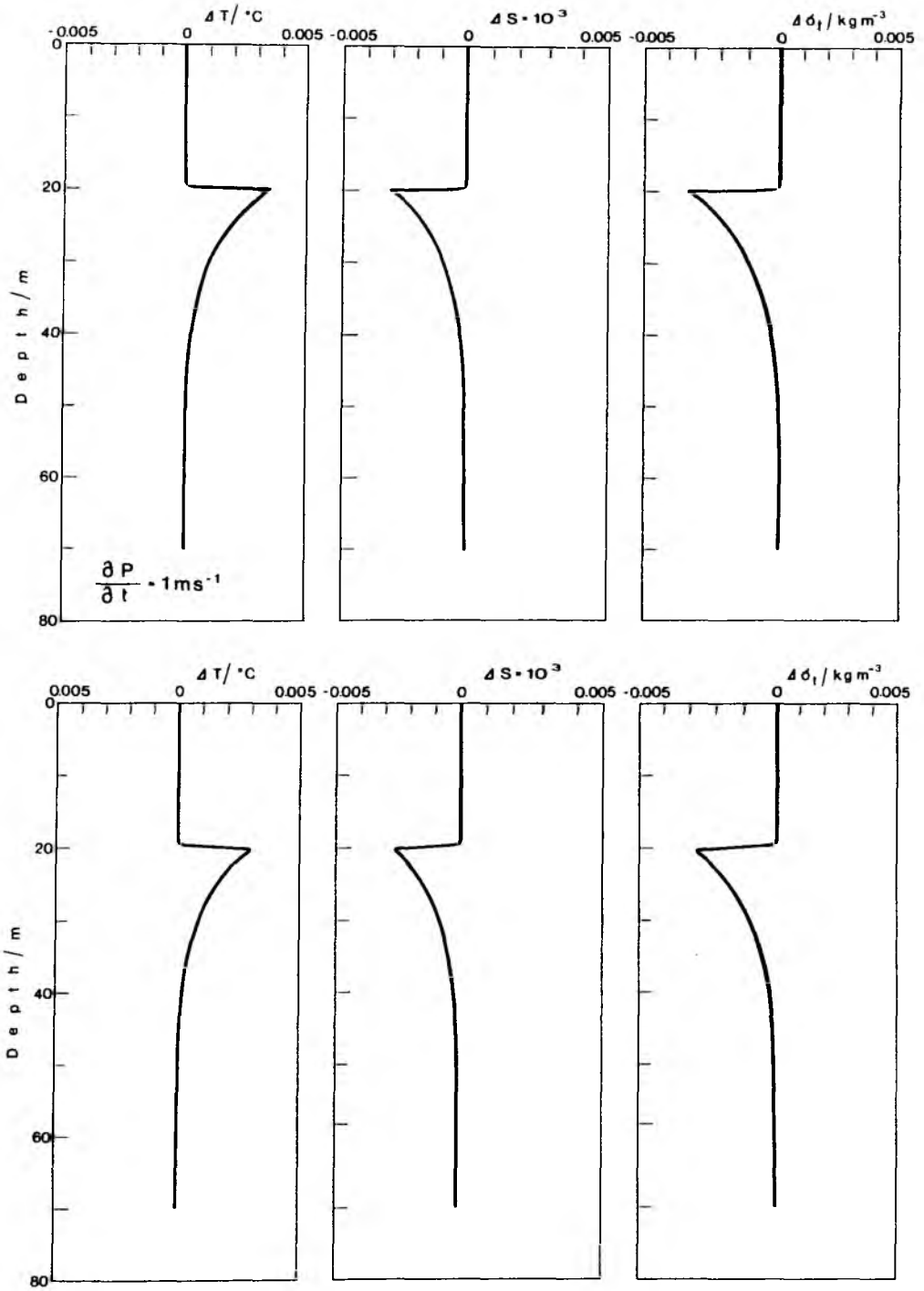

Fig. 8.2: Profiles of numerically estimated errors in temperature, salinity and density before (upper panels) and after (lower panels) correction of errors. There is little change but the errors are small anyway.

8.3 Errors in objectively analysed fields

The deviation of confidence limits for the objectively analysed scalar field was described in Bauer et al. (1985). The weighted confidence limits (WCL) were calculated from the weighted number of contributions (WNC) and the weighted rms-error (WRMSE) at each grid point by using

$$WCL = t_{\nu}(1 - \frac{\alpha}{2}) \cdot WRMSE/(WNC)^{1/2} \quad . \qquad (8.1)$$

With $\alpha = 5$ these are the 95 % confidence limits (Jenkins and Watts, 1986) for ν = WNC-1 degrees of freedom. The weighting factors were determined from the smoothed autocorrelation function (Bauer et al., 1985).

The statistical parameters WNC, WRMSE and WCL will be discussed for the depth of the isopycnal $\sigma_t = 26.85$ kg m^{-3} (Fig. 7.2). While Bauer et al. (1985) have chosen WNC = 1.0 as the boundary between sufficient and too sparse data coverage, Fischer (1986) has taken a WNC isopleth, which was everywhere within half the correlation distance for the NOA'81 data set. As a consequence of the regular survey pattern in the NOA'83 experiment the WNC-field exceeds 80.0 almost everywhere (Fig. 8.3). The second parameter used in equation (8.1) is the weighted rms-error (Fig. 8.4), which is calculated from the sum of the weighted differences between measured values and the corresponding grid-point value.

The combination of both fields WNC and WRMSE gives the weighted 95 % confidence levels shown in Figure 7.23 and 7.24 for the depth of $\sigma_t = 26.85$ kg m^{-3} and spacing between $\sigma_t = 26.8 - 26.9$ kg m^{-3}. Table 8.1 summarizes the 95 % confidence levels for the hydrographic data on the density surface $\sigma_t = 26.85$ kg m^{-3}. All values in the figures and tables were displayed in the same units as the scalar distributions shown in section 7.1.

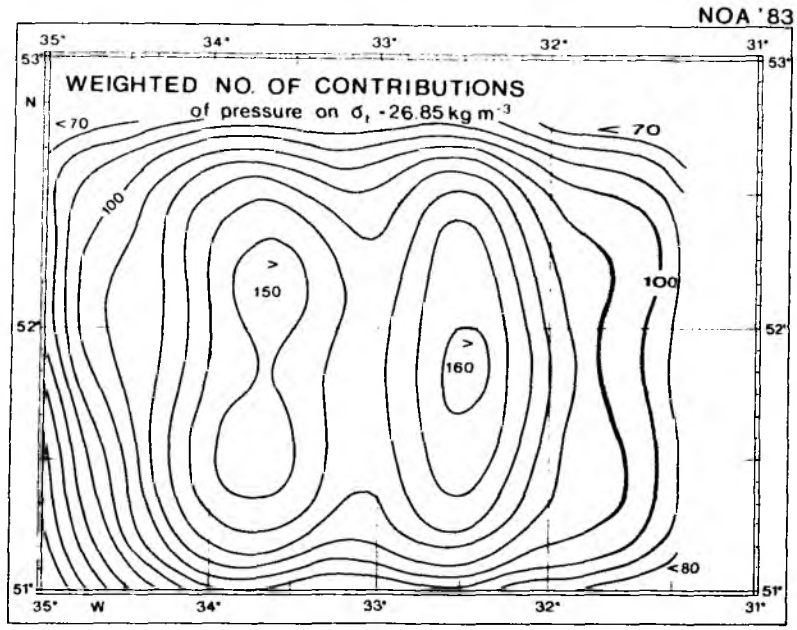

Fig. 8.3: The weighted number of contributions for the depth of the isopycnals σ_t = 26.85 kg m^{-3}.
Contour interval is 10 contributions.

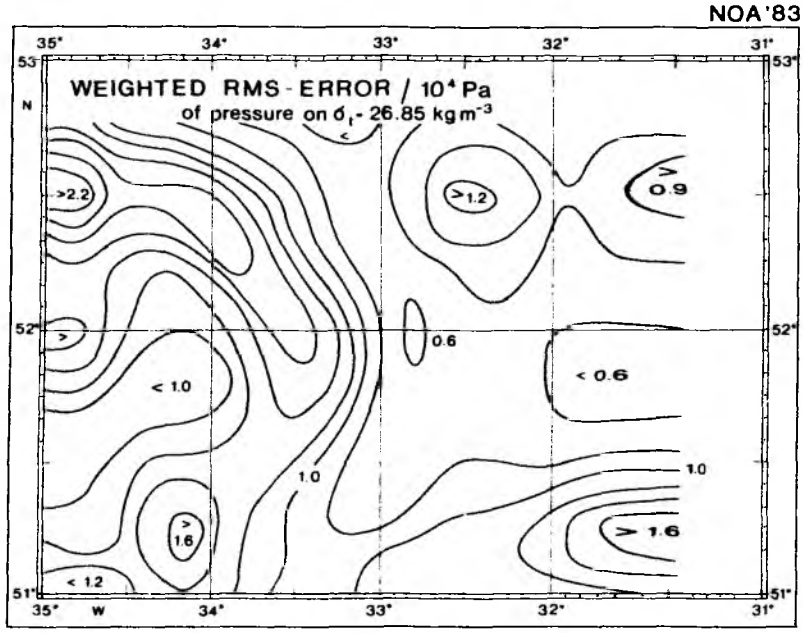

Fig. 8.4: The weighted rms-error for the depth of the isopycnal σ_t = 26.85 kg m^{-3}.
Contour interval is 0.2 m.

Table 8.1: Weighted confidence limits of objectively analysed scalar fields

Parameter	WNC	WRMSE	WCL
Temperature		0.04°K	0.01°K
$T]_{\sigma_t} = 26.85$ kg m^{-3}	> 80	- 0.16°K	- 0.03°K
Salinity		$0.01 \cdot 10^{-3}$	$0.002 \cdot 10^{-3}$
$S]_{\sigma_t} = 26.85$ kg m^{-3}	> 80	$- 0.04 \cdot 10^{-3}$	$- 0.01 \cdot 10^{-3}$
Depth		0.6 m	0.1 m
$z]_{\sigma_t} = 26.85$ kg m^{-3}	> 80	- 1.8 m	-0.3 m
Spacing Δz between $\sigma_t = 26.8$ kg m^{-3} and $\sigma_t = 26.9$ kg m^{-3}	> 60	0.5 m - 1.0 m	0.1 m - 0.2 m

8.4 Synopticity

The survey of the Polar Front took nine days and was conducted in a spatially systematic way. Frequent cloud cover during the time of the experiment prevented the regular acquisition satellite images (Viehoff, 1987). Therefore, it was only possible to estimate the asynopticity directly from the time of the measurements (Bauer et al., 1985). Data points contributing to a grid-point value were measured within 0.2 days on average; the weighted rms-time was 0.2 days. This interval was assumed to be short compared with the likely time scale of such meanders. Nevertheless, there could be a systematic distortion of the large-scale structures over the nine-day period of the experiment.

8.5 Errors in attenuation, K_d

A variety of error sources in the attenuation K_d has been identified by Horch (1987). These errors were caused either by the type of measurements or have been introduced during the processing. The radiation measurements were treated as being correct in this investigation of errors.

Errors due to vertical averaging

The measured radiation E_d (500) decreased exponential with depth and block averaging E_d (500) will cause an error in K_d which depends on the optical thickness of the water. Extreme values of this error occur in regions where the curvature of the exponential is extreme. Nevertheless, this error did not exceed 1 % of K_d for the range of values measured during NOA'83.

Errors due to variable irradiance at the sea surface

Summarizing the results from Horch (1987) a tolerable error in K_d ($\varepsilon_{K_d} = 0.01$) will be caused by a 5 % change in E_o over the 5-second averaging interval. Such short-time variations were seldom observed and data from these times have been rejected.

Errors due to surface waves

Sea surface waves will effect the measured radiation either due to the variability in the path length of the light or due to the refraction of light by very short waves. The total effect of the surface waves was estimated to be less than 15 % of K_d for the situation of NOA'83.

Changes of the fish's attitude

The radiometer was fixed at the top of the fish (Fig. 2.2) and downwelling radiation will be accurately measured only if the fish is horizontal. Any deviation from the horizontal, i.e. pitch and roll angles not equal to zero, will cause an error, which was estimated to be less than $\varepsilon_{K_d} = 0.01\ m^{-1}$ on the ascending profiles, where the pitch and roll angles were generally smaller than on the descending profiles (Fig. 3.1).

Influence of solar elevation on the attenuation

The attenuation is not only a function of turbidity but also on the distribution of the downwelling radiation. A correction of this effect was carried out by Horch (1987) for clear sky situations (see also Fischer and Horch, 1987). It was only possible to correct the data relative to a reference value obtained for a totally overcast sky with the light being 100 % diffuse. The correction applied was up to 20 % dependent on the solar elevation. The residual error was assumed to be less than this value. No correction could be applied for cloudy weather situations.

9. ANALYSIS OF ERRORS OF CURRENT DATA

9.1 Measurement errors

The currents along the ship track were estimated from the vector difference between velocity relative to the water (ADCP-measurements) and mean ship motion between satellite fixes (navigation). Both vectors are subject of measurement errors.

The error of the time-averaged relative velocity partly depends on the variance resulting from a random error of the Doppler frequency measurement. In Didden (1987) it is shown that the frequency standard deviation for a pulse and bin-width of 4.8 ms (corresponding to vertical bin width of 3.15 m) is σ_f = 60 Hz. The resulting standard deviations of the horizontal and vertical velocity measurements are σ_h = 62 cm/s and σ_v = 26 cm/s, respectively. The 95 % confidence interval for the mean horizontal velocity sampled over N pings is $2\sigma_h/\sqrt{N}$ and thus with a sample rate of 1/2.5 s the relative velocity error is about 3.3 cm/s for a 1-hour averaging interval (N = 1440 pings). For longer averaging intervals the error decreases with $1/\sqrt{N}$.

A further error source for the vector-averaged relative velocity is due to unsteady ship motion (roll, pitch, surge, sway, heave) and to transducer misalignment. For R.V. "Poseidon" with actively controlled stabilizing fins roll and pitch amplitudes rarely exceeded 2° and the amplitudes of fluctuating ship velocities (surge, sway, heave) were typically less than 1 m/s. These motions introduced a large variance into the time record of the velocity signal. The bias of the time-averaged horizontal ship velocity - due to correlation between oscillating velocities and angles - was estimated to be less than 2 cm/s (Didden, 1987). Further the transducer misalignment with the ship's longitudinal axis (or, equivalent, a compass error) can introduce a serious systematic error; for a misalignment angle γ the cross-track velocity component (port velocity v_P) is contaminated by the along-track component (forward velocity v_F) by an amount $\Delta v_P = v_F \cdot \sin\gamma$, i.e. 1.7 % of the ship speed for $\gamma = 1°$. From tests with the ADCP bottom-track in shallow water, however, the misalignment angle was found to be very small (~ 0.1°). Thus the total ADCP measurement error of the relative velocity between satellite fixes is assumed to be about 5 cm/s.

The accuracy of the satellite navigation is estimated from the rms distance of satellite fix positions measured when the ship was stationary

in harbour. The rms distance from the mean position of 20 satellite fixes was 0.07 nmi. For a mean time interval of 1 hour between satellite fixes this corresponds to an rms ship speed error of 5 cm/s. An additional systematic fix position error of 0.2 nmi occurs for each 1 knot of error in specifying the absolute ship velocity during the satellite fix measurement. Thus the accuracy of the ship speed between pairs fo satellite fixes is typically 5 - 10 cm/s.

From the above discussion the accuracy of ADCP current measurements derived from the vector difference between absolute and relative ship velocities is about 10 cm/s. This error is largely due to navigational error and thus decreases with increasing time intervals between satellite fixes.

9.2 Estimate of errors in the objectively analysed fields

The errors in the objectively analysed velocity fields and the fields of the quantities derived from them, namely vorticity, streamfunction and divergence-free currents, were calculated by the methods described in Leach (1986). These are also discussed by Fiekas (1987).

Due to the regular spacing of the data and rectangular survey area filling the analysis area there were only regions of poor data coverage at the very edges of the analysis area, see Figures 7.25 and 7.26, for example.

Taking the DCP currents for the bins 6 - 10, corresponding to a depth range of 22 - 37.5 m, as an example the method of Leach (1986) gave weighted confidence limits (WCL) for the objectively analysed velocity components u and v of approximately 0.035 and 0.020 m s^{-1} respectively within the area of small confidence limits. The fields of confidence limits for vorticity and streamfunction are shown in Figures 7.25 and 7.26. Throughout most of the analysis area the WCL for vorticity is less than 4 rad Ms^{-1} and for streamfunction less than $1.0 \cdot 10^{3}$ m^{2} s^{-1}.

The divergence-free currents showed confidence limits between 0.03 and 0.07 m s^{-1}. For the calculation of the confidence limits the length scale used was the grid-spacing of 15 km. It can be argued that a correlation length scale should be used instead. If this were done it would lead to smaller confidence limits for vorticity and larger limits for the stream-function.

10 METEOROLOGY

The meteorological system on board "Poseidon" built by Dr. K. Uhlig from the Department for Maritime Meteorology was interfaced to the navigation system (see section 2.3), so that the data could be logged there.

The meteorological parameters thus recorded were the wind speed and direction, the dry and wet bulb temperature, the incoming short-wave radiation, air pressure and surface water temperature. Measurements were occasionally made by hand to check these quantities and in addition observations of the cloud cover and type, the sea and swell and the weather were made. The wind and temperature sensors were duplicated on both sides of the ship and the measurements from the windward side were taken to be the correct ones.

Fig. 10.1 shows a time-series of the air temperature, wind speed and direction, air pressure and short-wave irradiance. Particularly apparent is the period of more unsettled weather lasting from 28th June till about 5th July which lead to heavy swell at the beginning of the Polar Front Survey thus invalidating some of the acoustic current measurements.

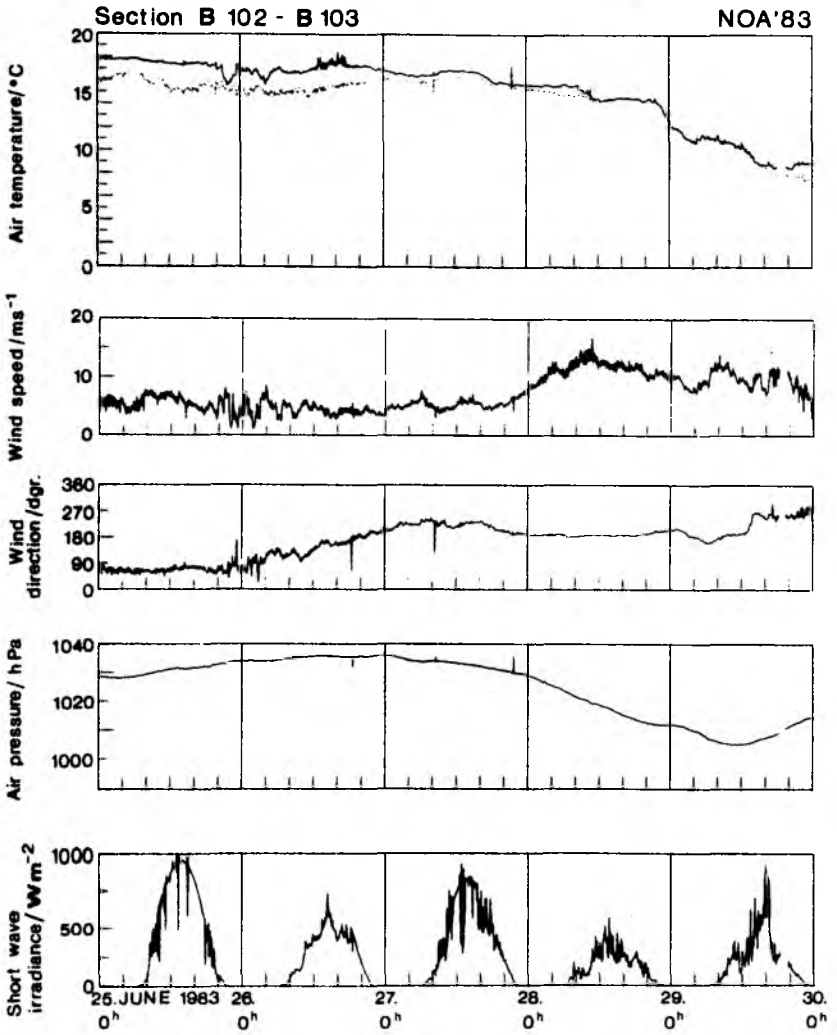

Fig. 10.1 a):

Meteorological parameters air temperature, wind speed and direction, air pressure and short-wave irradiance for the period 25th - 29th June.

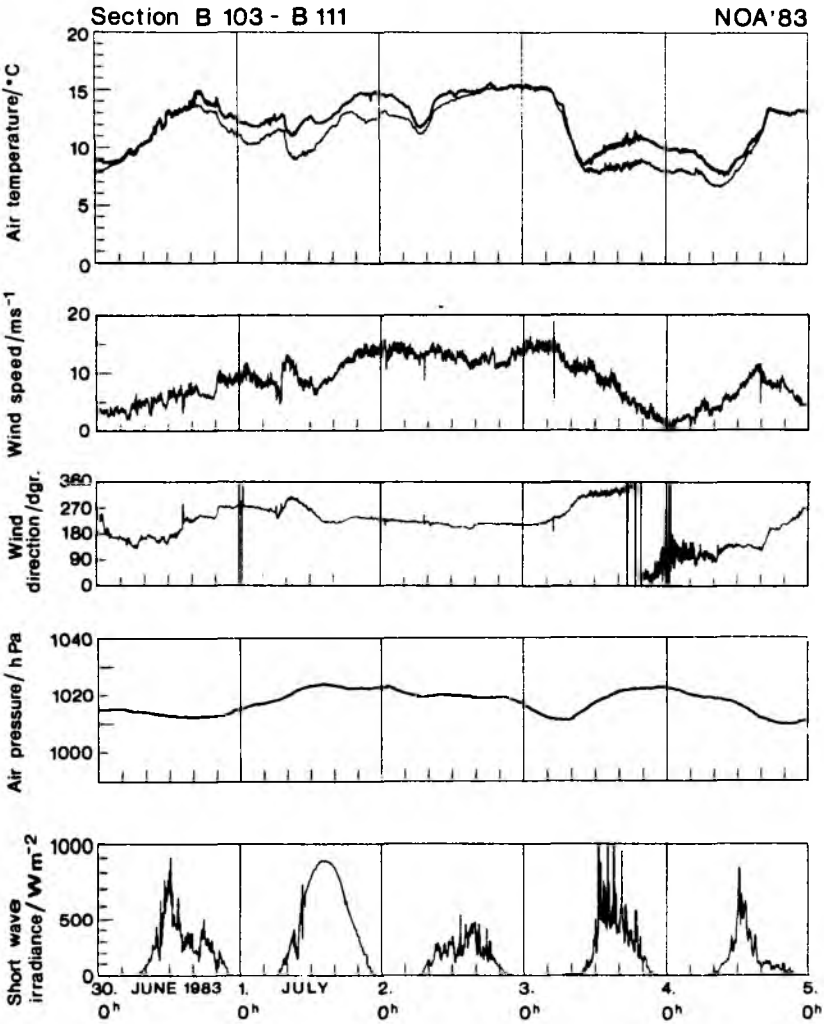

Fig. 10.1 b):

Meteorological parameters for the period 30th June - 4th July.

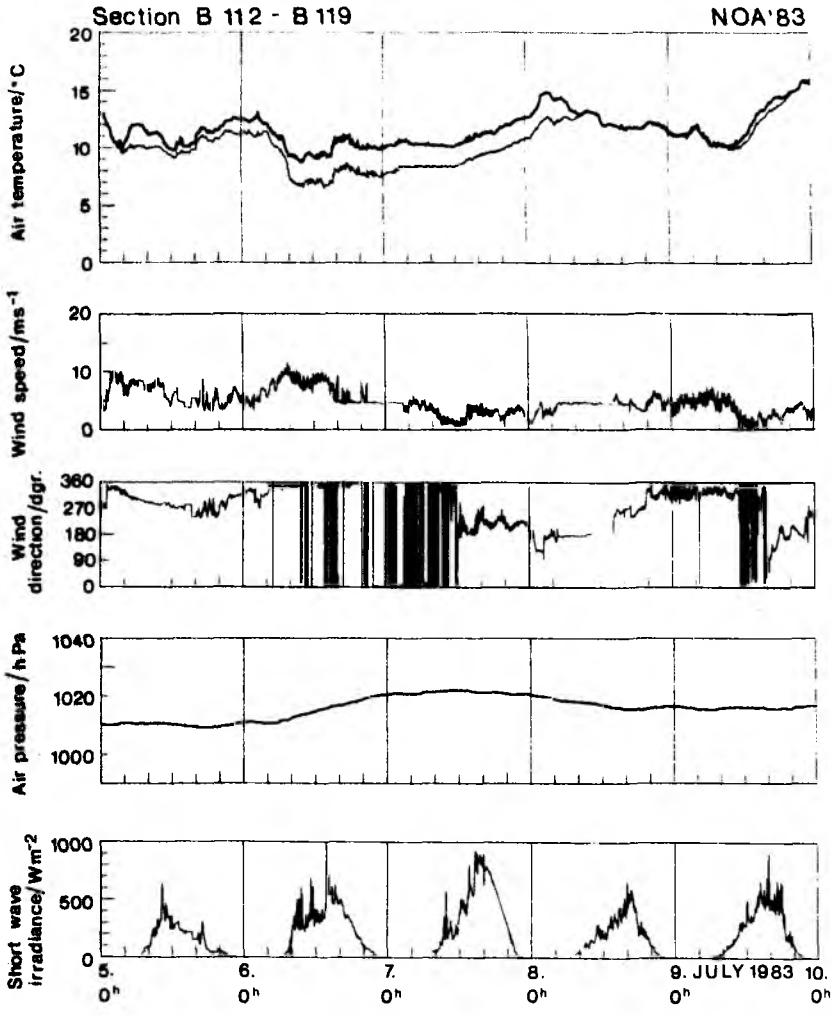

Fig. 10.1 c):

Meteorological parameters for the period 5th - 9th July.

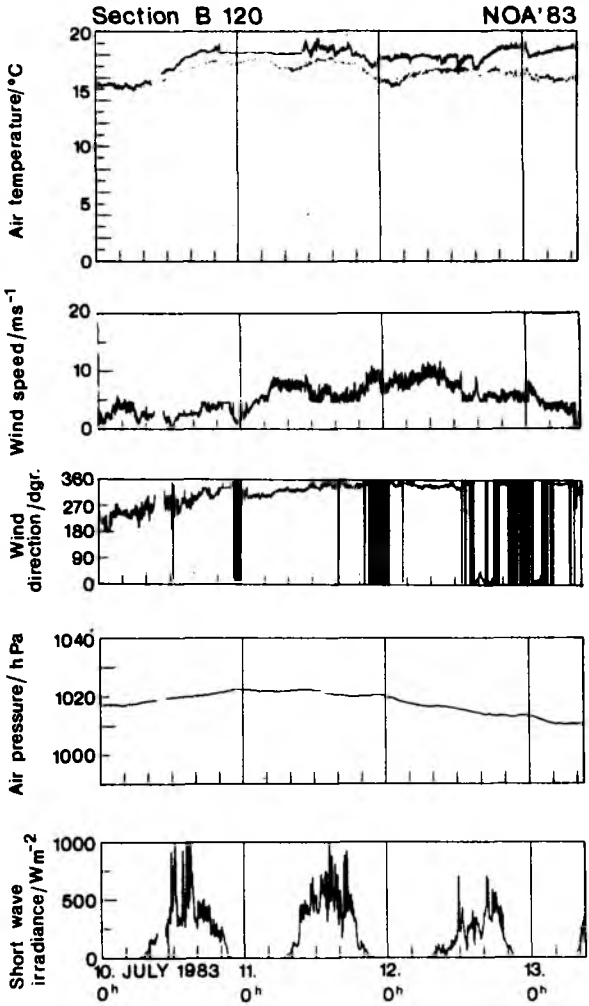

Fig. 10.1 d):

Meteorological parameters for the period 10th - 13th July.

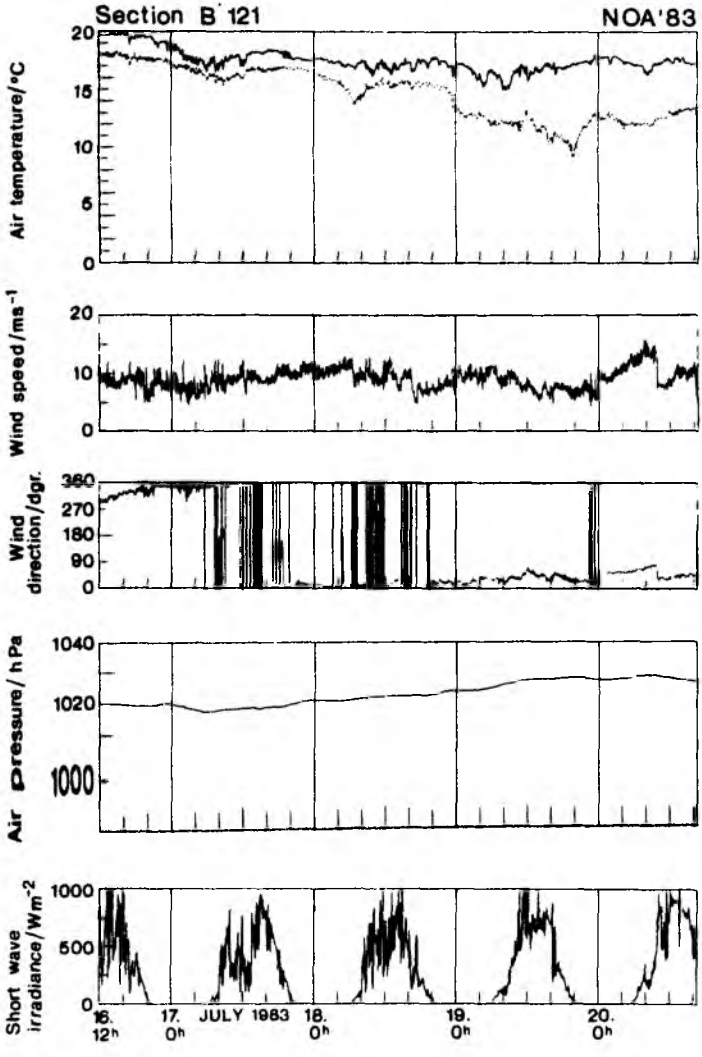

Fig. 10.1 e):

Meteorological parameters for the period 16th - 20th July.

11 CONCLUSIONS

The expedition described in this report, NOA'83, was the second using the SEA ROVER system. Again data were collected along Long Sections and a Polar Front Survey was made. The measurements were enhanced by the inclusion of acoustically measured currents and optically measured water turbidity. The Long Sections contributed to the programme of acquiring a data set describing the annual cycle of the upper ocean in the North Atlantic (see Bauer, 1987). The Polar Front Survey was to some extent a repeat of the 1981 survey but the regular spacing of the data collected systematically has undoubtedly helped in the analysis of the results. The extra information provided by the acoustic current profiler and the radiometer are enabling this data set to give more insight into the dynamics of the synoptic scale than the 1981 data set (Fiekas, 1987; Horch, 1987).

In the subsequent SEA ROVER expeditions (1984, 1985, 1986, 1987) a fluorometer was included in the fish which gave more information about the phytoplankton distribution than the attenuation derived from the radiometer. In these expeditions however no Polar Front Survey was made and data were only collected along Long Sections.

12. REFERENCES

Baumgartner, A. and E. Reichel, 1975: The World Water Balance.
Elsevier, Amsterdam, 179 pp.

Bauer, J., 1987: Sommerliche Ausbreitung von Labradorwasser über die Polarfront in den Nordatlantischen Strom.
Ph.D. Thesis, University of Kiel (in preparation).

Bauer, J., J. Fischer, H. Leach and J. Woods, 1985: SEA ROVER Data Report I, North Atlantic Summer 1981 - NOA'81.
Ber. Institt. Meeresk. Kiel, 143.

Bauer, J. and J.D. Woods, 1984: Isopycnic Atlas of the North Atlantic Ocean.
Ber. Inst. f. Meeresk. Kiel, 132, 173 pp.

Budyko, M.I., 1974: Climate and Life.
International Geophys. Series, Vol. 18, Academic Press, London, 508 pp.

Dettmann, E., 1981: Konzeption, Gestaltung und Anwendung eines ozeanographischen Schleppsystems.
Ph.D. Thesis, University of Hannover.

Didden, N., 1987: Performance evaluation of a shipboard 155 kHz acoustic Doppler current profiler.
Cont. Shelf Res. (in press).

Dietrich, G., 1969: Atlas of the Hydrography of the Northern North Atlantic Ocean.
Conseil International pour l'Exploration de la Mer, Service Hydrographique, Charlottenlund Slot - Denmark, 140 pp.

Dietrich, G., K. Kalle, W. Krauss and G. Siedler, 1980: General Oceanography. An Introduction. 2nd edition (translated from German), John-Wiley, New York, 626 pp.

Fiekas, V., 1987: Die Rolle der ageostrophischen Bewegungen im synoptischskaligen Wirbelfeld der Nordatlantischen Polarfront.
Ph.D. Thesis, University of Kiel (in preparation).

Fischer, J. and A. Horch, 1988: Determination of chlorophyll in the open ocean from quasi-inherent optical properties.
To be submitted to J. Geophys. Res.

Fischer, J., H. Leach and J.D. Woods, 1988: A synoptic map of isopycnic potential vorticity in the seasonal thermocline at the North Atlantic Polar Front.
(in preparation)

Fischer, J., C. Meinke, P.J. Minnett, V. Rehberg and V. Strass, 1985:
A description of the Institut für Meereskunde Schleppfisch-System.
Technischer Bericht Nr. 1 der Abt. Regionale Ozeanographie des Instituts für Meereskunde, Kiel, 2. Auflage.

Gould, W.J., 1985: Physical oceanography of the Azores Front.
Proc. Oceanogr., 14, 167-190.

Hardtke, P.G. and J. Meincke, 1984: Kinematical interpretation of infrared surface pattern in the North Atlantic.
Oceanologica Acta 7(3), 373-378.

Helland-Hansen, B. and F. Nansen, 1926: The eastern North Atlantic.
Geofysiske Publikasjoner, Vol.IV, No.2, 76 pp.

Horch, A., 1984: Eine Beschreibung der NOVA-Software für Schleppfisch-Experimente.
Technischer Bericht Nr. 5 der Abt. Regionale Ozeanographie des Instituts für Meereskunde, Kiel, 2. Auflage.

Horch, A., 1987: Meerwassertrübung, Erwärmungsraten und Chlorophyllgehalt im Nordatlantik aus Messungen der kurzwelligen Einstrahlung bei 500 nm mit einem geschleppten Meßsystem.
Ph.D. Thesis, University of Kiel (in preparation).

Iselin, C. O'D., 1936: A study of the circulation of the western North Atlantic.
Papers in Physical Oceanography and Meteorology, Woods Hole, 4,(4), 1-101.

Isemer, H.-J. and L. Hasse. 1985: The Bunker climate atlas of the North Atlantic Ocean. Vol.1: Observations. Springer Verlag, Heidelberg, New York, Tokyo.

Isemer, H.-J. and L. Hasse, 1987: The Bunker climate atlas of the North Atlantic Ocean. Vol.2: Air Sea Interactions. Springer Verlag, Heidelberg, New York, Tykyo.

Jenkins, G.M. and D.G. Watts, 1968: Spectral Analysis and its applications.
Holden-Day, pp. 525.

Krauss, W., 1986: The North Atlantic Current.
J. Geophys. Res., 91, 5061-5074.

Krauss, W. and R. Käse, 1984: Mean circulation and eddy kinetic energy in the eastern North Atlantic.
J. Geophys. Res. 89, 3407-3415.

Krauss, W. and J. Meincke, 1982: Drifting buoy trajectories in the North Atlantic Current.
Nature, 296, 737-740.

Leach, H., 1984: Eine Beschreibung des wissenschaftlichen Navigationssystems des FS "Poseidon".
Technischer Bericht Nr. 2 der Abt. Regionale Ozeanographie des Instituts für Meereskunde, Kiel, 2. Auflage.

Leach, H., 1986: The analysis of currents measured from a moving ship in the region of the North Atlantic Polar Front.
Deep-Sea Res., 33, 1069-1081.

Leach, H., P.J. Minnett and J.D. Woods, 1985: The GATE Lagrangian Batfish Experiment.
Deep-Sea Res. 32, 575-597.

Lewis, E.L. and R.A. Perkin, 1978: Salinity: Its definition and calculation. J. Geophys. Res., 83, 466-478.

Meincke., J. and A. Sy, 1983: Large-scale effects of the Mid-Atlantic Ridge on the North Atlantic Current.
ICES Report, C.M./C:8, 10 pp.

Morel, A. and N.K. Højerslev, 1979: Conversion of quasi-monochromatic downward irradiance into downward quanta irradiance (370-700 nm).
Proc.-Verb. No. 15, IUGG, XVII General Assembly, Canberra, 1979.

Olbers, D.J., M. Wenzel and J. Willebrand, 1985: The inference of North Atlantic circulation patterns from climatological hydrogaphic data.
Rev. Geophys., 23, 313-356.

Robinson, M.K., R.A. Bauer and E.H. Schroeder, 1979): Atlas of North Atlantic - Indian Ocean monthly mean temperatures and mean salinities of the surface layer.
U.S. Naval Oceanographic Office Ref. Pub. 18, Washington D.C.

Stammer, D., 1986: Die potentielle Vorticity in der Warmwassersphäre des Nordatlantiks: Analyse der saisonalen Variabilität in klimatologischen Atlas-Daten und quasisynoptischen "Sea Rover"-Messungen.
Diplom-Dissertation, University of Kiel.

Stammer, D., N. Didden, H. Leach, V. Strass and J.D. Woods (1988) Compendium of Sea Rover Long Sections 1981-1987.
Ber. Inst. Meeresk. Kiel (in Vorbereitung)

Sy, A.,1985: An alternative editing technique for oceanographic data.
Deep-Sea Res., 32, 1591-1599.

Sy, A., 1987a: Untersuchungen zum großskaligen Feld der Zirkulation des Nordatlantiks im Bereich des Mittelatlantischen Rückens.
Ph.D. Thesis, University of Hamburg.

Sy, A., 1987b: Investigation of large scale circulation patterns in the central North Atlantic: The North Atlantic current, the Azores current and the Mediterranean water plume in the area of the Mid-Atlantic ridge.
Deep-Sea Res. (accepted).

Viehoff, T. (1987) Bestimmung mesoskaliger Variabilitäten der Oberflächentemperatur und der Attenuation im Nordatlantik aus Satellitenmessungen.
Ber. Inst. f. Meeresk. Kiel, 162.

Woods, J.D., 1985: The physics of thermocline ventilation.
In J.C.J. Nihoul (Editor), Coupled Ocean-Atmosphere Models. Elsevier, Amsterdam.

Woods, J.D., H. Leach and P. Minnett, 1981: The GATE Lagrangian Batfish Experiment.
Ber. Inst. Meeresk. Kiel, 88 and 89.

Woods, J.D. and P.J. Minnett, 1979: Analysis of mesoscale thermoclinicity with an example from the tropical thermocline during GATE.
Deep-Sea Res. 26A, 85-96.